UNIVERSITY OF CALIFORNIA, SAN DIEGO

Reception and Performance Enhancement Techniques for Constant Envelope OFDM

A dissertation submitted in partial satisfaction of the

requirements for the degree

Doctor of Philosophy

in

Electrical Engineering (Communication Theory and Systems)

by

Ahsen U. Ahmed

Committee in charge:

Professor James R. Zeidler, Chair
Professor Robert R. Bitmead
Professor William S. Hodgkiss
Professor Laurence B. Milstein
Professor Bhaskar D. Rao

2014

This dissertation of Ahsen U. Ahmed is approved,

and it is acceptable in quality and form for

publication on microfilm and electronically:

_____

_____

_____

_____

_____

Chair

University of California, San Diego

2014

DEDICATION

To my father, who always encouraged us to explore new frontiers of knowledge and experience. He passed away at the age of 58 from multiple myeloma.

To my mother, for her countless sacrifices and her endless encouragement.

EPIGRAPH

"The seeker after truth is not one who studies the writings of the ancients and, following his natural disposition, puts his trust in them, but rather the one who suspects his faith in them and questions what he gathers from them, the one who submits to argument and demonstration, and not the sayings of a human being whose nature is fraught with all kinds of imperfection and deficiency. Thus the job of the man who investigates the writings of scientist, if learning the truth is his goal, is to make himself an enemy of all that he reads, and applying his mind to the core and margins of its content, attack it from every side. He should also suspect himself as he performs his critical examination of it, so that he may avoid falling into either prejudice or leniency."

- Abu Ali Ibn al-Haytham (Alhazen, 965-1040AD, father of the modern scientific method)

"*If the end of the world is upon you and you are holding a seedling, plant it*."

-Muhammad (pbuh)

TABLE OF CONTENTS

LIST OF FIGURES

ACKNOWLEDGEMENTS

I would like to first express my heartfelt gratitude to my advisor, Professor Zeidler, for his invaluable guidance and advice on this research work and beyond as well as his encouragement on balancing my research work alongside work constraints. I am grateful for all his guidance and advice over the years. I would like to thank Professor Milstein for serving on my committee, for his advice and for him teaching some of the best classes anywhere, on any topic. I would like to thank Professor Bitmead, Professor Hodgkiss, and Professor Rao for taking the time to serve as committee members. I would also like to thank Professor Proakis for his valuable advice and guidance during my early research. I would also like to remember Professor Wolf, who previously served on my committee. His kindness and personal advice made a lasting impact on many students.

I would like to especially thank Steve Thompson for his collaboration on many aspects of CE-OFDM and for also providing invaluable advice, feedback, and encouragement on my research work. I would like to also thank Dr. Roy Axford for his advice and support from the very beginning and for making this journey possible. I would like to express my gratitude to Debbie Brady, my branch supervisor, for continually supporting and encouraging my research work and for always accommodating my irregular schedule. I would like to thank David Chi for his advice and suggestions on research work. I would also like to especially thank graduate advisor, Shana Slebioda, for being incredibly helpful on many occasions. I would like to thank Professor Maqusi for inspiring me to pursue the area of Wireless Communications and Professor Vines for teaching us many valuable lessons beyond the classroom, both from Texas Tech University. I would also like to thank my teachers in high school at the Government College of Science, in Lahore, Pakistan, especially Professor Riaz Hussain, Professor Mazhar Hayat and Professor Aftab Hussain, for their dedication to teaching and their many wisdoms of life.

Finally, I would like to thank my family, my wife, Fariha, and my daughters, Mariam and Maliha, for the constant support and encouragement and for the many sacrifices over the years.

Chapters 1, 4, 5, and 6 have, in part, been submitted for publications to the *IEEE Transactions on Signal Processing* as: A. U. Ahmed and J. R. Zeidler, "Novel Linear Receivers for Constant Envelope OFDM." Chapters 4 and 6 were, in part, originally published in: A. U. Ahmed, S. C. Thompson, and J. R. Zeidler, "Constant Envelope OFDM with Channel Coding," in *Proc. of IEEE Milcom*, Washington, DC, Oct. 2006. Chapters 4 and 7 were, in part, originally published in: A. U. Ahmed, S. C. Thompson, and J. R. Zeidler, "Threshold extending receiver structures for CE-OFDM," in *Proc. of IEEE Milcom*, Orlando, FL, Nov. 2007. Chapter 5 was, in part, originally published in: A. U. Ahmed, S. C. Thompson, and J. R. Zeidler, "Channel estimation and equalization for CE-OFDM in multipath fading channels," in *Proc. of IEEE Milcom*, San Diego, CA, Nov. 2008. Chapter 7 was, in part, originally published in: A. U. Ahmed, S. C. Thompson, D. W. Chi, and J. R. Zeidler, "Subcarrier based threshold performance enhancement in Constant Envelope OFDM," in *Proc. of IEEE Milcom*, Orlando, FL, Nov. 2012.

VITA

2000 B.S. in Electrical Engineering
Texas Tech University.

2002 M.S. in Electrical Engineering
Purdue University.

2014 Ph.D. in Electrical Engineering (Communication Theory and Systems)
University of California, San Diego.

PUBLICATIONS

A. U. Ahmed and J. R. Zeidler, "Novel Linear Receivers for Constant Envelope OFDM," submitted for publication to the *IEEE Transactions on Signal Processing*, 2014.

A. U. Ahmed, S. C. Thompson, D. W. Chi, and J. R. Zeidler, "Subcarrier based threshold performance enhancement in Constant Envelope OFDM," in *Proc. of IEEE Milcom*, Orlando, FL, Nov. 2012.

A. U. Ahmed, S. C. Thompson, and J. R. Zeidler, "Channel estimation and equalization for CE-OFDM in multipath fading channels," in *Proc. of IEEE Milcom*, San Diego, CA, Nov. 2008.

S. C. Thompson, A. U. Ahmed, J. G. Proakis, J. R. Zeidler, and M. J. Geile, "Constant envelope OFDM," in *IEEE Transactions on Communications*, 56(8), pp. 1300-1312, Aug. 2008.

A. U. Ahmed, S. C. Thompson, and J. R. Zeidler, "Threshold extending receiver structures for CE-OFDM," in *Proc. of IEEE Milcom*, Orlando, FL, Nov. 2007.

A. U. Ahmed, S. C. Thompson, and J. R. Zeidler, "Constant Envelope OFDM with Channel Coding," in *Proc. of IEEE Milcom*, Washington, DC, Oct. 2006.

S. C. Thompson, A. U. Ahmed, J. G. Proakis, J. R. Zeidler, "Constant envelope OFDM phase modulation: spectral containment, signal space properties and performance." in *Proc. of IEEE Milcom,* Monterey, CA, Nov. 2004.

ABSTRACT OF THE DISSERTATION

Reception and Performance Enhancement Techniques for Constant Envelope OFDM

by

Ahsen U. Ahmed

Doctor of Philosophy in Electrical Engineering (Communication Theory and Systems)

University of California, San Diego, 2014

Professor James R. Zeidler, Chair

Constant Envelope OFDM provides a solution to the issue of a high peak-to-average power ratio in OFDM by using angle modulation to transform the OFDM signal to a constant envelope signal. However, Constant Envelope OFDM is based on nonlinear angle modulation and therefore presents its own unique set of challenges. These challenges are studied in this dissertation and addressed through the application of signal reception, equalization and error correction coding techniques to enable robust Constant Envelope OFDM performance.

The impact of the threshold effect on Constant Envelope OFDM is studied. More specifically, the impact of cycle slip noise, both due to the threshold effect and phase wrapping issues, on Constant Envelope OFDM performance is considered. A novel cycle slip mitigation technique is developed which results in significant threshold extension. Novel receivers for Constant Envelope OFDM are also developed which allow for a lower complexity receiver implementation. These receivers alleviate the need to employ a phase demodulator at the receiver also resulting in immunity from the threshold effect and phase wrapping issues. The performance of these linear receivers is studied in additive white

Gaussian noise (AWGN) and multipath fading channels and they are shown to perform well compared to the conventional arctangent based receiver. In frequency selective fading channels, a frequency domain equalizer is applied to Constant Envelope OFDM and shown to provide good performance in all cases. Since the performance of the frequency domain equalizer depends on the quality of the channel estimate, the effect of the amplifier nonlinearities on the channel estimate is studied for the case of alternate channel estimation training symbols. Furthermore, the application of error correction coding to Constant Envelope OFDM is also studied for the alternate receivers in AWGN and multipath fading channels. Finally, the impact of narrowband interference on Constant Envelope OFDM is studied. A prediction error filter (PEF) is employed to mitigate the narrowband interference resulting in significant performance improvement at low signal to interference ratios.

1. Introduction

OFDM is widely used for wireless communication for both commercial and military applications [1]-[5]. Despite its many advantages, OFDM also suffers from major limitations including a high peak-to-average power ratio (PAPR) [6], [7] which results in intermodulation distortion among subcarriers and out-of-band spectral radiation at the non-linear power amplifier. It is customary to use a significant backoff and operate in the linear region of the amplifier to reduce, but not completely eliminate, the unwanted distortion and the accompanying spectral broadening. Such a backoff not only reduces the transmit power but also results in low power amplifier efficiency [8], [9]. This is especially detrimental for mobile devices operating on battery power. For example, a class A amplifier operating with a 6 dB backoff has a maximum efficiency of only 12.5% [8]. In fact, being limited to a more linear amplifier such as a class A amplifier due to design constraints and operating with a backoff can consume five times or more power than an alternate amplifier feasible for a constant envelope signal [10].

1.1. OFDM Peak-to-Average Power Ratio (PAPR) Issue

One of the major issues that affect OFDM is its high peak-to-average power ratio (PAPR) as shown in Figure 1. The large power fluctuations in OFDM are susceptible to power amplifier nonlinearities and result in intermodulation distortion and out-of-band spectral growth.

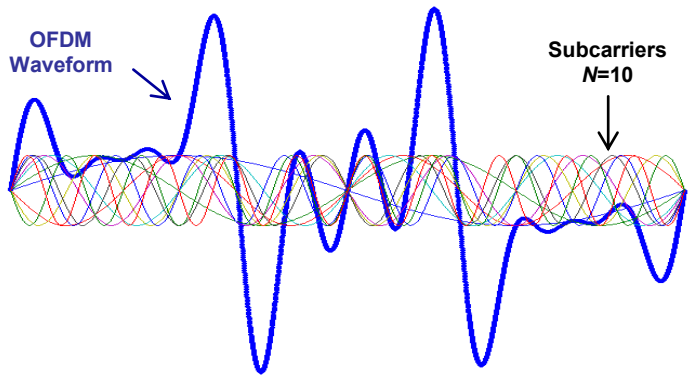

Figure 1. OFDM waveform which is the sum of N=10 modulated subcarriers.

A typical power amplifier transfer function is shown in Figure 2. The amplifier transfer function consists of a region of linear response followed by a region of increasingly nonlinear response close to saturation. The maximum amplifier efficiency is attained by operating in the highly nonlinear region close to saturation.

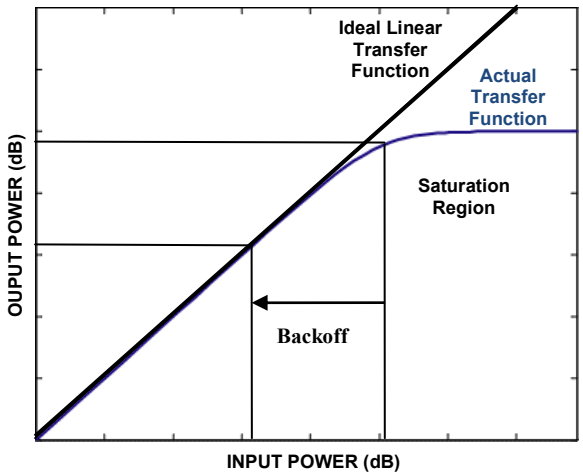

Figure 2. A typical power amplifier transfer function.

The OFDM transmit signal has a large dynamic range and is distorted by the power amplifier nonlinearities. The amplifier nonlinearities result in intermodulation distortion along with out-of-band spectral growth. Therefore, an output power backoff (OBO) is needed for OFDM to operate closer to the linear region thereby reducing the adverse affects of the power amplifier nonlinearities at the expense of radiated power and power amplifier efficiency. A power backoff results in essentially an equivalent loss in transmit power due to the reduction in radiated power. In addition, the amplifier efficiency is reduced significantly with an increase in power backoff e.g. a class A power amplifier operating at a 6 dB backoff has an efficiency of less than 13% (compared to 50% with no backoff) [8], [9]. This reduction in efficiency is highly detrimental to the battery life of mobile communication devices and is accompanied by an increase in heat dissipation.

1.2. Constant Envelope OFDM and its Applications

Constant Envelope OFDM (CE-OFDM) provides one solution to the high PAPR issue in OFDM [11]-[14]. Various PAPR reduction techniques have been previously developed for OFDM but these don't completely eliminate the OFDM PAPR issue [7]. In comparison, CE-OFDM transforms the high PAPR OFDM signal to a constant envelope signal using phase modulation. This not only eliminates the need for a backoff at the power amplifier, maximizing both transmit power and efficiency, but it also enables the use of even more non-linear, power efficient and cost effective amplifiers that are not feasible for OFDM [8].

Due to the major advantage of a constant envelope, CE-OFDM is being researched for applications as varied as wireless [11-26], optical [27]-[31], powerline [32] and satellite [33] communication as well as radar [34]-[37]. The advantages of CE-OFDM for energy efficiency in cellular wireless networks are discussed in detail in [38].

With the continuing rapid growth of wireless communication based applications and the expected increase in future demand, the need for further spectrum will remain high. The availability of 7GHz of unlicensed spectrum around 60GHz, which is much greater than the current combined allocation for radio, TV, cellular, satellite and WiMAX bands, makes it an ideal candidate for future high rate communication [39]. A further benefit of operating at such high frequencies is that the size of components including the antenna is very small enabling the transceiver implementation on a chip. Advances in CMOS technology have made CMOS an attractive choice for low cost, highly integrated transceiver implementation at high frequencies [40], [41]. However, component design, including the power amplifier, remains challenging at high frequencies with added requirements for linearity coming at the expense of performance and a further increase in complexity and cost [42]. CE-OFDM with its constant envelope reduces design complexity and cost while enabling maximum performance and power efficiency thereby providing a very attractive choice for communication at high frequencies including the 60GHz band. These advantages more than compensate for the reduction in bandwidth

efficiency for CE-OFDM compared to OFDM [11], especially with the vast amount of bandwidth available at high frequencies.

1.3. CE-OFDM Challenges

CE-OFDM is based on angle modulation and therefore, under certain conditions during phase demodulation, it is susceptible to the well known threshold effect whereby the demodulated signal to noise ratio (SNR) falls off much more rapidly than the input carrier to noise ratio (CNR) [20], [26]. The threshold effect is encountered at low CNR due to the appearance of phase cycle slips at the output of the phase demodulator, resulting in a degradation of the demodulated SNR and, consequently, the performance. The threshold effect is an issue for larger modulation indices ($2\pi h \geq 0.8$) when phase wrapping requires tracking the phase or using a phase unwrapper at the phase demodulator in the case of the arctangent receiver which estimates the phase on a sample by sample basis. However, for lower modulation indices, the phase wrapping is less frequent and operation without a unwrapper is possible. In this case, there still is less frequent phase wrapping which also results in cycle slips.

In addition to cycle slip noise, since CE-OFDM is based on angle modulation, unlike linear modulation techniques, it requires the study of the noise statistics for performance evaluation and the application of error correction coding and other performance improvement techniques. Additionally, while CE-OFDM is based on OFDM, the efficacy of applying digital communication techniques that work well for OFDM to the CE-OFDM waveform needs to be established. In some cases, such as channel estimation, the training signal that may work well in an OFDM system operating with a backoff may not provide the best performance in a CE-OFDM system operating without a backoff. Therefore, the channel estimation performance for alternate training signals in the presence of an amplifier needs to be studied.

The unique operating conditions and waveform characteristics of CE-OFDM require the study and application of advanced digital communications techniques tailed specifically for CE-OFDM and its own unique challenges.

1.4. Acknowledgements

Chapter 1 has, in part, been submitted for publication to the *IEEE Transactions on Signal Processing* as: A. U. Ahmed and J. R. Zeidler, "Novel Linear Receivers for Constant Envelope OFDM."

2. OFDM

Orthogonal Frequency Division Multiplexing (OFDM) is a spectrally efficient transmission scheme which provides many advantages for wideband, high data rate communications. In OFDM, multiple orthogonal subcarriers are modulated with low-rate, parallel data streams. This is in comparison to modulating a single carrier with a single high-rate data stream. Employing multiple overlapping but orthogonal subcarriers results in high bandwidth efficiency. The transmission of multiple symbols in parallel also results in a longer OFDM symbol time and therefore provides robustness to intersymbol interference (ISI) caused by multipath induced delay spread. Furthermore, the introduction of a cyclic prefix can completely eliminate ISI while preserving orthogonality among the subcarriers. The OFDM transmitter and receiver can be efficiently implemented through the utilization of the fast Fourier transform and the inverse fast Fourier transform pair (FFT/IFFT). Such an implementation of OFDM has become very practical in recent years due to advances in very large scale integration (VLSI) and with the widespread availability of economical, high speed digital signal processors (DSPs). These advantages have resulted in the selection of OFDM for leading commercial applications such as wireless local area networks (802.11a/ g/n/ac/ad), WiMAX, 4G LTE and digital audio and video broadcasting in Europe.

2.1. OFDM Signaling

Orthogonal Frequency Division Multiplexing (OFDM) signaling consists of a set of orthogonal subcarriers that are independently modulated by data. The OFDM signal is the sum of these modulated subcarriers. It is represented in complex baseband notation as

$$s(t) = \sum_{k=0}^{N-1} d_{nk} q_k (t - nT_s), \quad nT_s \le t \le (n+1)T_s \tag{1}$$

where N is the number of OFDM subcarriers and Ts is the OFDM symbol period. The complex data symbols (d_{nk}) modulate the k-th OFDM subcarrier $q_k(t)$ over the n-th signaling interval. The OFDM subcarriers $q_k(t)$ must satisfy the orthogonality requirement,

$$\int_0^{T_s} q_l(t) q_m(t) dt = \begin{cases} E_q, & l = m \\ 0, & l \neq m \end{cases}. \tag{2}$$

In conventional OFDM, full sine and cosine subcarriers separated by $1/T_s$ are used to fulfill the subcarrier orthogonality requirement. These subcarriers can be represented in baseband as complex exponentials and the resulting OFDM signal can be represented as

$$s(t) = \sum_{k=0}^{N-1} d_{nk} e^{j\frac{2\pi kt}{T_s}}, \quad nT_s \le t \le (n+1)T_s. \tag{3}$$

A simple block diagram depicting the OFDM transmit waveform generation is shown below. A high-rate serial data stream is broken up into many low-rate parallel data streams. These parallel data streams are then mapped to modulation symbols (e.g. ± 1 ± j for QPSK) which are then modulated onto the orthogonal subcarriers. The sum of the modulated subcarriers produces the OFDM signal.

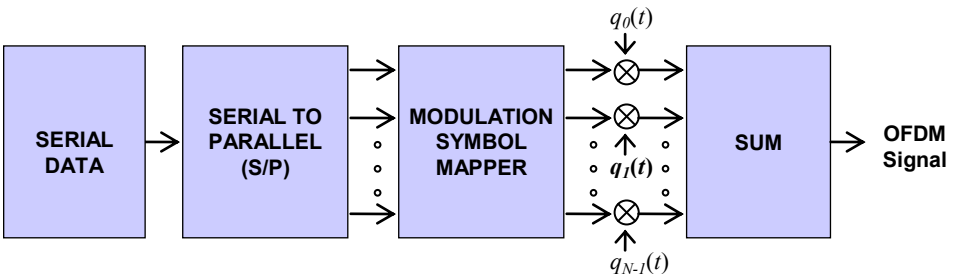

Figure 3. Generating the OFDM signal form a high-rate serial data stream.

The subcarrier modulation scheme can be chosen based on the application with M-ary QAM employed for higher spectral efficiency.

2.2. Efficient Implementation Using FFT/IFFT

The implementation of an OFDM system as depicted in Figure 1 would require a large number of oscillators at the transmitter corresponding to the OFDM subcarriers. These oscillators would need to be synchronized in order to preserve the orthogonality of the subcarriers. Similarly, at the receiver, a bank of matched filters would be needed, one for each subcarrier. Such an implementation would be cumbersome and costly [1]. Weinstein and Ebert [2] were the first to propose the use of discrete Fourier transform (DFT) for the implementation of an OFDM system. Over the years, highly efficient DSP algorithms have been developed for computation of the DFT, most notably, the famous radix-2, fast Fourier transform (FFT) algorithm. The advent of the radix-2 FFT which only requires multiplications on the order of $N\log_2 N$ as opposed to N^2 for the DFT provides all the more reason for such an efficient implementation of an OFDM system.

The OFDM signaling is achieved by modulating complex data symbols onto orthogonal subcarriers. Each subcarrier represents a unique, orthogonal, frequency tone and, therefore, the OFDM signal can be generated through application of the inverse fast Fourier transform (IFFT). This may be thought of as modulating in the frequency domain and then obtaining a time domain waveform by application of the IFFT. Consider a complex data sequence $\{d_0, d_1, \ldots, d_{N-1}\}$ that represents the modulation symbols which modulate the N subcarriers. Application of the IFFT results in a set of time samples $(s_0, s_1, \ldots, s_{N-1})$ that represents the OFDM time waveform for a given OFDM symbol,

$$s_m^n = \sum_{k=0}^{N-1} d_{nk} e^{-j(\frac{2\pi k}{N})m}, \quad m = 0,1,...N-1 \tag{4}$$

where s^n_m corresponds to the m-th time sample at time $t=mT_0$ (where $T_0=T_s/N$) of the n-th OFDM symbol. Similarly, the fast Fourier transform can be employed at the receiver to recover the original transmit symbols,

$$d_{nk} = \sum_{m=0}^{N-1} s_m^n e^{j(\frac{2\pi k}{N})m}, \quad k = 0,1,...N-1. \tag{5}$$

Figures 4 and 5 show the OFDM transmitter and receiver implementation respectively by using the FFT/IFFT pair.

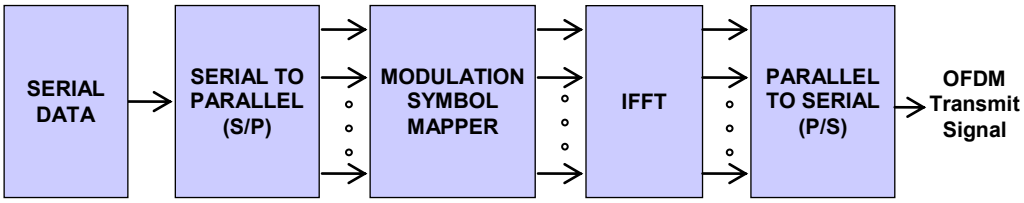

Figure 4. An IFFT based OFDM transmitter.

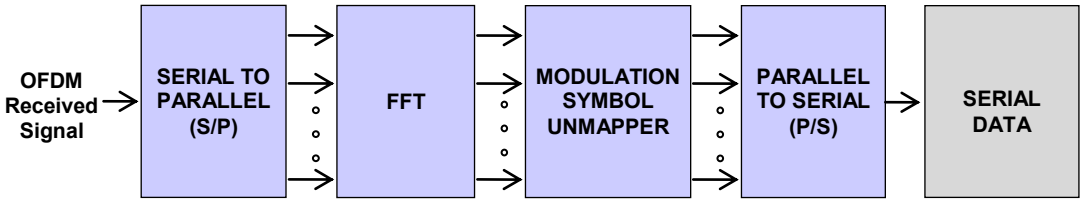

Figure 5. A FFT based OFDM receiver.

2.3. Cyclic Prefix

OFDM has a large symbol time compared to high rate serial communication techniques. This property is instrumental in reducing the effect of intersymbol interference (ISI) caused by multipath induced delay spread of the channel. Although, the ISI is reduced to a relatively small fraction of the symbol time, it is still harmful to the overall bit error rate performance and can results in an error floor at high signal-to-noise ratios (SNRs). One widely used technique to counter the ISI is the addition of a guard time in the form of a cyclic prefix between the OFDM symbols with the purpose of absorbing any delayed versions of the previous symbol. The ISI is completely eliminated if the cyclic prefix is longer than the impulse response (delay spread) of the channel.

While the cyclic prefix can be exploited for other purposes such as synchronization, one of its main advantages is the ability to transform the effect of the channel on the received signal to a circular convolution between the channel impulse response and the transmitted signal. This property of circular convolution is preserved if the guard interval consists of a cyclic prefix which is just a repetition of the last section of the following symbol as shown in Figure 6. At the receiver, the cyclic prefix is stripped

away. This results in removal of the ISI while at the same time preserving the circular convolution property needed for correct demodulation by FFT at the receiver.

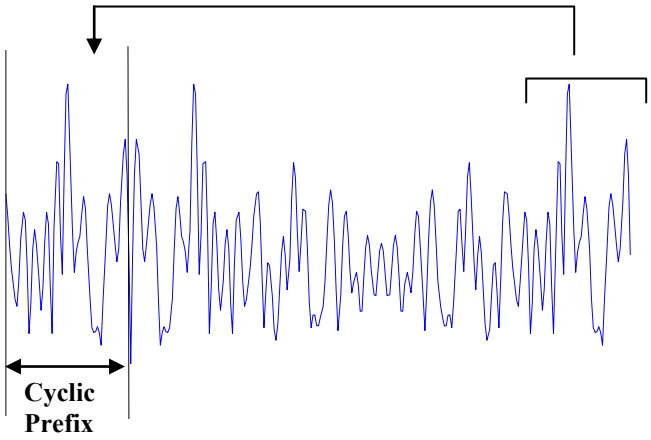

Figure 6. Addition of the cyclic prefix.

2.4. Performance

The performance of OFDM signaling in an ideal environment is that of the underlying modulation scheme. This is based on the assumptions that neither intersymbol interference (ISI), nor interchannel interference (ICI) exist. In a practical system, the ISI can be reduced to negligible levels by designing the cyclic prefix based on the delay spread of the physical channel. On the other hand, the ICI is eliminated if the orthogonality of the subcarriers is preserved. This can be achieved by removing all nonlinearities from the transmit system and by transmitting through a fading channel which does not change over the duration of a symbol. In a real world environment, nonlinear system components (such as amplifiers) and time-variations (doppler) in the channel affect the orthogonality of the subcarriers and cause ICI. Therefore, the performance of the underlying modulation in absence of ISI and ICI should be treated as the ideal performance.

It should be noted that in a frequency selective channel, the OFDM subcarriers can be treated as undergoing independent flat fading. This simplifies the performance analysis and also points to the possibility of using coding and interleaving to achieve both frequency and time diversity. In comparison

to a single carrier system where deep fades may completely wipe out a series of symbols, the longer symbol time implies that the same scenario may only result in some distortion in an OFDM symbol.

2.5. Spectrum and Bandwidth Efficiency

The OFDM subcarriers are spaced at $1/T_s$ in the frequency domain to assure orthogonality. Such a spacing results in the subcarrier spectra to overlap with the nulls of each falling at the center of other subcarriers. This property results in increased spectral efficiency while preserving the subcarrier orthogonality. For rectangular pulse shaping, the spectrum occupancy of OFDM can be computed by considering the main lobes of the *sinc* functions corresponding to the subcarriers. The main lobe of the first subcarrier occupies a frequency band of width $2/T_s$ while each additional subcarrier main lobe only occupies an additional frequency band of $1/T_s$. This is due to spectral overlap among the subcarriers as shown in Figure 7. Hence, the bandwidth of an OFDM waveform with N subcarriers is given as:

$$BW_{mainlobe} = \frac{N+1}{T_s} \tag{6}$$

The bit rate of an M-ary modulation scheme employed to modulate the N OFDM subcarriers is given as:

$$R_b = \frac{N \log_2 M}{T_s} \tag{7}$$

This allows us to show that the spectral efficiency of OFDM is equal to the spectral efficiency of the underlying modulation scheme for a large number of subcarriers.

$$\eta = \frac{R_b}{BW_{mainlobe}} = \frac{\frac{N \log_2 M}{T_s}}{\frac{N+1}{T_s}} \xrightarrow{N \longrightarrow \infty} \log_2 M \tag{8}$$

Hence, it is clear that OFDM provides several advantages over single carrier communications without any loss in spectral efficiency.

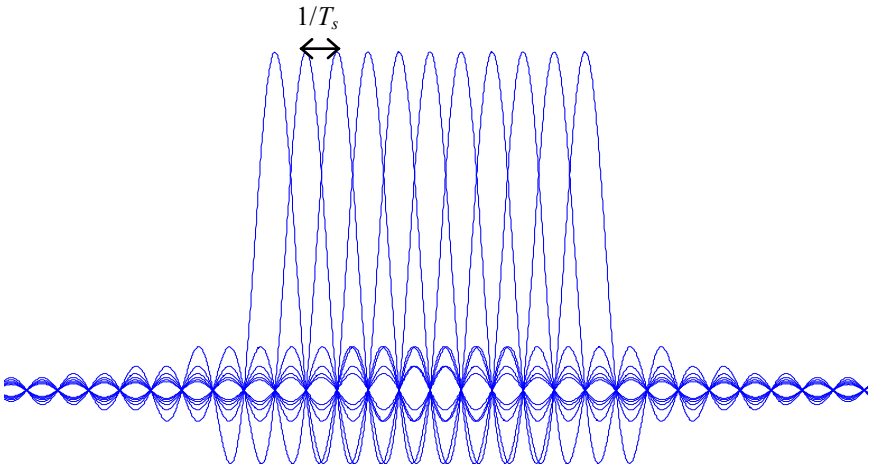

Figure 7. Spectrum overlap in OFDM.

3. Constant Envelope OFDM

The CE-OFDM signal is obtained by phase modulating a constant envelope signal with the OFDM signal. This can be regarded as a simple transformation of OFDM that can be implemented through a trivial modification of a standard OFDM system as shown in Figure 8.

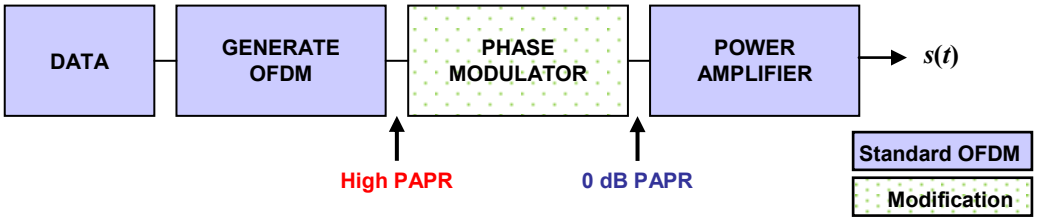

Figure 8. The modification of an OFDM system to obtain CE-OFDM.

The CE-OFDM signal is given as

$$s(t) = A\cos(2\pi f_c t + \phi(t)) \tag{9}$$

where A is the signal amplitude and f_c is the carrier frequency. The phase signal $\phi(t)$ with the embedded OFDM signal is given as

$$\phi(t) = 2\pi h C_N \sum_{k=1}^{N} d_{nk} q_k(t - nT_s) + \theta_n, \quad nT_s \le t \le (n+1)T_s . \tag{10}$$

The real data symbols d_{nk} modulate the orthogonal OFDM subcarriers $q_k(t)$ defined below. The normalizing constant $C_N = \sqrt{2/\sigma_I^2 N}$ ensures that the phase variance is independent of the number of OFDM subcarriers N and σ_I^2 is the data variance with σ_I^2=1 for binary data [12]. Binary data is assumed for all performance analysis in this thesis, however higher level data symbols can be used with CE-OFDM as well [11]. The modulation index h is the key parameter that controls the signal space properties (performance) and the spectral properties of CE-OFDM. The scaled modulation index ($2\pi h$) is also simply referred to as the modulation index here. The phase memory θ_n may be used to ensure a continuous phase at the symbol boundaries and hence better spectral containment. The CE-OFDM

received signal is often sampled at a 2X or higher sampling rate at the receiver [11]. Therefore, an oversampling factor of R_{os} with $N_s = R_{os} N$ samples per CE-OFDM symbol is considered for the various simulation based performance evaluation cases. When a cyclic prefix of length G is added, the length of the CE-OFDM symbol with the cyclix prefix is $N_s + G$. As shown in section 6, CE-OFDM receiver can be operated without any oversampling (R_{os}=1) when error correction coding is employed to take care of any distortion induced error floor.

In conventional OFDM, full sine and cosine subcarriers (DFT) separated by $1/T_s$ are used to fulfill the subcarrier orthogonality requirement.

$$q_k(t) = \begin{cases} \cos(\frac{2\pi kt}{T_s}), & k = 0,2,4,...,N-2\ (even) \\ \sin(\frac{2\pi(k-1)t}{T_s}), & k = 1,3,5...,N-1\ (odd) \end{cases} \qquad 0 \le t \le T_s \tag{11}$$

Such a choice works well for CE-OFDM as well. The subcarrier orthogonality requirement is also fulfilled [12] by half-sine subcarriers (DST) separated by $1/2T_s$,

$$q_k(t) = \sin(\frac{\pi kt}{T_s}), \qquad 0 \le t \le T_s \tag{12}$$

and half-cosine subcarriers (DCT) separated by $1/2T_s$,

$$q_k(t) = \cos(\frac{\pi kt}{T_s}), \qquad 0 \le t \le T_s \tag{13}$$

Each of these subcarrier function sets has its advantages and disadvantages in performance and spectral containment. For example, one advantage of full sine and full cosine subcarriers is that it imparts CE-OFDM with immunity from constant phase offsets at the receiver.

Finally, all the simulation results in this thesis are based on the assumption of an ideal rectangular filter at the receiver input with bandwidth equal to the Nyquest bandwidth based on the sampling rate. Using a narrower filter can help the performance of the phase demodulator based receiver, especially when a phase unwrapper is used. In simulation cases where such a predetection filter with bandwidth narrower than the Nyquest bandwidth is used, the fT_b for the filter is indicated.

3.1. CE-OFDM Spectrum

The spectrum of CE-OFDM is a function of the phase signal. In other words, the smoothness of the phase signal controls the spectral containment of CE-OFDM. A crude estimate of the spectrum may be obtained by application of FFT to obtain the frequency component of a CE-OFDM signal and then squaring to obtain a periodogram. However, such an estimate has a large variance. A good estimate of the spectrum of CE-OFDM can be obtained by application of the Welch method. The Welch method provides a low variance estimate of the spectrum. This is accomplished by windowing the signal and averaging over a large number of periodograms [54].

Since the spectrum of a phase modulated signal depends on the smoothness of the phase signal, analyzing the effects of different subcarrier choices on the CE-OFDM spectrum is important. The half-cosine subcarriers (DCT) and the full-sine/full-cosine subcarriers (DFT) result in a non-continuous phase signal at the symbol boundaries and hence the worst spectral containment. On the other hand, the half-sine subcarriers (DST) always return to zero at the symbol boundaries providing a continuous phase and good spectral containment. The phase signal for the half-cosine (DCT) and the full sine/full-cosine (DFT) cases can be made continuous by adding or subtracting a phase offset (memory) at the symbol boundaries. This results in the continuous phase half-cosine (CP-DCT) and the continuous phase full-sine/full-cosine (CP-DFT) signals. The affect of this continuous phase (memory) is to provide an even smoother phase signal compared to half-sine subcarriers (DST) and hence better spectral containment. The spectral containment can be depicted by plotting the fractional out-of-band power (FOBP) as a function of the frequency as shown in Figure 9.

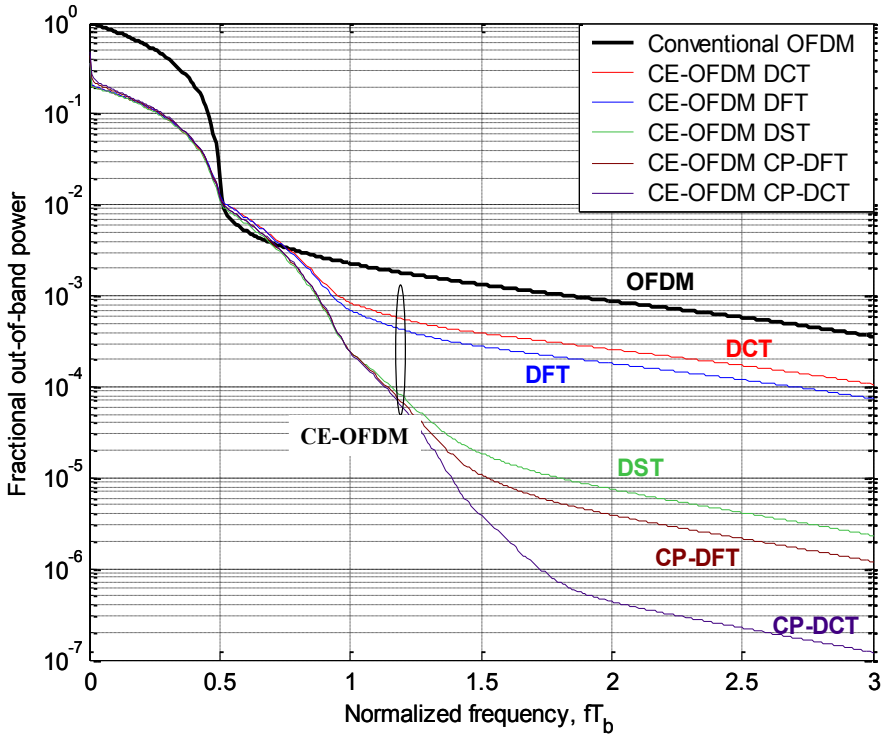

Figure 9. CE-OFDM fractional out-of-band power as a function of normalized frequency for various subcarriers (N=64, $2\pi h$=0.6).

In addition to the subcarrier choice, the bandwidth of CE-OFDM is also a function of the modulation index. Below is a plot of the fractional out-of band power (FOBP) of CE-OFDM with half-sine subcarriers (DST) for various modulation indices. The FOBP of ideal OFDM is also plotted for comparison purposed.

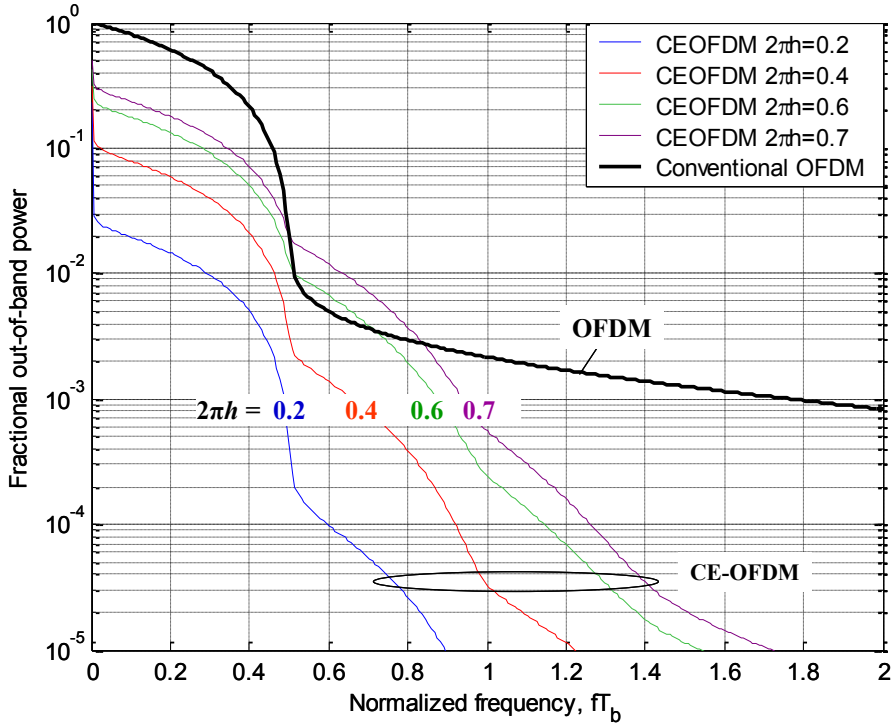

Figure 10. CE-OFDM fractional out-of-band power as a function of normalized frequency for modulation indices (N=64) in comparison to OFDM.

As expected, the CE-OFDM bandwidth grows with an increase in the modulation index. The CE-OFDM waveform is more spectrally confined than OFDM for low modulation indices but a higher CE-OFDM modulation index results in bandwidth expansion. For OFDM, the amplifier present in a real world system results in undesirable spectral growth, especially in the absence of an input power backoff (IBO) at the amplifier. In comparison, since CE-OFDM is constant envelope, it is unaffected by amplifier nonlinearities.

4. CE-OFDM Receiver Structures

4.1. Optimum Receiver

A matched filter based receiver is optimum for maximizing the signal to noise ratio (SNR) at its output. The optimum CE-OFDM receiver match filters the received signal with every possible CE-OFDM transmit signal. For the case of binary data modulating N subcarriers, there are 2^N unique phase message signals based on OFDM and therefore 2^N unique CE-OFDM transmit signals. Hence, the CE-OFDM optimum receiver for the case of N subcarriers modulated with binary data consists of 2^N matched filters corresponding to the 2^N unique transmit signals.

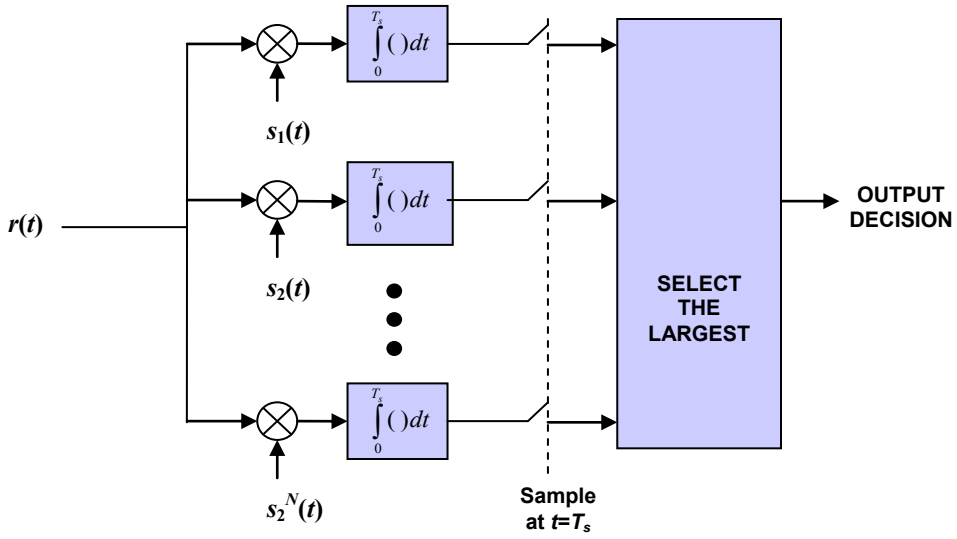

Figure 11. Optimum CE-OFDM receiver.

The implementation of such an optimum receiver is not practical for a large N, for example, $2^N=2^{64}=1.8447 \times 10^{19}$ matched filters are needed for the case of N=64 subcarriers.

4.2. Phase Demodulator Receiver

The conventional receiver structure for CE-OFDM consists of a phase demodulator, to undo

the phase modulation transformation, followed by a standard OFDM demodulator as shown in Figure 12. The phase demodulator extracts the OFDM signal embedded within the phase of the CE-OFDM received signal. This provides for a practical receiver implementation for CE-OFDM [11], [13].

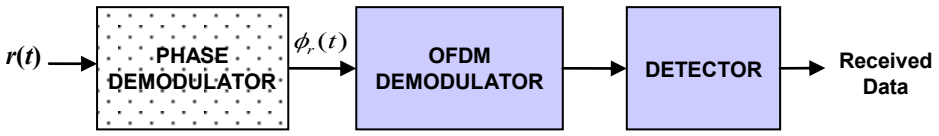

Figure 12. The modification of a standard OFDM receiver to obtain a CE-OFDM receiver.

The received CE-OFDM signal is given as

$$r(t) = A\cos(2\pi f_c t + \phi(t)) + n_w(t) \tag{14}$$

where $n_\omega(t)$ represents the AWGN with a two sided power spectral density of $N_0/2$ W/Hz. The baseband received CE-OFDM signal is given as

$$r(t) = Ae^{j\phi(t)} + n(t) = I_r(t) + jQ_r(t) \tag{15}$$

where $n(t) = n_c(t) + jn_s(t)$ is the baseband Gaussian distributed noise with power spectral density

$$\Phi_n(f) = \begin{cases} N_0, & |f| \le B/2 \\ 0, & |f| \ge B/2 \end{cases} \tag{16}$$

where B is the system front-end bandwidth. The in phase and quadrature noise components are independent with autocorrelation $R_{n_c n_c}(\tau) = R_{n_s n_s}(\tau) = N_0 \frac{\sin(\pi B\tau)}{\pi\tau}$ [43, p. 158]. The sampling rate (F_s=1/T_0) is taken to equal the bandwidth B resulting in independent Gaussian noise samples [12, p. 32] at the receiver.

4.2.1. Arctangent Based Receiver

A phase demodulator that employs the arctangent to obtain the phase estimate on a per sample basis works well for Constant Envelope OFDM. Such an inverse tangent based phase demodulator can be implemented as shown in Figure 13. The phase of the received signal is estimated by taking the inverse tangent of the ratio of the quadrature and in phase components of the received signal

$$\phi_r(t) = \tan^{-1}\frac{r_s(t)}{r_c(t)}. \tag{17}$$

The receiver structure using an arctangent based phase demodulator is known as the arctangent based receiver.

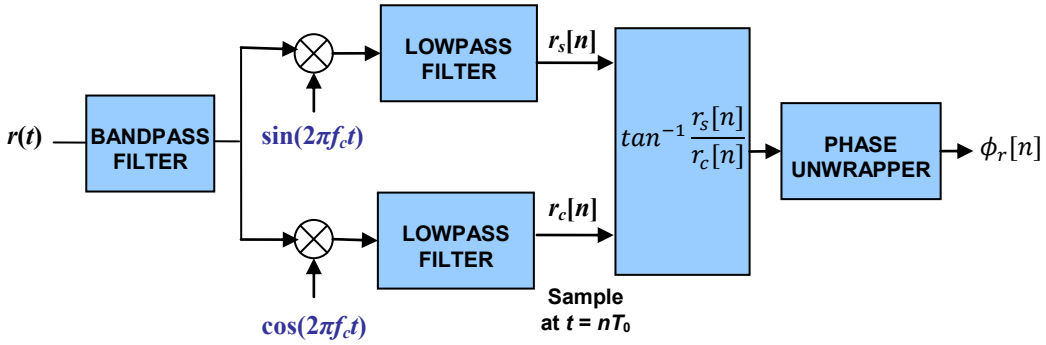

Figure 13. Quadrature inverse tangent phase demodulator.

The arctangent based phase demodulator is memoryless. The received signal $r(t)$ is passed through a bandpass filter to reject the out-of-band noise while allowing the signal component to pass through. This improves the performance of the phase demodulator. The filtered signal is then decomposed into orthogonal components and the phase is extracted by taking the inverse tangent of the samples of the quadrature components. This is followed up by a simple phase unwrapper to unwrap the demodulated phase. The arctangent based phase demodulator is less complex than well known phase demodulators such as a phase locked loop. Since the phase excursions are small for small modulation indices, phase tracking is not critical for small modulation indices and therefore the arctangent based receiver works well. Alternate phase demodulators such as a phase locked loop can also be used based on a tradeoff in complexity and performance.

4.2.1.1. Phase wrapping issues

The phase estimate from the inverse tangent phase demodulator is confined to the 2π range from $-\pi$ to $+\pi$. The original transmit phase that deviates outside the $-\pi$ to $+\pi$ range is wrapped to within this range at the phase demodulator e.g. a transmit phase of $3\pi/2$ is wrapped to $-\pi/2$ by the inverse

tangent phase demodulator. Phase wrapping is more frequent for higher modulation indices as the signal phasor traverses a larger section of the unit circle in the phase plane as shown in Figure 14.

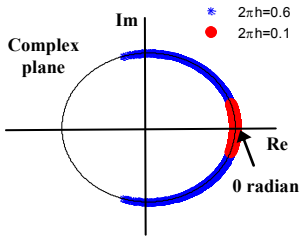

Figure 14. CE-OFDM phase deviation as a function of modulation index.

Large fluctuations in the OFDM message signal result in large fluctuations in the CE-OFDM transmit phase causing it to deviate more frequently outside the boundaries of the $-\pi$ to $+\pi$ range. In addition, the random carrier phase shift may also push the transmit phase closer to the $-\pi$ / $+\pi$ boundary causing phase wrapping at the phase demodulator. An example of phase wrapping is depicted in the figure below.

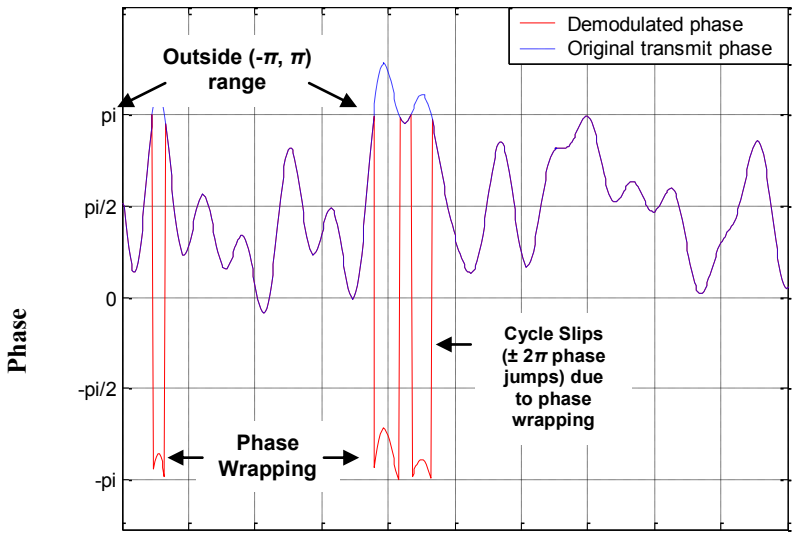

Figure 15. An example of phase wrapping at the phase demodulator.

The CE-OFDM phase with the embedded OFDM signal can be modeled as Gaussian distributed based on the central limit theorem [52] with variance $(2\pi h)^2$ [12, p. 48]. Based on this, the probability of CE-OFDM phase wrapping, $p(|\phi|>\pi)$, at the phase demodulator for various modulation

indices is shown in Figure 16. As expected, phase wrapping is more frequent for higher modulation indices. The likelihood of phase wrapping at the phase demodulator increases further in the presence of noise.

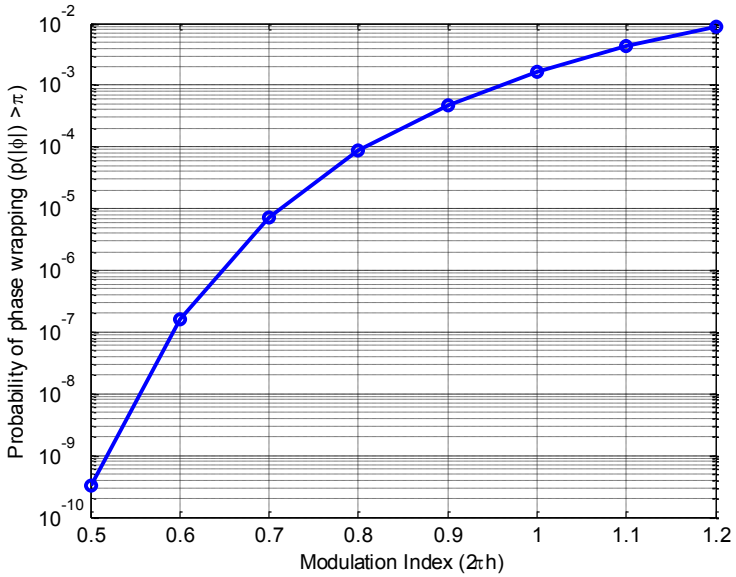

Figure 16. Probability of CE-OFDM phase wrapping as a function of the modulation index.

4.2.1.2. Phase Unwrapper

The purpose of the phase unwrapper is to undo the phase wrapping and restore the received phase to the unrestricted original range. The phase unwrapper operates by looking at consecutive samples of the phase estimate and determining the phase change from one phase sample to the next. This can be visualized by considering the received signal samples on the complex unit circle.

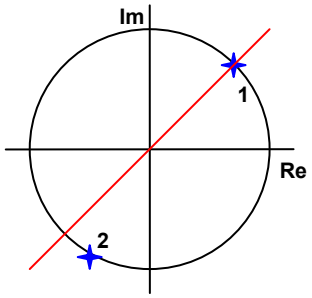

Figure 17. An example of two received signal samples on the complex unit circle.

The shortest angular path from the previous sample to the current sample is determined and the current sample phase is computed by either adding or subtracting this phase change to the previous sample phase. The phase change is added to the previous sample phase if the shortest angular path is anti-clockwise and the phase change is subtracted if the shortest angular path is clockwise. In effect, the unwrapped phase is obtained by computing the cumulative phase at each sample using this technique. Phase unwrapping errors occur when the noise results in the selection of the incorrect angular path (i.e. clockwise instead of anti-clockwise and vice versa). The phase unwrapping error is always equal to 2π due to the combined effect of the correct phase change and the incorrect phase change. It is analogous to a cycle slip in a phase locked loop.

While using the conventional receiver, it is necessary to use a phase unwrapper for larger modulation indices to reconstruct the original unrestricted phase. The phase unwrapper is prone to making errors resulting in phase cycle slips due to the presence of noise, especially at low CNR when significant noise is present [20], [26]. For low and moderate modulation indices, while phase wrapping is less frequent and the arctangent based receiver can be employed without a phase unwrapper, phase wrapping does occur infrequently resulting in burst errors [19].

4.2.1.3. OFDM Demodulator

The demodulated CE-OFDM phase, which is the OFDM signal, is then demodulated by a standard OFDM demodulator consisting of *N* matched filters. The OFDM demodulator performs matched filter based demodulation for each orthogonal subcarrier. The OFDM demodulator for one subcarrier is shown below.

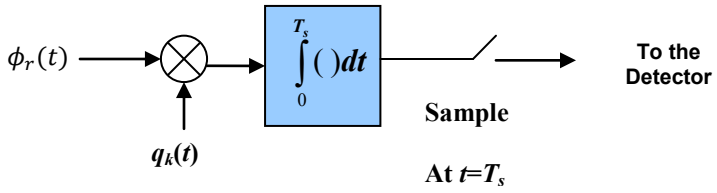

Figure 18. One branch (matched filter) of the OFDM demodulator.

4.2.2. Performance Evaluation

The performance of CE-OFDM when a phase demodulator receiver is employed can be evaluated based on the noise statistics at the output of the phase demodulator. The noise $n(t)$ at the input of the OFDM receiver from the phase demodulator output can be represented in polar form as [46, p. 236]

$$\boldsymbol{n(t)} = \sqrt{\boldsymbol{n_c^2(t) + n_s^2(t)}}\, \boldsymbol{e}^{\,j\left(\arctan\left(\frac{n_s(t)}{n_c(t)}\right)\right)} = \boldsymbol{V_n(t) e^{j\phi_n(t)}}, \tag{18}$$

where $V_n(t)$ and $\boldsymbol{\phi_n(t)}$ are the envelope and phase of the noise process respectively. Using this representation, the phasor diagram of the signal and noise is shown in Fig. 19 below.

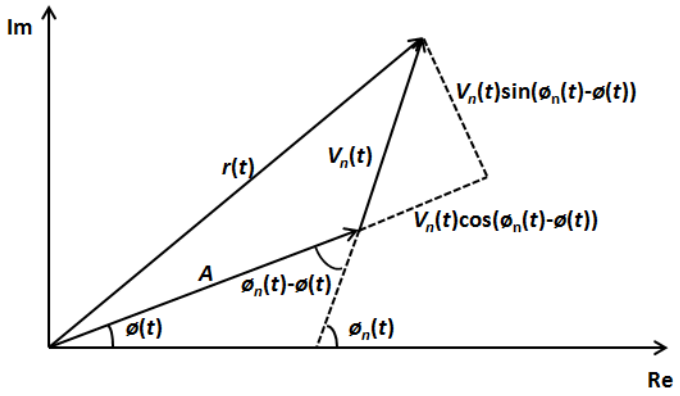

Figure 19. Phasor diagram of the phase of an angle modulated signal with noise.

It is evident from the phasor diagram that the received phase is given as

$$\phi_r(t) = \phi(t) + \arctan\left(\frac{V_n(t)\sin\left(\phi_n(t)-\phi(t)\right)}{A + V_n(t)\cos\left(\phi_n(t)-\phi(t)\right)}\right). \tag{19}$$

Using this and assuming high CNR, the output of the phase demodulator can be approximated as [46, p. 237]

$$\phi_r(t) \approx \phi(t) + \frac{V_n(t)}{A}\sin\left(\phi_n(t)-\phi(t)\right) = \phi(t) + Z_n(t). \tag{20}$$

$Z_n(t)$ provides a good approximation for the noise component at high CNR. The distribution for the noise has been previously computed as [55], [56, p. 417]

$$p(\phi_r \mid \phi) = \frac{1}{2\pi} e^{-\frac{A^2}{2\sigma^2}} \left[1 + \frac{\sqrt{2\pi} A}{\sigma} \cos(\phi_r - \phi) e^{\frac{A^2 \cos^2(\phi_r - \phi)}{2\sigma^2}} \Phi\left(\frac{A \cos(\phi_r - \phi)}{\sigma} \right) \right] \tag{21}$$
$$= \frac{1}{2\pi} e^{-CNR} \left[1 + \sqrt{4\pi CNR} \cos(\phi_r - \phi) e^{CNR \cos^2(\phi_r - \phi)} \Phi\left(\sqrt{2CNR} \cos(\phi_r - \phi) \right) \right],$$

where σ^2 is the variance of bandpass noise at the receiver input and

$$\Phi(x) = 1/\sqrt{2\pi} \int_{-\infty}^{x} e^{-\frac{y^2}{2}} dy \,. \tag{22}$$

This phase noise distribution approaches Gaussian for high CNR [57], therefore, the phase noise is well approximated as Gaussian distributed for high CNR [58, p. 28]. Furthermore, the power spectral density of the noise component for a phase modulated signal can be approximated as $S_Z(f) \approx N_0 / A^2$ W/Hz when the modulated signal bandwidth is much larger than the message bandwidth. Therefore, the noise at the output of the phase demodulator can be characterized as Gaussian noise with a flat power spectral density of N_0 / A^2 W/Hz over the message bandwidth.

The phase demodulator is followed by a conventional OFDM demodulator as shown in Figure 18. Considering the *i*-th CE-OFDM symbol and A=1 without loss of generality, the output of the *k*-th matched filter of the OFDM demodulator is given as

$$Y_k = \int_{(i-1)T_s}^{iT_s} \phi_r(t) q_k(t - iT_s) dt = S_k + N_k, \tag{23}$$

where

$$S_k = \int_{(i-1)T_s}^{iT_s} \phi(t) q_k(t - iT_s) dt = 2 d_k \pi h C_N E_q \in \pm 2\pi h C_N E_q \tag{24}$$

and

$$N_k = \int_{(i-1)T_s}^{iT_s} Z_n(t) q_k(t - iT_s) dt. \tag{25}$$

Since the noise process $Z_n(t)$ is well approximated as Gaussian for high CNR and $\{q_k(t)\}$ are an orthogonal set spanning an N-dimensional space, the N_k's are independent zero mean Gaussian random variables with variance $\sigma_N^2 = N_0 E_q / A^2$. The CE-OFDM performance for a phase demodulation receiver is then given as

$$P_b = Q\left(\sqrt{\frac{{s_{k_1}}^2}{\sigma_n^2}}\right) = \left(\sqrt{\frac{(2\pi h C_N E_b N)^2}{N_0 E_b N}}\right) = \left(2\pi h\sqrt{\frac{2E_b}{N_0}}\right). \quad (26)$$

where $E_b N = E_s = T_s/2 = E_q$.

The analytical performance of CE-OFDM for a phase demodulator based receiver is plotted along with simulation performance of the arctangent based receiver for various modulation indices in Figure 20 and shows good agreement.

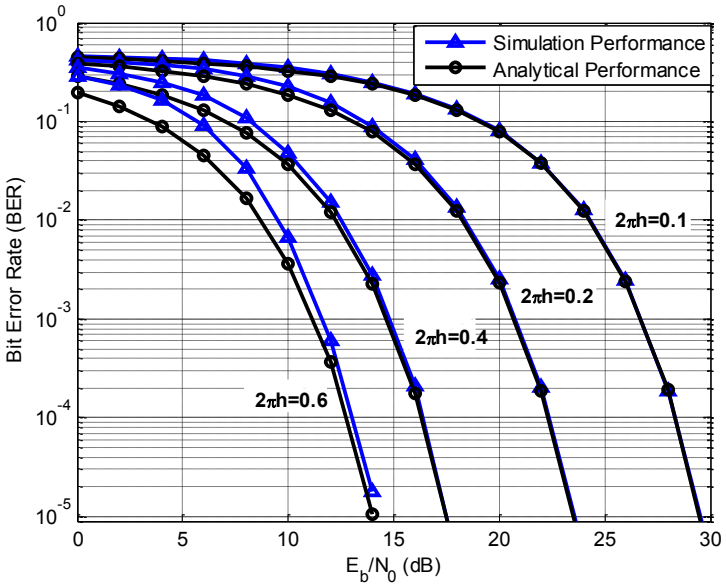

Figure 20. Analytical performance of CE-OFDM in AWGN compared to simulation performance of the arctangent based receiver for *N*=64 for various modulation indices with 2X oversampling.

4.3. Novel Linear Receivers

The need to implement a phase demodulator in the conventional CE-OFDM receiver results in increased receiver implementation complexity. The arctangent based receiver requires the computation of the arctangent at the receiver. This can be accomplished by using a lookup table at the receiver, however, this lookup table needs to be quite large for high accuracy. Additionally, the table address values still needs to be computed at the receiver. Alternately, several algorithms are available for computing the arctangent, but due to the fact that the arctangent is a highly nonlinear function, these

algorithms require a high computational complexity e.g. the popular CORDIC algorithm requires 10-12 iterations to attain a 0.1 degree accuracy. Other lower complexity algorithms still require several multiplications and divisions [44], [45].

Two novel linear receivers for CE-OFDM are developed based on the Taylor series expansion of CE-OFDM for low and moderate modulation indices ($2\pi h \leq 0.7$). These linear receiver structures eliminate the need for a phase demodulator, thus also eliminating phase cycle slips due to the threshold effect or phase wrapping. Due to this reason, while employing these receivers, CE-OFDM is not affected by the threshold effect or any phase wrapping issues. These receiver structures perform well compared to the arctangent receiver and as clear from later results, they also significantly outperform the conventional arctangent based receiver for coded CE-OFDM performance.

4.3.1. Basic Linear Receiver (BLR)

The Basic linear receiver is based on the Taylor series expansion of the CE-OFDM signal. With $m(t)$ representing the normalized OFDM signal, the CE-OFDM signal can be given as $s(t) = Ae^{j2\pi hm(t)}$. Without loss of generality, the amplitude (A) is set to 1. The CE-OFDM signal can then be expressed as

$$s(t) = e^{j2\pi hm(t)} = cos\big(2\pi hm(t)\big) + j\, sin\big(2\pi hm(t)\big) = I(t) + jQ(t). \tag{27}$$

By employing the Taylor series expansion [46], the in phase and quadrature components of CE-OFDM are given as

$$\cos\big(2\pi hm(t)\big) = \sum_{n=0}^{\infty} \frac{(-1)^n}{(2n)!}\big(2\pi hm(t)\big)^{2n} = 1 - \frac{(2\pi hm(t))^2}{2!} + \frac{(2\pi hm(t))^4}{4!} - \frac{(2\pi hm(t))^6}{6!} + \cdots \tag{28}$$

$$\sin\big(2\pi hm(t)\big) = \sum_{n=0}^{\infty} \frac{(-1)^n}{(2n+1)!}\big(2\pi hm(t)\big)^{2n+1} = 2\pi hm(t) - \frac{(2\pi hm(t))^3}{3!} + \frac{(2\pi hm(t))^5}{5!} - \frac{(2\pi hm(t))^7}{7!} + \cdots \tag{29}$$

Note that the first term of the Taylor series expansion of the quadrature component is the normalized OFDM signal. The contribution from the remaining higher order terms decreases with a decrease in the modulation index ($2\pi h$). Therefore, for small modulation indices when the higher order terms in the Taylor expansion are relatively negligible compared to the first term, a simple linear

receiver can be devised by only employing the quadrature component of the received CE-OFDM signal as shown in Figure 21.

Figure 21. The Basic Linear Receiver (BLR) structure for CE-OFDM.

This Basic linear receiver for small modulation indices is essentially a direct OFDM receiver applied to the quadrature component of the received CE-OFDM signal thereby reducing the overall CE-OFDM receiver complexity.

4.3.2. Enhanced Linear Receiver (ELR)

The Basic linear receiver works well for small modulation indices ($2\pi h \leq 0.5$) as the higher order terms are negligible. However the higher order terms become more significant for higher modulation indices. The first term of (29) is the desirable OFDM signal while the other higher order terms contribute to distortion with their contributions decreasing as their order increases for the case of modulation indices below 1 ($2\pi h<1$). It is clear that the second term, $(2\pi hm(t))^3/3!$, contributes the largest amount of distortion. An improved linear receiver can be developed by using both the in phase and quadrature components of CE-OFDM to cancel out the most significant cubic distortion term. This improved linear receiver is given as

$$\begin{aligned} Q(t)\big(4 - I(t)\big) &= sin\big(x(t)\big)\big(4 - \cos\big(x(t)\big)\big) \\ &= \Big(x(t) - \frac{x^3(t)}{3!} + \frac{x^5(t)}{5!} - \cdots\Big)\Big(3 + \frac{x^2(t)}{2!} - \frac{x^4(t)}{4!} + \cdots\Big) \\ &= 3x(t) - \frac{1}{10}x^5(t) + \frac{1}{84}x^7(t) - \frac{41}{60480}x^9(t) + \cdots \end{aligned} \quad (30)$$

where $x(t)= 2\pi hm(t)$. This improved linear receiver performs better than the Basic linear receiver for moderate modulation indices due to the removal of the cubic distortion term. It is shown below that the cubic term degrades the performance as distortion only when it is present with a negative sign (as in (29)) and that it in fact contributes constructively at the receiver when it is additive to the OFDM

component (first term). Therefore, further improvement can be obtained by using an Enhanced linear receiver with an additive cubic term, given as

$$R(t) = Q(t)\big(2 - I(t)\big) = sin\big(x(t)\big)\big(2 - \cos\big(x(t)\big)\big)$$
$$= \left(x(t) - \frac{x^3(t)}{3!} + \frac{x^5(t)}{5!} - \cdots\right)\left(1 + \frac{x^2(t)}{2!} - \frac{x^4(t)}{4!} + \cdots\right)$$
$$= x(t) + \frac{x^3(t)}{3} - \frac{7x^5(t)}{60} + \frac{31}{2520}x^7(t) - \frac{41}{60480}x^9(t) + \cdots \quad (31)$$

Figure 22 shows the block diagram of this Enhanced linear receiver structure. The Enhanced linear receiver, while not strictly linear, is an enhancement of the linear receiver. This receiver is low complexity, requiring only one addition and one multiplication per CE-OFDM received sample, resulting in a large reduction in complexity compared to the arctangent based receiver. The performance of the Basic and Enhanced linear receivers for several modulation indices ($2\pi h$) is shown in Figures 23 and 24 where they are compared with the conventional arctangent based receiver for the case of an AWGN channel.

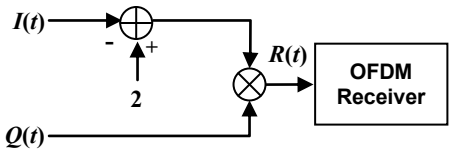

Figure 22. The Enhanced Linear Receiver (ELR) structure for CE-OFDM.

While the Basic linear receiver performs well for small modulation indices ($2\pi h \leq 0.5$), the Enhanced linear receiver outperforms it, as expected, especially for moderate modulation indices ($0.5 \leq 2\pi h \leq 0.7$) when the contribution from the cubic term is significant. The linear receivers also perform well compared to the arctangent based receiver. For higher modulation indices, while the arctangent receiver performs better at low BERs, the ELR outperforms it at higher BERs.

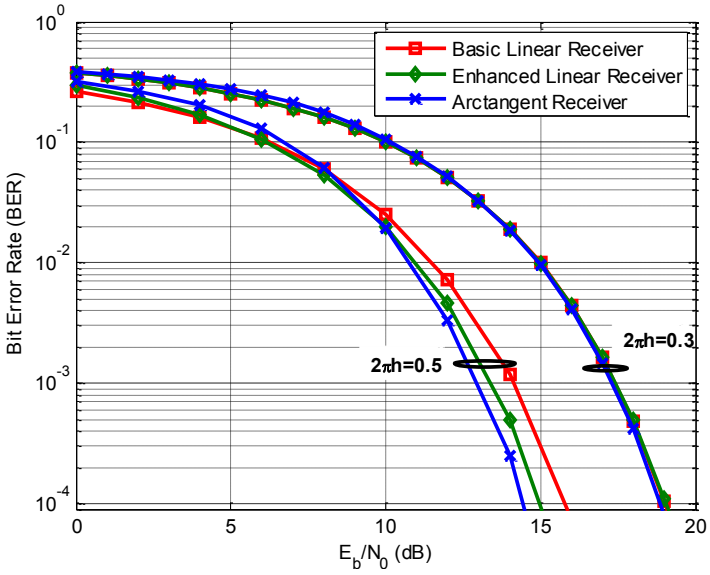

Figure 23. CE-OFDM simulation performance of the Basic and Enhanced linear receivers compared to the arctangent based receiver for *N*=64 with 2X oversampling.

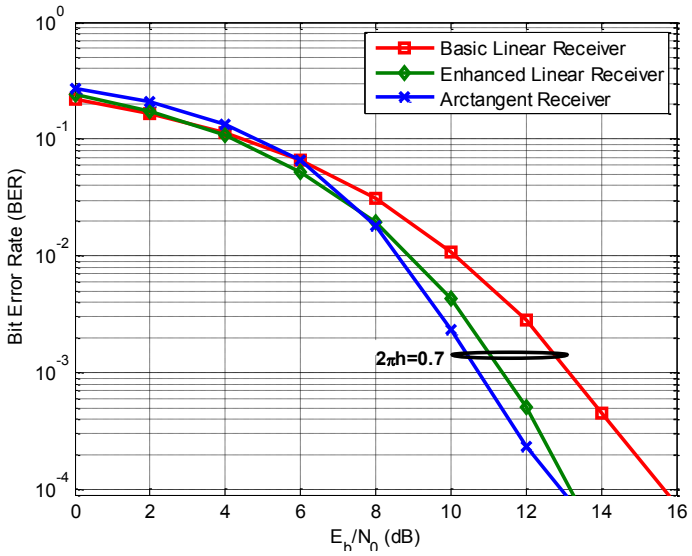

Figure 24. CE-OFDM simulation performance of the Basic and Enhanced linear receivers compared to the arctangent based receiver for *N*=64 with 2X oversampling.

4.3.2.1. Contribution of the cubic term

Let us further examine the cubic term and its contribution at the receiver. For the case of sine and cosine subcarriers, with ds_k and dc_k as the k-th data symbols present on the sine and cosine subcarriers respectively, the cubic term is given as

$$x^3(t) = \left(2\pi h C_N \left(\sum_{k=1}^{\frac{N}{2}} dc_k cos\left(\frac{2\pi kt}{T_s}\right) + ds_k sin\left(\frac{2\pi kt}{T_s}\right)\right)\right)^3. \tag{32}$$

By expanding out the terms and through repeated use of trigonometric identities as shown in appendix A, the cubic term can be represented as

$$\begin{aligned} x^3(t) = (2\pi h C_N)^3 \sum_{l=1}^{\frac{N}{2}} \sum_{m=1}^{\frac{N}{2}} \sum_{n=1}^{\frac{N}{2}} \Bigg(& \frac{1}{4}(dc_l dc_m dc_n + ds_l ds_m dc_n - dc_l ds_m ds_n + ds_l dc_m ds_n) cos\left(\frac{2\pi(-l+m+n)t}{T_s}\right) \\ & + \frac{1}{4}(dc_l dc_m dc_n + ds_l ds_m dc_n + dc_l ds_m ds_n - ds_l dc_m ds_n) cos\left(\frac{2\pi(l-m+n)t}{T_s}\right) \\ & + \frac{1}{4}(dc_l dc_m dc_n - ds_l ds_m dc_n + dc_l ds_m ds_n + ds_l dc_m ds_n) cos\left(\frac{2\pi(l+m-n)t}{T_s}\right) \\ & + \frac{1}{4}(dc_l dc_m dc_n - ds_l ds_m dc_n - dc_l ds_m ds_n - ds_l dc_m ds_n) cos\left(\frac{2\pi(l+m+n)t}{T_s}\right) \\ & + \frac{1}{4}(dc_l ds_m dc_n - ds_l dc_m dc_n + dc_l dc_m ds_n + ds_l ds_m ds_n) sin\left(\frac{2\pi(-l+m+n)t}{T_s}\right) \\ & + \frac{1}{4}(-dc_l ds_m dc_n + ds_l dc_m dc_n + dc_l dc_m ds_n + ds_l ds_m ds_n) sin\left(\frac{2\pi(l-m+n)t}{T_s}\right) \\ & + \frac{1}{4}(dc_l ds_m dc_n + ds_l dc_m dc_n - dc_l dc_m ds_n + ds_l ds_m ds_n) sin\left(\frac{2\pi(l+m-n)t}{T_s}\right) \\ & + \frac{1}{4}(dc_l ds_m dc_n + ds_l dc_m dc_n + dc_l dc_m ds_n - ds_l ds_m ds_n) sin\left(\frac{2\pi(l+m+n)t}{T_s}\right)\Bigg) \end{aligned} \tag{33}$$

This expression for the cubic term contains four sine terms and four cosine terms which results in sines and cosines at different locations for different combinations of l, m, and n over the triple summation (total terms = $8(N/2)^3$). Only sines and cosines that fall on the OFDM sine and cosine subcarrier locations have an impact on the CE-OFDM performance. Consider the k-th cosine matched filter at the

receiver, corresponding to the $\cos(2\pi kt/T_s)$ subcarrier. As shown in appendix B, the number of cosine/sine terms from the triple sum representing $x^3(t)$ in (33) that impact the k-th cosine matched filter is given as

$$N_{Total}^{k} = 3\left(\frac{N^2}{8} - \frac{N}{4} + \frac{kN}{2} - k^2 + k\right) + \left(\frac{k^2}{2} - \frac{3k}{2} + 1\right)u(k-3). \tag{34}$$

It is also shown in appendix B that the number of these terms that contribute constructively is given as

$$N_{correct} = 6\left(\frac{N}{2} - 1\right) + 3 = 3(N-1). \tag{35}$$

The contribution due to the non-constructive terms at the subcarrier matched filter output can be shown to be Gaussian distributed. Consider the coefficient of the first cosine term in (33). It is given as

$$dc_l dc_m dc_n + ds_l ds_m dc_n - dc_l ds_m ds_n + ds_l dc_m ds_n \tag{36}$$

The data coefficients (dc_k, $ds_k \in \pm 1$) are zero mean, independent, identically distributed with a uniform probability density. Thus, each of the terms in (36) is also distributed with a uniform probability density (± 1). Furthermore, the terms in (36) are uncorrelated Bernoulli random variables and thus pairwise independent [47] for any combination of (l, m, n) that generates unique terms.

The application of the central limit theorem is well known for the case of the sum of independent Bernoulli trials to model the resulting binomial distribution [48, p. 325]. Although the central limit theorem has been shown to hold for certain cases of pairwise independent identically distributed random variables [49], [50], pairwise independence is not a sufficient condition in general [49, p. 109] for the central limit theorem. Therefore, Monte Carlo simulations were performed to show that the sum of the coefficients in (33) is well modeled as Gaussian distributed. Further examination also shows that each coefficient term from (33) that affects the k-th cosine or sine matched filter is generated 6 times. For example, for k=4, the coefficient term $dc_1 dc_2 dc_3$ is generated 6 times from the combinations of (l, m, n) of (1,2,3), (1,3,2), (2,1,3), (3,1,2), (2,3,1) and (3,2,1). Therefore, based on this observation and from (34) and (35), there are $N_{Distort}^{k} = {4 * (N_{Total}^{k} - N_{correct})}/{6}$ unique distortion causing coefficient terms with unit variance, each appearing 6 times, at the k-th cosine or sine matched

filter. The sum of these coefficient terms is Gaussian distributed with variance, based on the sum of individual variances due to pairwise independence, given as

$$\sigma^2_{k,cubic} = \frac{6^2*(2\pi h C_N)^6}{(3!)^2*4^2} N^k_{Distort} = \frac{(2\pi h)^6 N^k_{Distort}}{2N^3}. \quad (37)$$

Figure 25 shows the histogram generated by simulating the coefficients of all terms from (33) (excluding the scaling at the front) that impact the k-th cosine matched filter for N=64 with dc_k=+1. The non-zero mean represents the terms that contribute constructively.

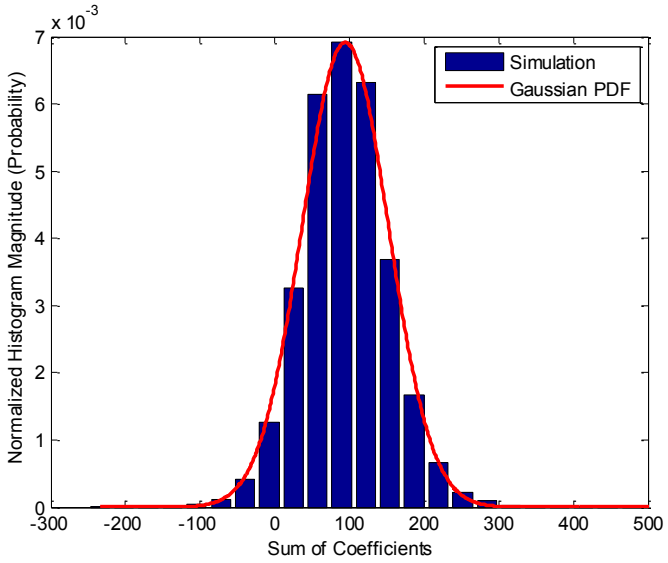

Figure 25. Histogram of the sum of the coefficients of all terms in (33) (excluding the scaling) that impact the k-th matched filter for N=64 with dc_k=+1. The Gaussian PDF with mean based on (35) and variance from (37) is also plotted.

The sum of the coefficients that appear at the k-th cosine matched filter due to the cubic term (33) matches well with the plotted Gaussian distribution with a mean of 3*(N-1)/2 as predicted by (35) and variance given by (37). The bias in the mean towards dc_k is the reason that the presence of the additive cubic term helps improve the performance of the Enhanced linear receiver compared to the Basic linear receiver.

4.3.3. Performance in AWGN

A performance approximation for the Basic and Enhanced linear receivers in AWGN can be obtained by considering the dominant first and third order signaling terms from the Taylor series expansion. The higher order signaling terms make a smaller contribution for modulation indices below 1 (i.e., $2\pi h<1$).

4.3.3.1. Basic Linear Receiver (BLR)

For the Basic linear receiver, the output of the OFDM matched filter for the k-th cosine subcarrier based on the quadrature component of the received CE-OFDM signal is

$$Y_k = \sum_{n=0}^{N_S-1} Q_r(nT_o)\cos\left(\frac{2\pi kn}{N_S}\right)$$

$$\cong S_{k1} - S_{k2} + I_{k2} + N_k, \tag{38}$$

where S_{k1} is the signaling component due to the first term of (29), which is simply the embedded OFDM signal. It is given as

$$S_{k_1} = \sum_{n=0}^{N_S-1} 2\pi h C_N \phi(nT_o)\cos\left(\frac{2\pi kn}{N_S}\right)$$

$$S_{k_1} = dc_k 2\pi h C_N E_b N \tag{39}$$

where $E_bN = E_s = N_s/2$. S_{k2} is due to the component of the cubic term arising from terms with the correct data bits. The total number of terms with the correct data symbol is given in (35). The signal component due to the negative cubic term based on (29) and (35) is given as

$$S_{k_2} = dc_k \frac{(2\pi h C_N)^3}{4}(N-1)E_bN. \tag{40}$$

N_k is due to the baseband quadrature noise component,

$$N_k = \sum_{n=0}^{N_S-1} n_s(nT_o)\cos\left(\frac{2\pi kn}{N_S}\right). \tag{41}$$

It is Gaussian distributed since $n_s(t)$ is Gaussian distributed. The variance of N_k can be shown to be $\sigma_n^2 = N_0 E_b N$ [43, p. 158]. I_{k2} is the distortion component due to the cubic term which was previously shown to be well modeled as Gaussian distributed. Therefore, I_{k2} is Gaussian distributed with variance $\sigma_I^2 = E_b N \sigma_{k,cubic}^2$ where $\sigma_{k,cubic}^2$ is given in (37).

Without loss of generality, we can assume that dc_k=+1. The performance of the Basic linear receiver for the k-th subcarrier can then be given as

$$P_b^k = Q\left(\sqrt{\frac{\left(s_{k_1} - s_{k_2}\right)^2}{\sigma_n^2 + \sigma_I^2}}\right). \tag{42}$$

The overall performance over all subcarriers is then given as $P_b = \frac{2}{N}\sum_{k=1}^{N/2} P_b^k$. This performance approximation is plotted against the simulation performance in Figure 26.

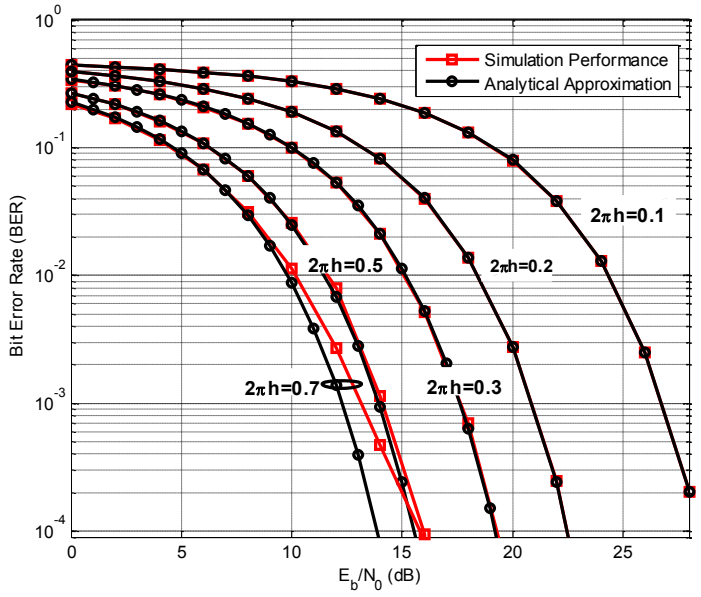

Figure 26. CE-OFDM simulation performance in comparison to the analytical approximation in AWGN for the Basic linear receiver for N=64 with 2X oversampling.

For low modulation indices ($2\pi h \leq 0.5$), the performance approximation is very accurate. For the higher modulation index of $2\pi h$=0.7, the higher order terms (fifth order and above) become more significant and therefore the approximation is not as accurate at low bit error rates (BERs).

At low modulation indices when the cubic term is negligible and can be ignored, the performance approximation can be simplified as

$$P_b = Q\left(\sqrt{\frac{S_{k_1}{}^2}{\sigma_n^2}}\right) = \left(\sqrt{\frac{(2\pi h C_N E_b N)^2}{N_0 E_b N}}\right) = \left(2\pi h\sqrt{\frac{2E_b}{N_0}}\right). \quad (43)$$

It should be noted that this performance approximation matches the performance approximation for the arctangent based receiver [11], [14]. Therefore, for low modulation indices, the AWGN performance of the arctangent and Basic linear receivers are a close match, as was the case in Figure 23.

4.3.3.2. Enhanced Linear Receiver (ELR)

The computation of the performance approximation for the Enhanced linear receiver is more involved due to the large number of signal and noise terms. Therefore, for the Enhanced linear receiver, we consider the case of low modulation indices ($2\pi h \leq 0.5$) when higher order terms are much smaller than the dominant signaling and noise terms and can thus be ignored. The received signal at the input of the OFDM demodulator in the Enhanced linear receiver is

$$\begin{aligned} R_r(t) = Q_r(t)\big(2 - I_r(t)\big) &= \Big(sin\big(x(t)\big) + n_s(t)\Big)\big(2 - \cos\big(x(t)\big) - n_c(t)\big) \\ &= R(t) + n_1(t) - n_2(t) - n_3(t) \end{aligned} \quad (44)$$

where $R(t)$ was previously defined in (9) and

$$n_1(t) = n_s(t)\big(2 - \cos\big(x(t)\big)\big)$$

$$n_2(t) = n_c(t) sin\big(x(t)\big)$$

$$n_3(t) = n_c(t) n_s(t).$$

The output of the OFDM matched filter for the k-th cosine subcarrier is then given as

$$\begin{aligned} Y_k &= \sum_{n=0}^{N_S-1} R_r(nT_o)\cos\left(\frac{2\pi kn}{N_S}\right) \\ &\cong S_{k1} + 2S_{k2} + 2I_{k2} + N_{k1} + N_{k2} + N_{k3}, \end{aligned} \quad (45)$$

where S_{k1} and S_{k2} are from the first two terms of $R(t)$ and were computed in (39) and (40) respectively. N_{k1}, N_{k2}, and N_{k3} are the noise terms due to $n_1(t)$, $n_2(t)$, and $n_3(t)$ respectively. I_{k2} is the distortion component due to the cubic term modeled as Gaussian distributed. Let us consider N_{k1} which is given as

$$N_{k1} = \sum_{n=0}^{N_s-1} n_s(nT_o)\left(2 - \cos\left(x(nT_o)\right)\right)\cos\left(\frac{2\pi kn}{N_S}\right)$$

$$= \sum_{n=0}^{N_s-1} n_s(nT_o)\left(1 + \frac{x^2(nT_o)}{2!} - \frac{x^4(nT_o)}{4!} + \cdots\right)\cos\left(\frac{2\pi kn}{N_S}\right) \quad (46)$$

Since the noise samples are uncorrelated, $E\{n_s(iT_o)n_s(jT_o)\} = N_0\delta[i-j]$, the variance of N_{k1} can be computed as

$$E\{N_{k1}^2\} = E\left\{\sum_{i=0}^{N_s-1}\sum_{j=0}^{N_s-1} \boldsymbol{n_s}(iT_o)\,\boldsymbol{n_s}(jT_o)\left(\mathbf{1} + \frac{\boldsymbol{x^2}(iT_o)}{\mathbf{2!}} - \frac{\boldsymbol{x^4}(iT_o)}{\mathbf{4!}} + \cdots\right)\left(\mathbf{1} + \frac{\boldsymbol{x^2}(jT_o)}{\mathbf{2!}} - \frac{\boldsymbol{x^4}(jT_o)}{\mathbf{4!}} + \cdots\right)\cos\left(\frac{2\pi ki}{N_S}\right)\cos\left(\frac{2\pi kj}{N_S}\right)\right\}$$

$$= N_0\sum_{i=0}^{N_s-1} E\left\{\left(\mathbf{1} + \frac{\boldsymbol{x^2}(iT_o)}{\mathbf{2!}} - \frac{\boldsymbol{x^4}(iT_o)}{\mathbf{4!}} + \cdots\right)^2\right\}\cos^2\left(\frac{2\pi ki}{N_S}\right)$$

$$= N_0\sum_{i=0}^{N_s-1} E\left\{1 + x^2(iT_o) + \frac{x^4(iT_o)}{6} - \frac{7x^6(iT_o)}{180} + \cdots\right\}\cos^2\left(\frac{2\pi ki}{N_S}\right) \quad (47)$$

The CE-OFDM phase, $x(t)= 2\pi hm(t)$, with the embedded OFDM signal can be modeled as Gaussian distributed based on the central limit theorem [52] with variance $(2\pi h)^2$ [12, p. 48]. The higher order moments for the case of a zero mean Gaussian random variable X are given as [53]

$$E\{X^v\} = \begin{cases}\sigma^v(v-1)!!, & v \text{ is even} \\ 0, & v \text{ is odd}\end{cases}, \quad (48)$$

where the double factorial is defined as $z!!\equiv z*(z-2)*\ldots*3*1$ for odd z. The variance of N_{k1} is then given as [43, p. 158]

$$\sigma_{n1}^2 = E\{N_{k1}^2\} \cong N_0E_bN\left(1 + (2\pi h)^2 + \frac{1}{2}(2\pi h)^4 - \frac{7}{12}(2\pi h)^6\right). \quad (49)$$

The higher order terms are ignored. Similarly, N_{k2} is given as

$$N_{k2} = \sum_{n=0}^{N_S-1} \boldsymbol{n_c}(nT_o)\,\mathbf{sin}\big(\boldsymbol{x}(nT_o)\big)\cos\left(\frac{2\pi kn}{N_S}\right)$$

$$= \sum_{n=0}^{N_s-1} \boldsymbol{n_s}(nT_o)\left(\boldsymbol{x(t)} - \frac{\boldsymbol{x^3(t)}}{\mathbf{3!}} + \frac{\boldsymbol{x^5(t)}}{\mathbf{5!}} + \cdots\right)\cos\left(\frac{2\pi kn}{N_S}\right) \quad (50)$$

with variance $\sigma_{n2}^2 = N_0 E_b N\left((2\pi h)^2 - (2\pi h)^4 + \frac{2}{3}(2\pi h)^6\right)$. Finally, N_{k3} is the cross noise term given as

$$N_{k3} = \sum_{n=0}^{N_s-1} \boldsymbol{n_c}(nT_o)\boldsymbol{n_s}(nT_o)\cos\left(\frac{2\pi kn}{N_S}\right). \quad (51)$$

Since the in phase and quadrature noise is uncorrelated, the variance of N_{k3} can be shown to be $\sigma_{n3}^2 = {N_0}^2 E_b N$.

The overall noise at the output of the k-th cosine matched filter is then given as $N_{k,Total}=N_{k1}+N_{k2}+N_{k3}$. Since N_{k1}, N_{k2}, and N_{k3} are uncorrelated, the variance of $N_{k,Total}$ is simply the sum of the individual variances, $\sigma_{n,Total}^2 = \sigma_{n1}^2 + \sigma_{n2}^2 + \sigma_{n3}^2$. Furthermore, $N_{k,Total}$ is the sum of non-identically distributed independent random variables, and as shown in appendix C, it satisfies the Lindberg condition which is a sufficient condition for the central limit theorem to hold [51]. Therefore, the overall noise, $N_{k,Total}$, can be modeled as Gaussian distributed with variance $\sigma_{n,Total}^2$. The performance approximation for the Enhanced linear receiver for small modulation indices ($2\pi h \leq 0.5$) for the k-th subcarrier is then given as

$$P_b^k = Q\left(\sqrt{\frac{\left(S_{k_1}+2S_{k_2}\right)^2}{\sigma_{n,Total}^2+4\sigma_I^2}}\right). \quad (52)$$

The performance over all subcarriers is given as $P_b = \frac{2}{N}\sum_{k=1}^{N/2} P_b^k$ and is plotted in Figure 27. It shows good agreement with simulation performance.

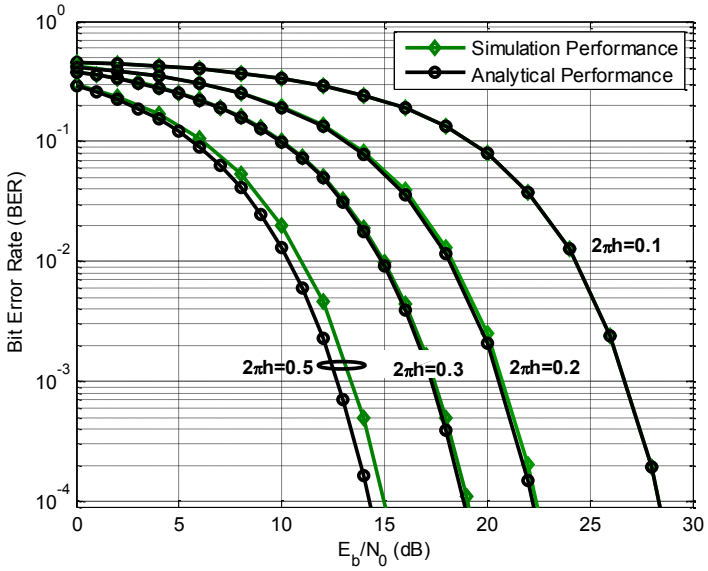

Figure 27. CE-OFDM simulation performance in comparison to the analytical approximation in AWGN for the Enhanced linear receiver for N=64 with 2X oversampling.

4.4. Acknowledgements

Chapter 4 has, in part, been submitted for publication to the *IEEE Transactions on Signal Processing* as: A. U. Ahmed and J. R. Zeidler, "Novel Linear Receivers for Constant Envelope OFDM." Chapters 4 was also, in part, originally published in: A. U. Ahmed, S. C. Thompson, and J. R. Zeidler, "Constant Envelope OFDM with Channel Coding," in *Proc. of IEEE Milcom*, Washington, DC, Oct. 2006 and A. U. Ahmed, S. C. Thompson, and J. R. Zeidler, "Threshold extending receiver structures for CE-OFDM," in *Proc. of IEEE Milcom*, Orlando, FL, Nov. 2007.

5. CE-OFDM in Multipath Fading: Equalization and Channel Estimation

In OFDM, the orthogonal subcarriers can be assumed to undergo independent flat fading in a frequency selective fading channel. This permits operation even without an equalizer especially for differential data encoding. However, in CE-OFDM, the embedded OFDM data symbols are spread out over the frequency domain [11] and therefore, an equalizer is needed for operation in frequency selective channels. A frequency domain equalizer (FDE) works well for OFDM and lends itself well to CE-OFDM due to the presence of a cyclic prefix. The performance of the equalizer is dependent on the quality of the channel estimate. In this chapter, the various channel estimation techniques for CE-OFDM using a training symbol are studied. It is desirable to have a training symbol with a constant envelope or a low PAPR to reduce distortion at the transmit amplifier. Additionally, a training signal with uniformly distributed power over the frequency domain provides the best performance. The performance of alternate training signals is studied such as a low PAPR OFDM signal, a CE-OFDM signal, a QPSK signal, and a Chu sequence. The least squares (LS) channel estimation technique provides a low complexity estimate of the channel and works well for high signal-to-noise ratios (SNRs). It is also needed for an initial estimate by other channel estimation techniques. The linear minimum mean-squared error (LMMSE) channel estimation technique takes advantage of the channel correlation knowledge to provide a more robust estimate. However, its complexity is large depending on the number of subcarriers. Low complexity channel estimation techniques such as those based on singular value decomposition (SVD) [59] have been developed and shown to perform well in certain conditions. The various channel estimation techniques for CE-OFDM are studied here.

5.1. Flat Fading

5.1.1. Rayleigh Flat Fading

When there is no direct signal propagation path (specular component), the channel response is zero mean with a Rayleigh distributed envelope and uniformly distributed phase in the interval (0,2π). The channel response for a flat fading channel with N signal scatterers is given as [43]

$$\mu(t) = \sum_{i=1}^{N} c_i(t) e^{j\phi_i(t)} e^{j2\pi f_i t} \delta(t - \tau_i(t)) \tag{53}$$

where $c_i(t)$, $\varphi_i(t)$, and f_i respectively represent the attenuation, phase shift, and the doppler frequency shift of the received signal component from the i-th scatterer. Since we are considering the case of flat fading, the signal components are assumed to arrive at the receiver at time delays τ_i with a relatively insignificant time delay spread (τ_d) i.e. $\tau_d << T_s$ (symbol period). The frequency f_i depends on the angle of arrival θ_i and is given as

$$f_i = f_{d\max} \cos\theta_i \tag{54}$$

where $f_{d\max}$ is the maximum doppler frequency shift and θ_i is uniformly distributed over the interval (0,2π). In the presence of a large number of scatterers with no direct path, $\mu(t)$ has a Rayleigh distributed envelope and a uniform phase over (0,2π). A non-zero doppler frequency shift ($f_{d\max} \neq 0$) indicates a time varying channel.

5.1.1.1. Performance Evaluation

The baseband received signal in a time invariant channel with Rayleigh flat fading is given as

$$r(t) = \alpha e^{-j\theta} s(t) + n(t) \tag{55}$$

where α is the Rayleigh distributed envelope and θ is uniformly distributed and can be estimated at the receiver. $n(t)$ is the additive white Gaussian noise. The expression for the error rate of CE-OFDM as a function of the received signal to noise ratio is then given as,

$$P(\gamma_b) = Q\left(\sqrt{b\gamma_b}\right) \tag{56}$$

where $\gamma_b = \alpha^2\bar{\gamma} = \alpha^2 {E_b}/{N_0}$ and b is based on the modulation and receiver structure. b=2 for BPSK and $b = 8\pi^2h^2$ for CE-OFDM when using the phase demodulator receiver. When α is the Rayleigh distributed, α^2 is Chi square distributed and therefore γ_b is also Chi square distributed with probability density function, $p(\gamma_b)$. The probability of error is then given as

$$P_b = \int_0^\infty P(\gamma_b)p(\gamma_b)d\gamma_b. \tag{57}$$

The general expression for the probability of error in a time invariant $(\boldsymbol{f_{d\max}} \approx 0)$ Rayleigh flat fading channel can be computed as [43]

$$P_b = \frac{1}{2}\left(1 - \sqrt{\frac{\lambda}{1+\lambda}}\right) \tag{58}$$

where

$$\lambda = \frac{b}{2}\bar{\gamma} \tag{59}$$

$\bar{\gamma}$ is the average signal energy per bit to noise power ratio $(\boldsymbol{E_b}/\boldsymbol{N_0})$. b depends on the modulation scheme and the receiver structure employed. For example, b=2 for BPSK modulation and b=1 for coherent orthogonal FSK. b can be obtained from the performance expression for each of the CE-OFDM receivers in AWGN,

$$\text{Arctangent Receiver: } P_b = \left(2\pi h\sqrt{\frac{2E_b}{N_0}}\right), \tag{60}$$

$$\text{Basic Linear Receiver: } P_b^k = Q\left(\sqrt{\frac{\left(S_{k_1} - S_{k_2}\right)^2}{\sigma_n^2 + \sigma_I^2}}\right), \tag{61}$$

$$\text{Enhanced Linear Receiver: } P_b^k = Q\left(\sqrt{\frac{\left(S_{k_1} + 2S_{k_2}\right)^2}{\sigma_{n,Total}^2 + 4\sigma_I^2}}\right), \tag{62}$$

where $S_{k_1} = dc_k 2\pi h C_N E_b N$ and $S_{k_2} = dc_k \frac{(2\pi h C_N)^3}{4}(N-1)E_b N$. When the distortion component of the cubic term is ignored in the linear receivers for the case of small modulation indices (which also removes the dependence on the subcarrier k), b for the performance approximation is obtained as,

$$\text{Arctangent Receiver: } b = 8\pi^2 h^2, \tag{63}$$

$$\text{Basic Linear Receiver: } b = 8\pi^2 h^2 \left(1 - \frac{(2\pi h C_N)^2 (N-1)}{4}\right)^2, \tag{64}$$

$$\text{Enhanced Linear Receiver: } b = \frac{8\pi^2 h^2 \left(1 + \frac{(2\pi h C_N)^2 (N-1)}{2}\right)^2}{G}, \tag{65}$$

where $G = A + B + N_0 \cong A + B$ for high SNR with $A = 1 + (2\pi h)^2 + \frac{1}{2}(2\pi h)^4 - \frac{7}{12}(2\pi h)^6$ and $B = (2\pi h)^2 - (2\pi h)^4 - \frac{2}{3}(2\pi h)^6$.

Based on the *b* terms noted above, the analytical probability of error approximation for CE-OFDM for the simple case of the arctangent receiver in a Rayleigh flat fading channel can be obtained from (58) and (63) obtained as

$$\boldsymbol{P_b} = \frac{1}{2}\left(1 - \sqrt{\frac{4\pi^2 \boldsymbol{h}^2 \frac{\boldsymbol{E_b}}{\boldsymbol{N_0}}}{1 + 4\pi^2 \boldsymbol{h}^2 \frac{\boldsymbol{E_b}}{\boldsymbol{N_0}}}}\right) \tag{66}$$

where *h* is the CE-OFDM modulation index. The expanded expressions for the Basic and Enhanced linear receiver can similarly be obtained by substituting (64) and (65) into (58) respectively.

5.1.2. Rician Flat Fading

Rician fading occurs when there is a direct path (specular component) from the transmitter to the receiver in addition to the multipath components. The direct, or line of sight (LOS), component is called the deterministic or specular signal component while the signal due to the scatterers is known as the diffuse signal component. The channel response for the case a specular (LOS) component with *N* diffuse scatterers is given as

$$\mu(\boldsymbol{t}) = \boldsymbol{k_d} \boldsymbol{e}^{\boldsymbol{j}(2\pi \boldsymbol{f_d} \boldsymbol{t} + \phi_d)} \delta(\boldsymbol{t} - \tau_d) + \sum_{\boldsymbol{i}=1}^{\boldsymbol{N}} \boldsymbol{c_i}(\boldsymbol{t}) \boldsymbol{e}^{\boldsymbol{j}\phi_i(\boldsymbol{t})} \boldsymbol{e}^{\boldsymbol{j}2\pi \boldsymbol{f_i} \boldsymbol{t}} \delta(\boldsymbol{t} - \tau_i(\boldsymbol{t})) \tag{67}$$

where k_d represents the strength of the direct component while f_d and ϕ_d represent the doppler frequency shift and phase of the direct component. For the case of a flat fading channel, the difference in time delay of the direct and indirect path is considered negligible. The channel model in the presence of a

specular component has a Rician distributed envelope and a uniformly distributed phase in the interval (0,2π). The ratio of the specular signal power (direct path) and the diffuse signal power (indirect path) is known as the Rician factor (*K*) [60]

$$\boldsymbol{K}(\boldsymbol{dB}) = 10\log_{10}\left(\frac{\boldsymbol{k}_d^2}{2\sigma^2}\right) \tag{68}$$

where $\boldsymbol{k}_d^2$ is the power in the specular signal components while $2\sigma^2$ is the power in the diffuse signal components.

5.1.2.1. Performance Evaluation

The general expression for the probability of error in a time invariant $(\boldsymbol{f}_{d\max} \approx 0)$ Rician flat fading channel is given as [62]

$$P_b = \frac{1}{\pi}\int_0^{\pi/2} \frac{(1+K)\sin^2\theta}{(1+K)\sin^2\theta + b\frac{\bar{\gamma}}{2}} \exp\left(-\frac{Kb\frac{\bar{\gamma}}{2}}{(1+K)\sin^2\theta + b\frac{\bar{\gamma}}{2}}\right) d\theta \tag{69}$$

$\bar{\gamma}$ is the average signal energy per bit to noise power ratio $(\boldsymbol{E}_b/\boldsymbol{N}_0)$ and *K* is the Rician factor. The special case of the Rician factor, *K*=0, is the Rayleigh fading case. The *b* terms for the alternate CE-OFDM receiver structures were previously determined and provided in (63)-(65) for the arctangent, Basic linear and Enhanced linear receivers respectively.

5.1.3. Performance Results

5.1.3.1. Arctangent Based Receiver

For the arctangent based receiver, the CE-OFDM analytical probability of error along with simulation results for *N*=64 for modulation indices of 2π*h* =0.3, 0.5, and 0.7 in the Rician flat fading channel for Rician factors (*K*) of 0, 3, 6, and 10 dB are shown in Figure 28-30.

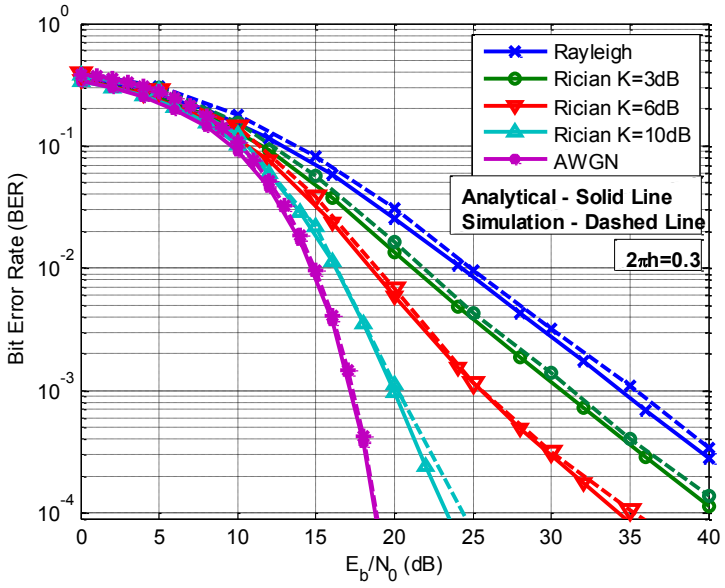

Figure 28. Performance of CE-OFDM (Arctangent Receiver) in Rician flat fading (N=64, $2\pi h$ =0.3, R_{os}=2).

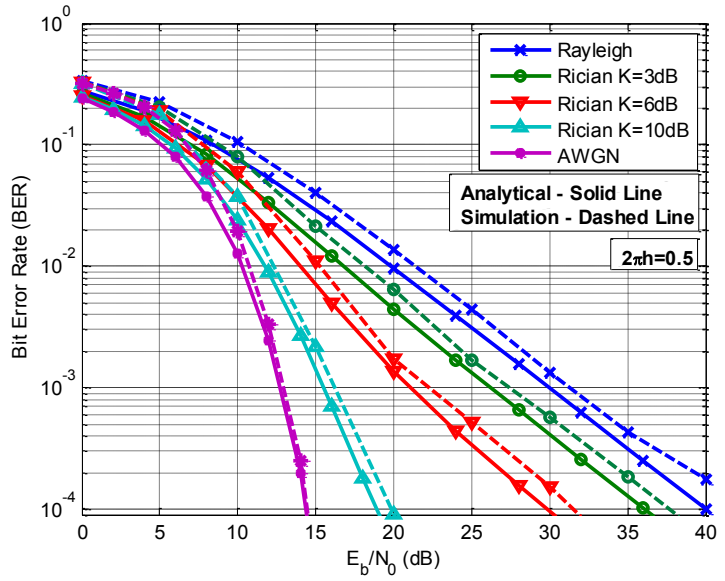

Figure 29. Performance of CE-OFDM (Arctangent Receiver) in Rician flat fading (N=64, $2\pi h$ =0.5, R_{os}=2).

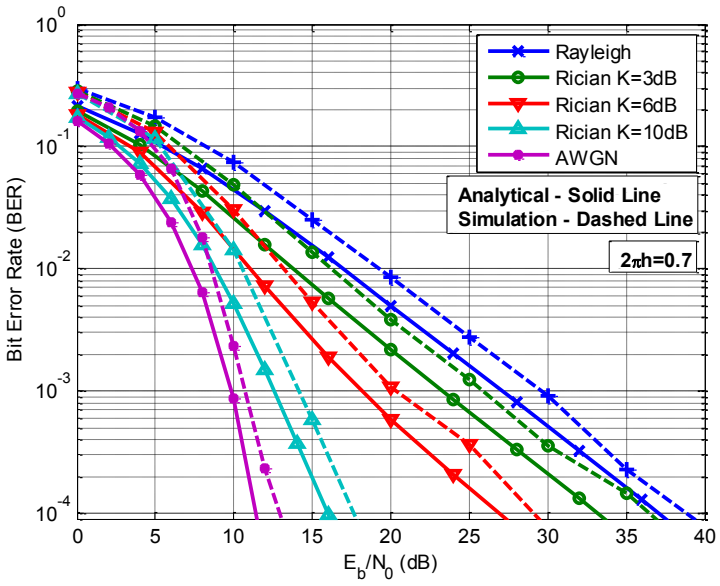

Figure 30. Performance of CE-OFDM (Arctangent Receiver) in Rician flat fading (N=64, $2\pi h$ =0.7, R_{os}=2).

The simulation performance matches well with the analytical approximation for low modulation indices ($2\pi h \leq 0.5$). At higher modulation indices, the simulation performance deviates more from the analytical approximation. This is mainly due to the phase wrapping that occurs more frequently at higher modulation indices. In this case, the performance approximation essentially represents lower bound.

5.1.3.2. Basic Linear Receiver

For the Basic linear receiver, the CE-OFDM analytical probability of error along with simulation results for N=64 for modulation indices of $2\pi h$ =0.3, 0.5, and 0.7 in the Rician flat fading channel for Rician factors (K) of 0, 3, 6, and 10 dB are shown in Figure 31-33.

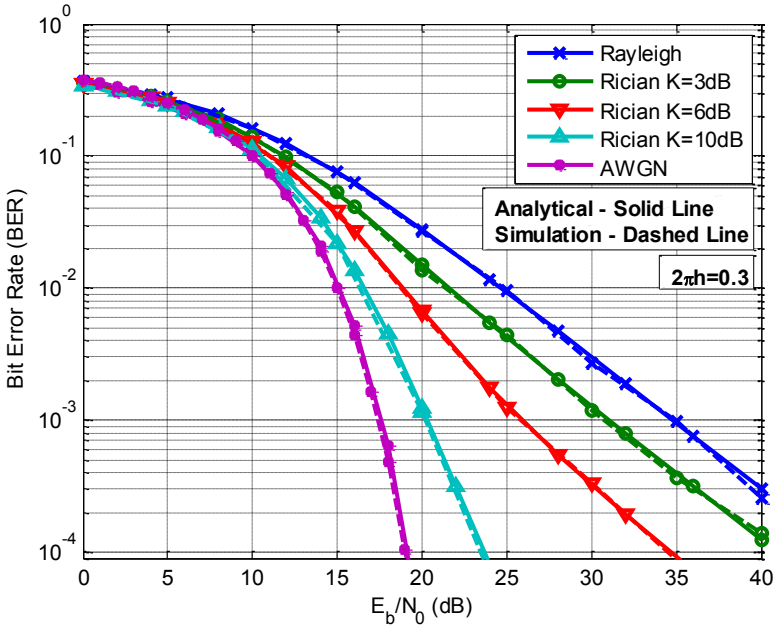

Figure 31. Performance of CE-OFDM (Basic Linear Receiver) in Rician flat fading (N=64, $2\pi h$ =0.3, R_{os}=2).

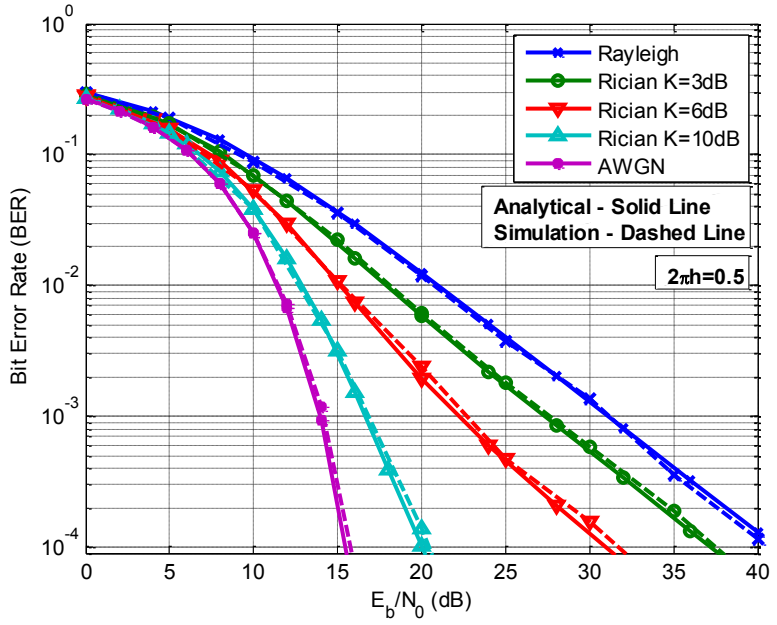

Figure 32. Performance of CE-OFDM (Basic Linear Receiver) in Rician flat fading (N=64, $2\pi h$ =0.5, R_{os}=2).

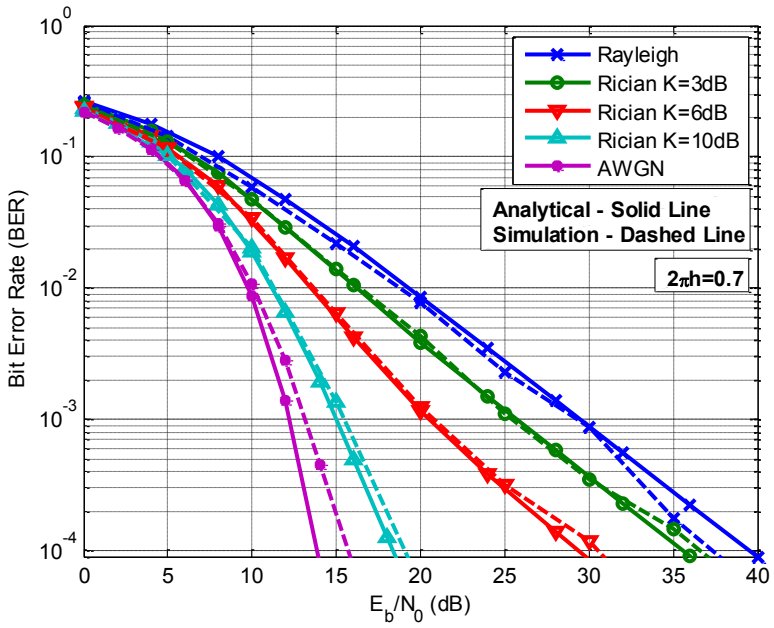

Figure 33. Performance of CE-OFDM (Basic Linear Receiver) in Rician flat fading (N=64, $2\pi h$ =0.7, R_{os}=2).

The simulation performance of the Basic linear receiver matches well with the analytical approximation for all cases. At the higher modulation index of $2\pi h$ =0.7, the simulation performance deviates slightly from the analytical approximation for AWGN. This is mainly due to the greater amount of distortion from higher order terms that are ignored at the receiver.

5.1.3.3. Enhanced Linear Receiver

For the Enhanced linear receiver, the CE-OFDM analytical probability of error along with simulation results for N=64 for modulation indices of $2\pi h$ =0.3 and 0.5 in the Rician flat fading channel for Rician factors (K) of 0, 3, 6, and 10 dB are shown in Figure 34-35. The performance approximation isn't provided for higher modulation indices since it is not as accurate due to distortion from higher order terms.

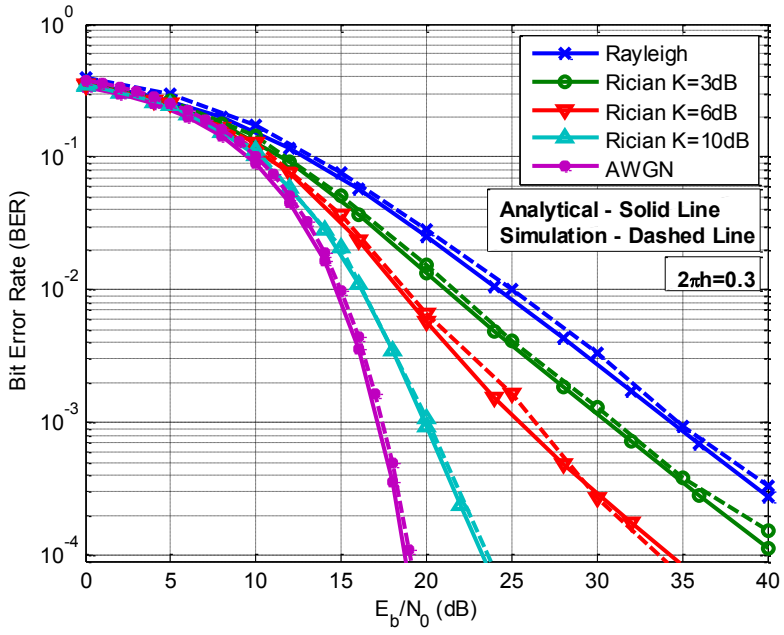

Figure 34. Performance of CE-OFDM (Enhanced Linear Receiver) in Rician flat fading (N=64, $2\pi h$ =0.3, R_{os}=2).

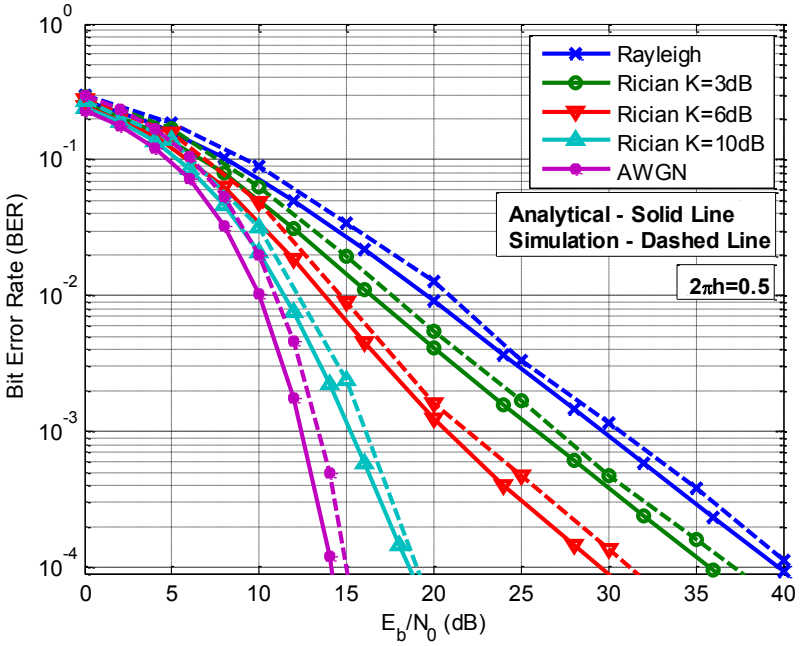

Figure 35. Performance of CE-OFDM (Enhanced Linear Receiver) in Rician flat fading (N=64, $2\pi h$ =0.5, R_{os}=2).

The simulation performance of the Enhanced linear receiver matches well with the analytical approximation. As expected, the performance matches more closely for the lower modulation index of $2\pi h$ =0.3, since the distortion from higher order terms in smaller in this case.

5.1.3.4. Receiver Performance Comparison

The simulation performance comparison of the arctangent, Basic and Enhanced linear receivers for the case of Rayleigh flat fading is shown in Figure 36. The performance approximation for the phase demodulator receiver is also plotted. The simulation performance comparison for the case of a dominant line of sight component (LOS) component resulting in Rician flat fading with Rician factor (K) of 10dB is shown in Figure 37. Perfect channel phase estimation is assumed for all cases. The linear receivers perform well comparable to the arctangent receiver with a slightly better performance for Rayleigh flat fading. For the Rician fading (K=10dB) case, the Enhanced linear receiver (ELR) provides around 0.8 dB better performance at a BER of 0.1 for $2\pi h$=0.6.

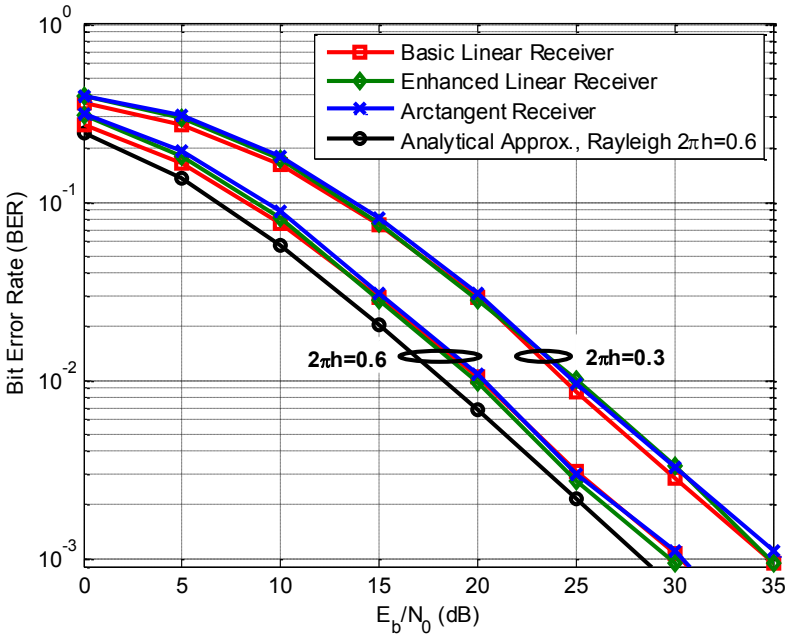

Figure 36. CE-OFDM receiver performance comparison in Rayleigh flat fading for N=64 assuming perfect channel phase estimate with R_{os}=2.

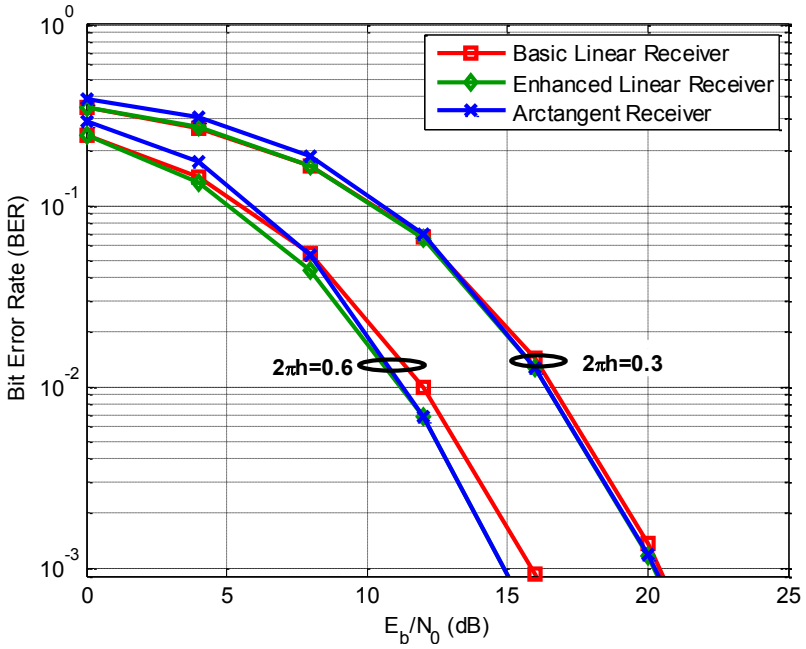

Figure 37. CE-OFDM receiver performance comparison for the case of Rician flat fading with Rician factor K=10dB for N=64 with R_{os}=2.

5.2. Frequency Selective Fading

Frequency selective fading is encountered when the coherence bandwidth of the channel is less than the bandwidth of the transmitted signal. In this situation, different frequency components of the signal encounter different attenuations. CE-OFDM is envisioned as a wideband waveform and is therefore more likely to encounter frequency selective fading. It is important to mitigate the effects of frequency selective fading to attain acceptable performance. An equalizer is customarily employed for this purpose.

5.2.1. Frequency Domain Equalizer

A frequency domain equalizer (FDE) provides an effective technique to mitigate the distortion due to a frequency selective channel. The use of a cyclic prefix in CE-OFDM (like OFDM) not only prevents interblock interference (IBI) but also transforms the linear convolutions common in time-dispersive channels into circular convolutions. This results in a circulant channel matrix composed of

the channel taps in the time domain with a diagonal channel matrix in the frequency domain allowing a single tap per subcarrier equalizer in the frequency domain. This characteristic is fundamental to the implementation of the frequency domain equalizer and allows the use of the DFT/IDFT pair. A block diagram of the frequency domain equalizer is shown below.

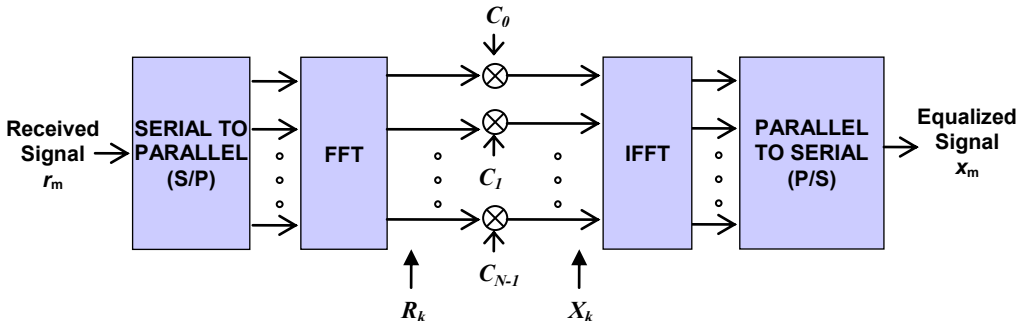

Figure 38. Frequency Domain Equalizer for CE-OFDM.

Frequency domain equalization is accomplished in three main steps on a per block basis. The received time signal is first transformed into the frequency domain by simple application of the FFT,

$$R_k = \sum_{m=0}^{N_{FFT}-1} r_m e^{-j(\frac{2\pi k}{N_{FFT}})m}, \quad k = 0,1,...N_{FFT}-1, \tag{70}$$

where $r_m=r[m]=r(mT_o)$ is the m-th time sample of the received time signal sampled at rate $f_s=1/T_o$ (T_o is the sampling period). R_k represents the frequency component of the received signal at frequency $f_k=k/T_s$ (where T_s is symbol period).

The actual frequency domain equalization is performed next. The frequency domain equalizer consists of a single tap equalizer with a complex tap at each of the discrete frequency components (f_k) obtained above through application of the DFT. Each received signal frequency component is multiplied by a complex coefficient (tap)

$$\boldsymbol{X_k = R_k C_k} \tag{71}$$

where C_k is the coefficient that attempts to invert the channel response at frequency $f_k=k/T_s$ while X_k represents the equalized received signal at that frequency. The C_k's are obtained from the channel

frequency response, $H(f)$, based on either the Zero Forcing (ZF) criterion or the Minimum Mean Square Error (MMSE) criterion [62]. The ZF criterion attempts to simply invert the channel

$$\boldsymbol{C_k} = \frac{1}{\boldsymbol{H_k}} \tag{72}$$

where $H_k=H(k/T_s)$ is the channel frequency response at frequency $f_k=k/T_s$. The ZF criterion results in noise enhancement unless the signal-to-noise ratio (SNR) is high. The MMSE criterion is preferred because it is more robust in the presence of noise

$$\boldsymbol{C_k} = \frac{\boldsymbol{H_k^*}}{\left|\boldsymbol{H_k}\right|^2 + \gamma^{-1}} \tag{73}$$

where $\gamma=E_b/N_0$ is the signal-to-noise ratio (SNR). It should be noted that the equalizer coefficient C_k at the discrete frequency $f_k=k/T_s$ only depends on the channel frequency response (H_k) at that frequency alone. This characteristic is in sharp contrast to the time domain equalizer where each tap coefficient is a function of the entire channel impulse response at all delays. Once the received signal has been equalized in the frequency domain, the final step entails transforming it back to the time domain. This is accomplished through application of the IDFT

$$x_m = \sum_{k=0}^{N_{FFT}-1} X_k e^{j(\frac{2\pi k}{N_{FFT}})m}, \quad m = 0,1,...N_{FFT}-1 \tag{74}$$

where $x_m=x[m]=x(mT_o)$ is the m-th time sample of the equalized received time signal.

5.2.2. Multipath Fading Channel Models

Four channel models representing frequency selective fading channels were considered in order to study the performance of the alternate receiver structures in frequency selective fading while employing a frequency domain equalizer [11]. The channel models were defined based on the statistics of the channel impulse response, $h[l]$ of length L, which was normalized as $\sum_{l=0}^{L-1} E\{|h[l]|^2\} = 1$. Channels A and B are two path models with the second path delayed by 5μs. Channel A has a weak second path (10dB below the first path in power) while the two paths are equal power for channel B. Channel C has an exponential power delay profile (PDP) with a delay spread of 9μs and $E\{|h[l]|^2\} \propto$

$e^{-\tau_l/2\mu s}$. Channel D has an uniform power delay profile (PDP) with a delay spread of 9μs and all paths having equal power.

5.2.3. Performance Results

The simulation performance evaluation of the arctangent, Basic and Enhanced linear receivers for channels A, B, C and D is presented in Figures 39-42. These cases were evaluated with a CE-OFDM symbol period of T_s=128μs, a cyclic prefix of 10μs and FDE based equalization with perfect channel state information (CSI).

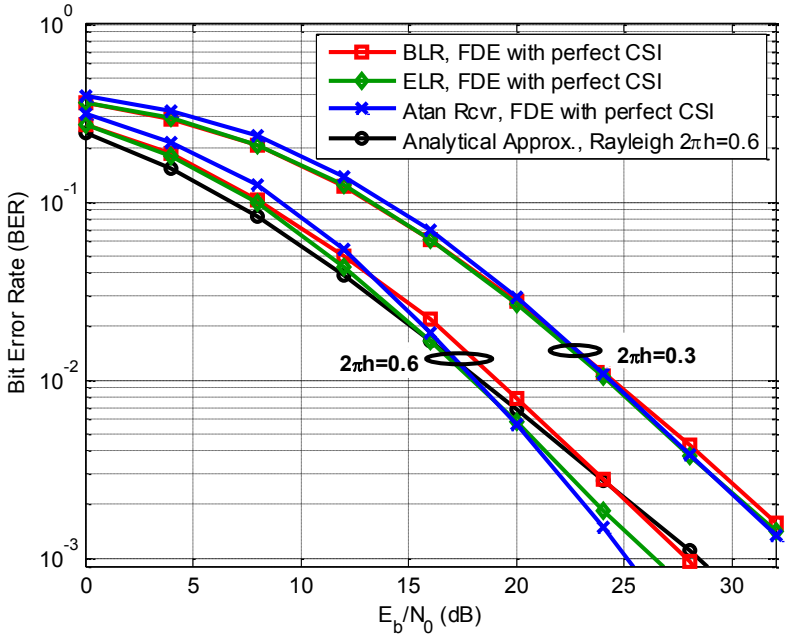

Figure 39. CE-OFDM receiver performance comparison in frequency selective fading (Channel A, two paths) using a FDE for N=64 with R_{os}=2.

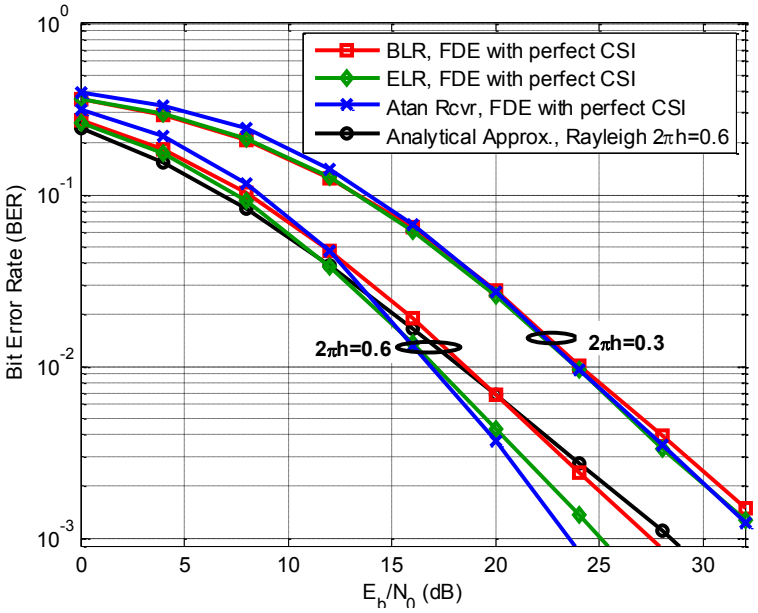

Figure 40. CE-OFDM receiver performance comparison in frequency selective fading (Channel B, two paths) using a FDE for N=64 with R_{os}=2.

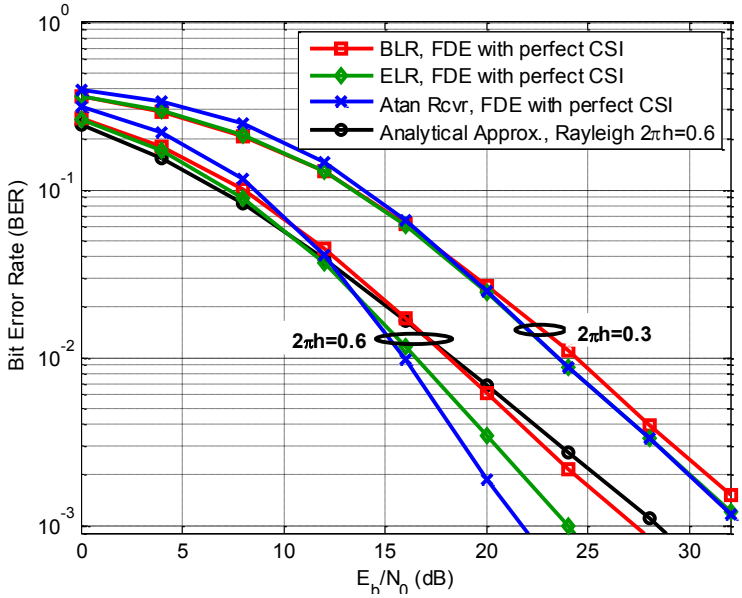

Figure 41. CE-OFDM receiver performance comparison in frequency selective fading (Channel C, exponential power delay profile) using a FDE for N=64 with R_{os}=2.

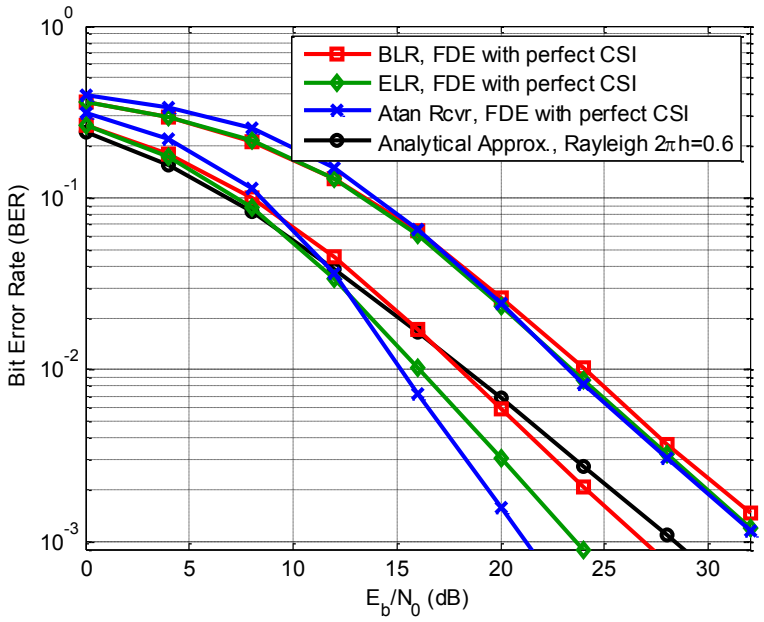

Figure 42. CE-OFDM receiver performance comparison in frequency selective fading (Channel D, uniform power delay profile) using a FDE for N=64 with R_{os}=2.

Both the linear receivers, BLR and ELR, perform well compared to the arctangent receiver for all cases. While the arctangent receiver provides better performance at low BERs for $2\pi h$=0.6, the ELR outperforms it at high BERs. For example, the ELR provides over 1.2 dB better performance at a BER of 0.1 in channels C and D. This has a significant impact on the error correction coding performance as shown in the next section.

5.3. Channel Estimation

The tap coefficients (C_k) in the frequency domain equalizer are obtained from the channel frequency response (H) by employing the Zero Forcing (ZF) or the Minimum Mean Square Error (MMSE) criterion. The channel frequency response (H) is typically not known at the receiver in advance and changes over time for a time-varying channel. Therefore, it is necessary to perform channel estimation at the receiver prior to equalization.

The performance of the equalizer depends on the quality of the channel estimate. The channel frequency response (H) is typically not known at the receiver in advance and changes over time for a

time-varying channel. Therefore, it is necessary to perform channel estimation at the receiver prior to equalization. It is preferable to perform channel estimation in the frequency domain to directly obtain the channel frequency response. This can be accomplished by transmitting a known training signal. It is desirable to choose a training signal with a uniform power level across the full channel frequency band. Since standard OFDM satisfies this requirement, consider an OFDM training signal for channel estimation here before comparing various training signals.

The received OFDM symbols at the receiver, after passing through the channel, are given in matrix notation as

$$\boldsymbol{R} = \boldsymbol{DH} + \boldsymbol{n} = \begin{bmatrix} \boldsymbol{d}_0 & 0 & 0 & 0 \\ 0 & \boldsymbol{d}_1 & 0 & 0 \\ 0 & 0 & . & 0 \\ 0 & 0 & 0 & \boldsymbol{d}_{N-1} \end{bmatrix} \begin{bmatrix} \boldsymbol{H}_0 \\ \boldsymbol{H}_1 \\ . \\ \boldsymbol{H}_{N-1} \end{bmatrix} + \begin{bmatrix} \boldsymbol{n}_0 \\ \boldsymbol{n}_1 \\ . \\ \boldsymbol{n}_{N-1} \end{bmatrix} \tag{75}$$

where $R=[R_1, R_2, \ldots, R_{N-1}]^T$ is the vector of received OFDM symbols (in the frequency domain), D is the diagonal matrix containing the OFDM transmit modulation symbols i.e. the known training symbols, and H represents the channel transfer function with entries $H_k=H(k/T_s)$, $k=0,1,\ldots,N-1$, corresponding to the channel transfer function at discrete frequencies $f_k=k/T_s$. The vector $\boldsymbol{n}$ comprises of independent, zero-mean, complex Gaussian noise with variance σ_n^2.

5.3.1. Least Squares (LS) Estimate

The Least Squares (LS) estimate is the simple low complexity estimate of the channel. Since the training symbols are known at the receiver, the LS estimate is obtained by simply dividing the received symbols by the known transmit symbols.

$$\hat{\boldsymbol{H}}_{LS} = \boldsymbol{D}^{-1}\boldsymbol{R} = \boldsymbol{H} + \boldsymbol{D}^{-1}\boldsymbol{n}. \tag{76}$$

It is obvious that the LS estimate improves with an increase in the signal-to-noise ratio (SNR) and provides a perfect estimate of the channel in the absence of noise. The LS estimate is commonly used as an initial estimate by other channel estimation schemes.

5.3.2. Training Signals

The structure of the training signal influences the quality of the channel estimate. A training signal, such as OFDM, with a flat power spectrum over the frequency domain is desirable to obtain the best estimate. However, the rationale for employing CE-OFDM is to avoid the inefficient power backoff at the amplifier and thus operate in the nonlinear saturation region where the amplifier is most efficient. This raises the challenge of employing a training signal for channel estimation which provides good performance in the presence of amplifier nonlinearities. CE-OFDM is not necessarily the ideal choice for channel estimation since it does not offer a uniform power distribution over the signal band. Also, while regular OFDM offer a uniform power distribution over the signal band, the large PAPR of OFDM results in distortion at the transmit power amplifier and therefore a degradation of the channel estimate. Therefore, it is desirable to ideally have a training signal with both a flat power spectrum over the frequency band as well as a constant envelope in the time domain. Four training signals are considered in this section for channel estimation.

5.3.2.1. Low PAPR OFDM

Standard OFDM signals have a large PAPR which results in distortions at the power amplifier. However, since training signals are known before transmission, a predetermined low PAPR OFDM signal can be employed for the purposes of channel estimation. A genetic algorithm discussed in [63] was used to find a low PAPR OFDM signal (N_{FFT}=256) with a PAPR of 3.18 dB to evaluate as a training signal.

5.3.2.2. CE-OFDM

A CE-OFDM training signal is also considered for channel estimation. Although, CE-OFDM doesn't have a flat power distribution in the frequency domain [11], it has a constant envelope in the time domain. A CE-OFDM signal with a relatively high modulation index ($2\pi h$=0.8) is considered due to its higher sidebands [11].

5.3.2.3. QPSK

A QPSK signal is another choice for the training signal. It has a constant envelope in time but a non-uniform power distribution in the frequency domain. The inverse of the low PAPR OFDM signal is used for the QPSK signal with constant envelope in the time domain and a PAPR of 3.18 dB in the frequency domain.

5.3.2.4. Chu Sequence

The Chu sequences (analogous to the chirp) are ideal for training as they have both a constant envelope in time and a uniform distribution of power over the frequency domain [64], [65]. The Chu sequence of length N_{FFT} is defined as

$$s[n] = \begin{cases} e^{j\pi rn^2 / N_{\mathrm{FFT}}}, & for\ even\ n \\ e^{j\pi rn(n+1) / N_{\mathrm{FFT}}}, & for\ odd\ n \end{cases}, \tag{77}$$

where n=0,1,…, N_{FFT} -1, and r is relatively prime to N_{FFT}. A Chu sequence with r = 1 is used here.

5.3.2.5. Performance Results

The mean squared error (MSE) is considered the main performance measure for frequency domain channel estimation [66] and it is defined as

$$MSE = E\left\{\left|H(k) - \hat{H}(k)\right|^2\right\} \tag{78}$$

where $\hat{H}(k)$ is the estimate of the channel at the k-th frequency bin. A MSE based comparison of the different training signals is provided in Figure 43. These simulation results were obtained for LS channel estimation.

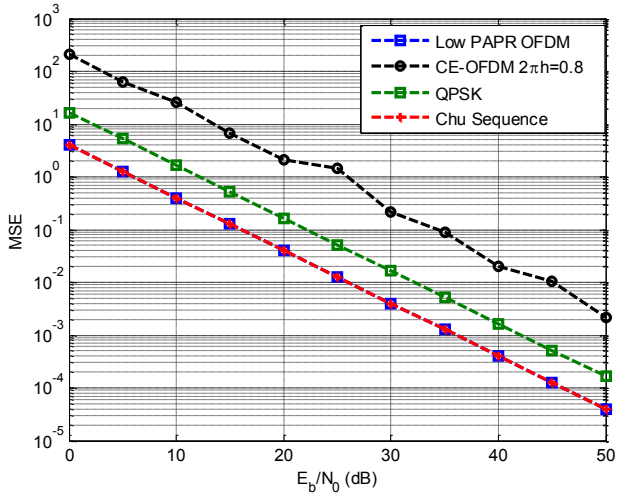

Figure 43. Comparison of the channel estimation MSE of various training signals with LS channel estimation for N=64 and R_{os}=4.

The low PAPR OFDM training signal and the Chu sequence training signal provide the best MSE performance due to their flat power distribution over the frequency bins. The QPSK signal has a PAPR of 3.18 dB in the frequency domain which results in a small performance degradation while CE-OFDM also suffers due to non-uniform power distribution over the frequency domain.

5.3.3. Effects of Amplifier Non-Linearities on Channel Estimation

The CE-OFDM, QPSK, and Chu sequence based training signals have a constant envelope in the time domain and are therefore not affected by the non-linearities at the transmit power amplifier. However, the low PAPR OFDM signal (PAPR=3.18 dB) suffers from distortions due to the amplifier and it is therefore important to take the affects of the power amplifier into account. Since CE-OFDM is based on OFDM, both OFDM and CE-OFDM are attractive choices for implementation in a CE-OFDM system for the purpose of channel estimation. However, the results presented here show that neither of them provide the most effective channel estimation performance. In this section, the affect of the amplifier nonlinearities on a non-constant envelope signal such as OFDM is evaluated and its performance is compared to CE-OFDM.

Various models for the affect of the amplifier non-linearities have been developed over the years that model the power amplifier as a memoryless non-linearity with a non-frequency selective response [12]. With the input to the power amplifier given as

$$s_{in}(t) = A(t)e^{j\phi(t)} \tag{79}$$

the output is

$$s_{out}(t) = G\left[A(t)\right]e^{j\{\phi(t)+\Phi[A(t)]\}} \tag{80}$$

where G(.) and Φ(.) are the AM/AM and AM/PM conversions respectively. The widely used Rapp model for the solid state power amplifier (SSPA) [67] is expressed as

$$G(A) = \frac{g_0 A}{\left[1+\left(A/A_{sat}\right)^{2p}\right]^{1/2p}}, and\ \Phi(A) = 0 \tag{81}$$

where g_0 is the amplifier gain and A_{sat} is the amplifier input saturation level. The factor p controls the sharpness of the AM/AM curve and is chosen as p=2 here. The more non-linear traveling wave tube amplifier (TWTA) is expressed by the Saleh model [68] as

$$G(A) = \frac{g_0 A}{1+\beta_a A^2}, and\ \Phi(A) = \frac{\alpha_\phi A^2}{1+\beta_\phi A^2} \tag{82}$$

where α_Φ and β_Φ control the AM/PM conversion. A common choice for these parameters is α_a=0.25 , α_Φ=π/12 and β_Φ=0.25 [67].

5.3.3.1. Performance Results

The Figure below shows the MSE performance of the low PAPR OFDM training signal when the power amplifier models for SSPA and TWTA are taken in account.

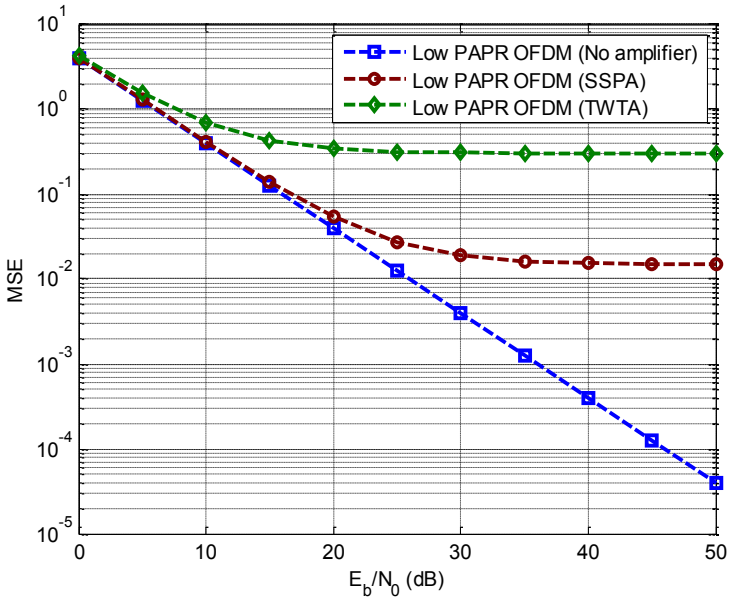

Figure 44. MSE performance of low PAPR OFDM training signal with LS channel estimation with SSPA and TWTA amplifier models for N=64 and R_{os}=4.

The channel estimation performance of low PAPR OFDM suffers considerably in the presence of a power amplifier. As expected, the performance is worse for the more non-linear TWTA case compared to the SSPA case. A comparison of the low PAPR OFDM training signal with a CE-OFDM training signal is provided in Figure 45 for an SSPA amplifier model with various power backoffs employed for the low PAPR OFDM training signal. CE-OFDM is not affected by amplifier nonlinearities due to its constant envelope.

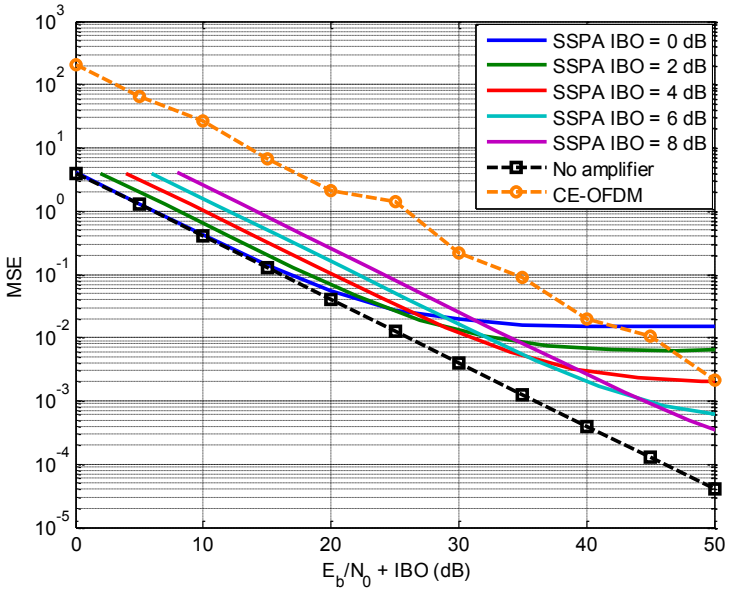

Figure 45. MSE performance of the low PAPR OFDM training signal while employing the SSPA amplifier model for various power backoffs for N=64 and R_{os}=4. Also plotted is the MSE performance of the CE-OFDM training signal.

The x-axis is defined as the E_b/N_0 plus the power backoff (E_b/N_0 + IBO) at the amplifier to provide a fair comparison by taking into account the transmit power lost due to the amplifier backoff for the case of the low PAPR OFDM training signal while this power is available for CE-OFDM. The results in Figure 45 indicate that for the SSPA, the low PAPR OFDM training signal provides better channel estimation performance than CE-OFDM for E_b/N_0 + IBO below 40 dB, with smaller backoffs providing better performance at lower SNRs. Above 40 dB, the low PAPR OFDM signal with a backoff larger than 4 dB provides better performance than CE-OFDM. Since the SSPA is less nonlinear when compared to the TWTA, the low PAPR OFDM signal performance degrades further when a more non-linear amplifier such as the TWTA is considered.

While low PAPR OFDM is impacted due to the SSPA amplifier non-linearities, it still provides better channel estimation performance than CE-OFDM when an appropriate power backoff is used. However, as previously shown, the Chu sequence training signal provides the best performance

for channel estimation in the presence of system non-linearities due to its constant envelope in the time domain in addition to the uniform power distribution in the frequency domain.

5.3.4. Linear Minimum Mean Square Error (LMMSE) Estimate

The Linear Minimum Mean Square Error (LMMSE) estimate of the channel is obtained by minimizing the mean square error (MSE) between the actual and estimated channel. This is accomplished by performing an optimizing linear transformation on the LS estimate of the channel using the frequency correlation of the channel. The optimum estimate of the channel frequency response is given by the Wiener-Hopf equation [59]

$$\hat{\boldsymbol{H}}_{LMMSE} = \boldsymbol{R}_{H\hat{H}_{LS}} \boldsymbol{R}^{-1}_{\hat{H}_{LS}\hat{H}_{LS}} \hat{\boldsymbol{H}}_{LS} \tag{83}$$

where $\boldsymbol{R}_{H\hat{H}_{LS}}$ is the N x N matrix representing the cross-correlation between the channel frequency response (H) and its LS estimate ($\hat{\boldsymbol{H}}_{LS}$) and $\boldsymbol{R}_{\hat{H}_{LS}\hat{H}_{LS}}$ is the N x N matrix representing the autocorrelation of the of the LS estimate ($\hat{\boldsymbol{H}}_{LS}$). Since the noise n is zero mean and independent of the channel response, the cross-correlation $\boldsymbol{R}_{H\hat{H}_{LS}}$ is reduced as

$$\boldsymbol{R}_{H\hat{H}_{LS}} = \boldsymbol{E}\left\{\boldsymbol{H}\hat{\boldsymbol{H}}^{\boldsymbol{H}}_{\boldsymbol{LS}}\right\} = \boldsymbol{E}\left\{\boldsymbol{H}(\boldsymbol{H}+\boldsymbol{D}^{-1}\boldsymbol{n})^{\boldsymbol{H}}\right\} = \boldsymbol{R}_{HH}\,. \tag{84}$$

The superscript $(.)^{H}$ denotes the Hermitian transpose. The autocorrelation $\boldsymbol{R}_{\hat{H}_{LS}\hat{H}_{LS}}$ of the channel LS estimate ($\hat{\boldsymbol{H}}_{LS}$) is also simplified below due to the independence of the noise and channel response

$$\begin{aligned}
\boldsymbol{R}_{\hat{H}_{LS}\hat{H}_{LS}} &= \boldsymbol{E}\left\{\hat{\boldsymbol{H}}_{LS}\hat{\boldsymbol{H}}^{\boldsymbol{H}}_{\boldsymbol{LS}}\right\} \\
&= \boldsymbol{E}\left\{(\boldsymbol{H}+\boldsymbol{D}^{-1}\boldsymbol{n})(\boldsymbol{H}+\boldsymbol{D}^{-1}\boldsymbol{n})^{\boldsymbol{H}}\right\} \\
&= \boldsymbol{E}\left\{\boldsymbol{H}\boldsymbol{H}^{\boldsymbol{H}}\right\} + \boldsymbol{D}^{-1}\boldsymbol{E}\left\{\boldsymbol{n}\boldsymbol{n}^{\boldsymbol{H}}\right\}(\boldsymbol{D}^{\boldsymbol{H}})^{-1} \\
&= \boldsymbol{R}_{HH} + \sigma_n^2(\boldsymbol{D}\boldsymbol{D}^{\boldsymbol{H}})^{-1}
\end{aligned} \tag{85}$$

Therefore, the Linear Minimum Mean Square Error (LMMSE) estimate of the channel can be expressed as

$$\hat{\boldsymbol{H}}_{LMMSE} = \boldsymbol{R}_{HH}[\boldsymbol{R}_{HH} + \sigma_n^2(\boldsymbol{D}\boldsymbol{D}^{\boldsymbol{H}})^{-1}]^{-1}\hat{\boldsymbol{H}}_{LS}\,. \tag{86}$$

We may further simplify by employing a training constellation with equal energy symbols (e.g. BPSK) such that

$$(\boldsymbol{DD}^{\boldsymbol{H}})^{-1} = \frac{1}{|\boldsymbol{d}|^2}\boldsymbol{I} \tag{87}$$

where I is the N x N identity matrix and $|d|^2$ is the energy of each training (modulation) symbol (d_k). By defining the signal-to-noise ratio (SNR) as $\gamma = \frac{\boldsymbol{E_b}}{\boldsymbol{N}_0} = \frac{|\boldsymbol{d}|^2}{2\sigma_{\boldsymbol{n}}^2}$, we can rewrite the LMMSE estimate of the channel response as

$$\hat{\boldsymbol{H}}_{\boldsymbol{LMMSE}} = \boldsymbol{R}_{\boldsymbol{HH}}[\boldsymbol{R}_{\boldsymbol{HH}} + \frac{\boldsymbol{I}}{2\gamma}]^{-1}\hat{\boldsymbol{H}}_{\boldsymbol{LS}}. \tag{88}$$

This equation represents the optimum transformation from the least squares channel estimate ($\hat{\boldsymbol{H}}_{\boldsymbol{LS}}$) to the linear minimum mean square error channel estimate ($\hat{\boldsymbol{H}}_{\boldsymbol{LMMSE}}$). This transformation is based on the signal-to-noise ratio (γ) and the frequency correlation of the channel ($\boldsymbol{R}_{\boldsymbol{HH}}$).

At first, the dependence of the LMMSE channel estimate on the channel correlation ($\boldsymbol{R}_{\boldsymbol{HH}}$) seems to be a contradiction. This is because in order to compute the LMMSE estimate of an unknown channel, you need to know the correlation matrix of that unknown channel. However, this problem may be solved by using a statistical model of the channel to obtain an estimate of the channel correlation ($\boldsymbol{R}_{\boldsymbol{HH}}$). For example, if the channel can be modeled as having an exponential or uniform power delay profile (PDP), then the channel correlation matrix ($\boldsymbol{R}_{\boldsymbol{HH}}$) computed for these PDPs can be used as an estimate of the true correlation matrix. Later on, a better estimate of channel correlation can be developed over time by averaging the channel correlation obtained from the channel estimates. It has been shown that a design for the worst correlation is robust to mismatch. Therefore, if the statistics of the channel are unknown, it is best to design for a uniform PDP [59]. The entries $\boldsymbol{R}_{\boldsymbol{HH}}(\boldsymbol{m},\boldsymbol{n})$ for the m-th row and n-th column of the channel correlation matrix for the case of a uniform PDP and guard band of length L is given by the expression [59]

$$\boldsymbol{R}_{HH}(\boldsymbol{m},\boldsymbol{n}) = \begin{cases} 1, & \boldsymbol{if}\ \boldsymbol{m} = \boldsymbol{n} \\ \dfrac{1-\boldsymbol{e}^{-j2\pi\boldsymbol{L}\frac{\boldsymbol{m}-\boldsymbol{n}}{\boldsymbol{N}}}}{j2\pi\boldsymbol{L}\dfrac{\boldsymbol{m}-\boldsymbol{n}}{\boldsymbol{N}}}, & \boldsymbol{if}\ \boldsymbol{m} \neq \boldsymbol{n} \end{cases}. \tag{89}$$

The other parameter needed for the LMMSE channel estimate is the signal to noise ratio (γ). The SNR needs to be estimated at the receiver frequently enough to track the time variations of the channel. Alternatively, a predetermined value of the SNR can be employed. It has been shown that robustness to mismatch is achieved by setting the predetermined SNR value to the highest SNR that would be encountered during transmission [59]. This is due to the fact that the channel estimation error is masked by the high noise level when the SNR is low. However, the channel estimation error due to mismatch at a high SNR would be apparent due to the low noise level and would result in an error floor.

The computation of the LMMSE channel estimate requires the calculation of the inverse of an N x N matrix ($[\boldsymbol{R}_{HH} + \frac{\boldsymbol{I}}{\boldsymbol{SNR}}]^{-1}$). The complexity of this calculation increases with the number of subcarriers N. When the correlation matrix ($\boldsymbol{R}_{HH}$) and the SNR (γ) are known beforehand and are set to fixed nominal values, the transformation factor can be computed beforehand ($\boldsymbol{R}_{HH}[\boldsymbol{R}_{HH} + \frac{\boldsymbol{I}}{\boldsymbol{SNR}}]^{-1}$). However, the transformation from the LS to the LMMSE estimate still requires N multiplications for each subcarrier. In other words, N^2 multiplications are required for each LMMSE channel estimate. A technique for reducing the complexity of the LMMSE channel estimation has been proposed [59]. In this technique, optimal rank reduction is performed on the channel correlation matrix through application of singular value decomposition (SVD).

5.3.4.1. Singular Value Decomposition

The computation of the LMMSE channel estimate requires the calculation of the inverse of an N x N matrix ($[\boldsymbol{R}_{HH} + \frac{\boldsymbol{I}}{\boldsymbol{SNR}}]^{-1}$). The complexity of this calculation increases with the number of subcarriers N. When the correlation matrix ($\boldsymbol{R}_{HH}$) and the SNR (γ) are known beforehand and are set to

fixed nominal values, the transformation factor can be computed beforehand ($\boldsymbol{R}_{\boldsymbol{HH}}[\boldsymbol{R}_{\boldsymbol{HH}}+\frac{\boldsymbol{I}}{\boldsymbol{SNR}}]^{-1}$). However, the transformation from the LS to the LMMSE estimate still requires N multiplications for each subcarrier. In other words, N^2 multiplications are required for each LMMSE channel estimate. A technique for reducing the complexity of the LMMSE channel estimation has been proposed in [59]. In this technique, optimal rank reduction is performed through application of singular value decomposition (SVD) on the channel correlation matrix, $R_{HH}=U\Lambda U^H$, where U is the unitary matrix containing singular vectors and Λ is a diagonal matrix containing the singular values (λ_i's) on its diagonal ($\lambda_1 \geq \lambda_2 \geq \ldots \geq \lambda_N$). The optimal rank-$p$ estimator is given as [59]

$$\hat{H}_p = U\Delta_p U^H \hat{H}_{LS} \tag{90}$$

where Δ_p is the diagonal matrix with entries

$$\delta_m = \begin{cases} \dfrac{\lambda_m}{\lambda_m + \dfrac{1}{2\gamma}}, & m = 1,2,\ldots,p \\ 0, & m = 1,2,\ldots,p \end{cases}. \tag{91}$$

The performance of the low rank estimator improves with increasing p as the magnitude of singular values decreases. While an error floor is present for an estimator with a small rank p, this error floor decreases rapidly for rank $p>L+1$ where L is the length of the cyclic prefix [59].

5.3.4.2. Performance Results

The LMMSE channel estimation provides a better quality channel estimate by using the knowledge of the frequency correlation of the channel. Figure 46 provides a performance comparison of the LS and LMMSE channel estimation techniques when a Chu sequence is employed for training. The lower complexity SVD based estimate is also considered. Both the cases with the actual channel correlation ($\boldsymbol{R}_{\boldsymbol{HH}}$) as well as the case where the channel correlation is unknown and therefore the channel is modeled as having a uniform power delay profile are considered.

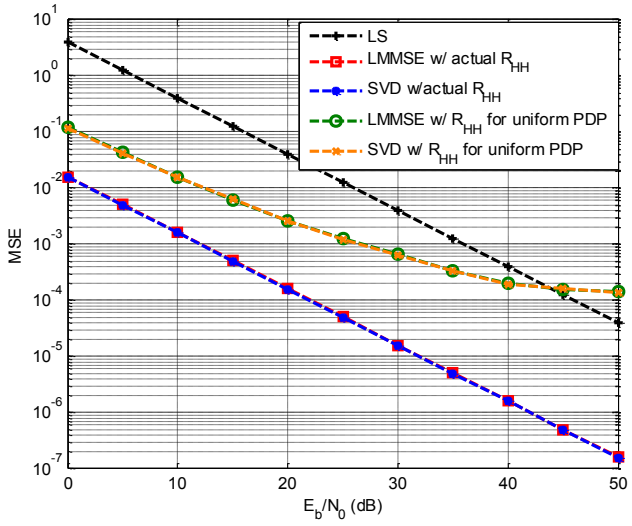

Figure 46. MSE performance comparison of LS channel estimation with LMMSE and SVD based channel estimation techniques using a Chu training sequence for N=64 and R_{os}=4.

The LMMSE channel estimation provides a much superior estimate of the channel when the channel statistics and hence the channel correlation is known. In the worst case scenario where the channel is unknown and modeled with a uniform power delay profile, the LMMSE performance is better than LS for lower E_b/N_0's up to 43 dB, however, the LS channel estimate is better for higher SNR. The low rank SVD estimator was considered with a rank of 15 and performs just as well as the LMMSE estimator. The performance of the low rank estimator would degrade with a reduction in rank.

5.4. Acknowledgements

Chapter 5 has, in part, been submitted for publication to the *IEEE Transactions on Signal Processing* as: A. U. Ahmed and J. R. Zeidler, "Novel Linear Receivers for Constant Envelope OFDM." Chapter 5 was also, in part, originally published in: A. U. Ahmed, S. C. Thompson, and J. R. Zeidler, "Channel estimation and equalization for CE-OFDM in multipath fading channels," in *Proc. of IEEE Milcom*, San Diego, CA, Nov. 2008.

6. Application of Error Correction Coding to CE-OFDM

6.1. Convolutional Coding

Channel error control coding has long been used to improve the performance of communication systems by adding redundancy at the transmitter and using it to correct errors at the receiver. Therefore, it is important to study the application of channel coding to CE-OFDM [69] and the resulting performance gain in light of the associated reduction in spectral efficiency. Convolutional coding (CC) is widely used in Communications systems today. It can be implemented at the transmitter using simple shift registers while near-optimal decoding can be performed at the receiver by employing an algorithm such as the Viterbi algorithm. The application of an optimum rate ½ convolutional code with constraint length K=9 [70] to CE-OFDM is studied. The generator polynomial of this code is [561,753] and the shift register structure is shown in Figure 47. The input bit stream is shifted into the shift register one bit at a time (k=1) producing two output bits (n=2). The constraint length of K=9 means that each output bit is generated from the current input bit and eight previous input bits.

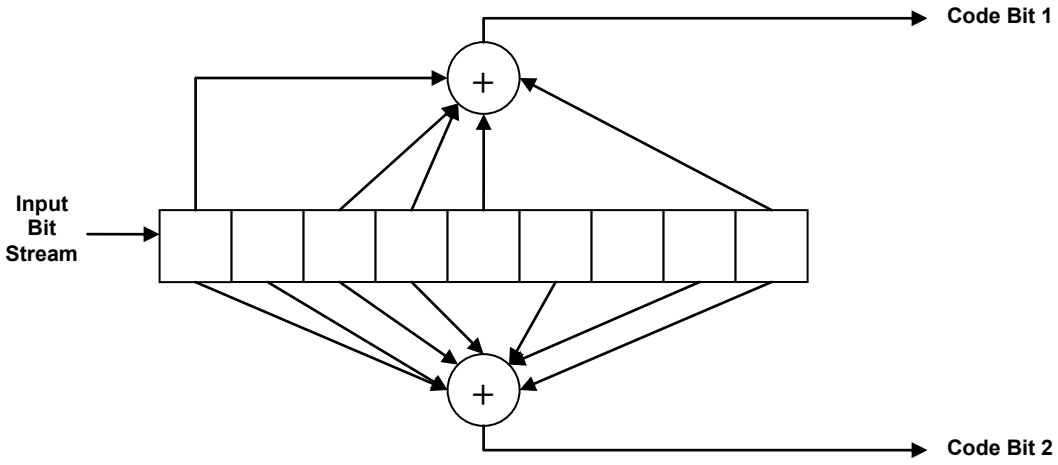

Figure 47. Convolutional encoder structure for constraint length K=9 with generator polynomial [561,753].

6.2. Viterbi Decoding

The convolutional encoder can be represented by a trellis diagram, whereby the transmitted sequence undertakes a path on the trellis based on the input bit stream. The convolutional encoder is a finite-state machine. Therefore, the optimum decoder for a convolutional code is a maximum likelihood sequence estimator (MLSE) [43]. The MLSE searches for the minimum distance path over the trellis based on the received signal. As such, it considers all possible transmit sequences and chooses the most probable one. A search over all possible transmit sequences is tedious; however, the Viterbi algorithm allows us to reduce the number of sequences in the trellis search by eliminating less probable sequences as new data is received. In essence, the Viterbi algorithm is a sequential trellis search algorithm. To understand the MLSE, consider a BPSK system (with some form of memory e.g. CC) shown in Figure 48.

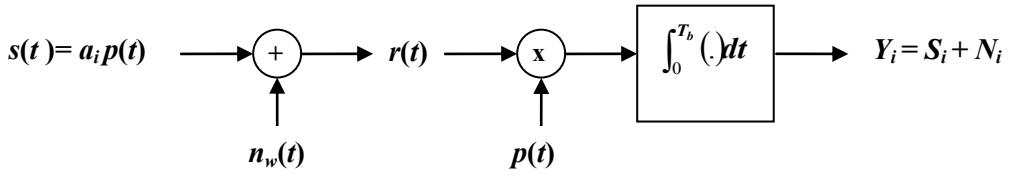

Figure 48. Decoding example of a BPSK communication system.

The input stream is represented by a_i=±1, while $p(t)$ is the signal pulse shaping, with $\int_0^{T_b} p^2(t)dt = E_b$. Also, $n_w(t)$ is the additive white Gaussian noise with power spectral density of $N_0/2$ watts/Hz. The output Y_i of the matched filter is composed of the signal component, S_i, and the noise component, N_i, given as

$$S_i = a_i \int_0^{T_b} p^2(t)dt = a_i E_b = \pm E_b \tag{92}$$

and

$$N_i = \int_0^{T_b} p(t) n_w(t)dt \tag{93}$$

where N_i are independent, zero mean Gaussian random variables with variance,

$$\begin{aligned} \sigma_N^2 &= E\left\{\int_0^{T_b} p(t_1) n_w(t_1)dt_1 \int_0^{T_b} p(t_2) n_w(t_2)dt_2\right\} \\ &= \int_0^{T_b}\int_0^{T_b} p(t_1)p(t_2)E\{n_w(t_1)n_w(t_2)\}dt_1dt_2 \\ &= \int_0^{T_b}\int_0^{T_b} p(t_1)p(t_2)\frac{N_0}{2}\delta(t_1 - t_2)dt_1dt_2 \\ &= \frac{N_0}{2}\int_0^{T_b} p^2(t)dt = \frac{N_0}{2}E_b \end{aligned} \tag{94}$$

The conditional probability density functions (PDFs) of the matched filter output Y_i given the two possible input a_i's are

$$p(Y_i \mid a_i = +1) = \frac{1}{\sqrt{2\pi}\sigma_N} e^{\frac{-(Y_i - E_b)^2}{2\sigma^2}} \tag{95}$$

and

$$p(Y_i \mid a_i = -1) = \frac{1}{\sqrt{2\pi}\sigma_N} e^{\frac{-(Y_i + E_b)^2}{2\sigma^2}} \tag{96}$$

Therefore, for a given transmitted sequence of length L, $a^{(m)}=\{a_1^{(m)},a_2^{(m)},\ldots,a_L^{(m)}\}$, the joint PDF of Y_1, Y_2, …, Y_L is [3]

$$\begin{aligned} p(Y_1, Y_2, ..., Y_L \mid a^{(m)}) &= \prod_{i=1}^{L} p(Y_i \mid a_i^{(m)}) \\ &= \prod_{i=1}^{L} \frac{1}{\sqrt{2\pi}\sigma_N} \exp\left(-\frac{(Y_i - a_i^{(m)} E_b)^2}{2\sigma^2} \right) \\ &= \left(\frac{1}{\sqrt{2\pi}\sigma_N} \right)^L \exp\left(-\sum_{i=1}^{L} \frac{(Y_i - a_i^{(m)} E_b)^2}{2\sigma^2} \right) \end{aligned} \tag{97}$$

where each a_i is either +1 or -1. The sequence $a^{(m)}$ which maximizes the conditional PDF is the maximum likelihood (ML) sequence.

By taking the log of both sides, we obtain the log likelihood function

$$\begin{aligned} \log p(Y_1, Y_2, ..., Y_L \mid a^{(m)}) &= \log\left(\frac{1}{\sqrt{2\pi}\sigma_N} \right)^L - \sum_{i=1}^{L} \frac{(Y_i - a_i^{(m)} E_b)^2}{2\sigma^2} \\ &= C_1 - C_2 \sum_{i=1}^{L} (Y_i - a_i^{(m)} E_b)^2 \end{aligned} \tag{98}$$

where C_1 and C_2 are constants with no dependency on $a^{(m)}$. Equivalently, the ML detector finds the sequence that minimizes the Euclidean distance metric, defined as

$$D = \sum_{i=1}^{L} (Y_i - a_i^{(m)} E_b)^2 \cdot \tag{99}$$

In theory, the Euclidean distance metric would need to be computed for all 2^L possible sequences. However, the Viterbi algorithm provides for a practical implementation whereby less probable sequences are discarded as new data is received. The Viterbi algorithm steps through the trellis in an incremental manner. It computes the Euclidean distance metric for all paths coming into a state. However, it only keeps one survivor path ending at each state resulting in a large reduction in complexity. This process is repeated for each received bit. Eventually, the decision on a bit can be reliably made when the trellis has worked its way to several constraint lengths into the future.

The Y_i in the equation above for the Euclidean distance metric represents the soft output of the matched filter; therefore, such decoding is referred to as soft decision decoding (SDD). An alternate decoding method is based on hard decision decoding (HDD), where hard decisions are made on the output of the matched filter before applying the Viterbi algorithm. The metric in this case is sometimes also referred to as the Hamming distance metric. In general, soft decision decoding results in better performance than hard decision decoding.

6.3. Noise Model

6.3.1. Phase Demodulator Receiver

In a conventional amplitude modulated signal, the message signal is amplitude modulated onto the carrier signal. Since the additive white Gaussian noise (AWGN) is additive in nature, it is simply added on to the message signal. However, for a phase modulated signal, the effect of noise on the message signal is not straightforward. While the AWGN is added to the modulated signal, it does not have an additive affect on the message signal embedded in the phase. In fact, this nonlinear affect of the noise on the message signal causes the threshold effect as witnessed in FM and other angle modulated signals.

The noise at the output of the phase demodulator was previously analyzed in chapter 4. The output of the phase demodulator is given as

$$\phi_r(t) = \phi(t) + Z_n(t) \tag{100}$$

where $Z_n(t)$ was shown to be well approximated as Gaussian distributed for high carrier to noise ratio (CNR) with power spectrum density of the noise component approximated as $S_z(f) = {N_0}/{A^2}$ [4] for low angular deviations (small modulation indices).

6.3.2. Linear Receivers

The noise at the output of the Basic linear receiver is a result of the matched filter output due to the quadrature baseband noise component and it is therefore Gaussian distributed. The noise at the input to the OFDM matched filters in the Enhanced linear receiver consists of multiple noise components, however, it was shown in chapter 4 that the noise component at the output of the matched filters that are part of the Enhanced linear receiver was well modeled as Gaussian distributed due to the central limit theorem.

6.4. Soft Decision Decoding for CE-OFDM

The noise at the matched filter outputs of the BLR is Gaussian distributed. Also, for the ELR and the arctangent receiver [12], [19], the noise is well modeled as Gaussian distributed. Therefore, the conditional probability density function (PDF) of the k-th matched filter output Y_k given input data d_k is given as

$$p(Y_k|d_k) = \frac{1}{\sqrt{2\pi\sigma_n^2}} e^{-\frac{(Y_k - S_k)^2}{2\sigma_n^2}} \tag{101}$$

where S_k is the signaling component of the matched filter output and σ_n^2 is the noise variance. The maximum likelihood (ML) sequence $\underline{d}$ of length L_d which maximizes the joint conditional PDF of the Y_k's then leads to the ML detector that minimizes the Euclidean distance metric. The resulting maximum likelihood decoding metrics for the arctangent, Basic linear and Enhanced linear receivers are given as

$$\text{Arctangent Receiver: } D = \sum_{l=1}^{L_d} (Y_l - d_l 2\pi h C_N N E_b)^2, \tag{102}$$

$$\text{BLR: } D = \sum_{l=1}^{L_d} \left(Y_l - d_l 2\pi h C_N E_b N \left(1 - \frac{(2\pi h C_N)^2}{4}(N-1)\right)\right)^2, \tag{103}$$

$$\text{ELR: } D = \sum_{l=1}^{L_d} \left(Y_l - d_l 2\pi h C_N E_b N \left(1 + \frac{(2\pi h C_N)^2}{2}(N-1)\right)\right)^2. \tag{104}$$

6.4.1. Performance in AWGN

Figures 49-52 show the performance of CE-OFDM in AWGN for the case where a rate ½ convolutional code with a constraint length of 9 with Viterbi decoding is applied for the arctangent and linear receivers. For the case of $2\pi h$=0.3 in Figure 49, a significant coding gain of over 4 dB is obtained at a BER of 10^{-3}. Both the linear receivers provide slightly better performance than the arctangent receiver, although the coded performance advantage of the linear receivers over the arctangent receiver is minimal at this low modulation index.

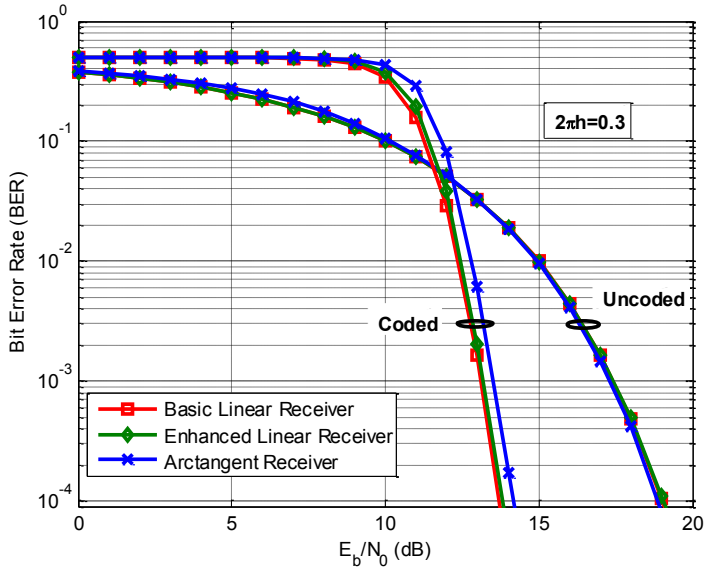

Figure 49. CE-OFDM ($2\pi h$=0.3) performance of linear and arctangent based receivers in AWGN using a rate ½ convolutional code of constraint length 9 for N=64 with a 2X oversampling rate.

Figure 50 shows the performance of coded CE-OFDM in AWGN for the arctangent and linear receivers for the case of $2\pi h$=0.6. The performance advantage of the linear receivers is much more significant, over 1.2 dB at a BER of 10^{-3}. While the arctangent based receiver generally provides slightly better performance than the ELR at low BERs for moderate modulation indices, the ELR provides better performance at high BERs (BER>0.05 in most cases). Since the error control coding corrects all errors that fall within the code's minimum distance, the performance advantage of the ELR at high BERs (> 10^{-2}) translates into a significant performance advantage in a coded system.

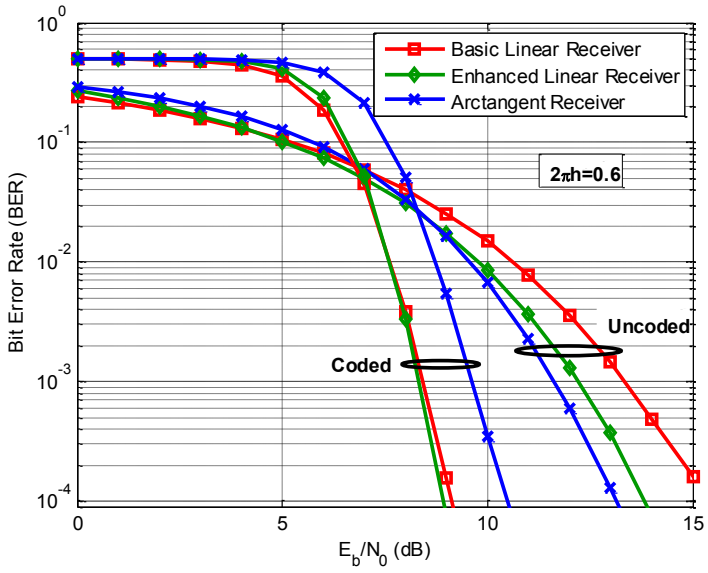

Figure 50. CE-OFDM ($2\pi h$=0.6) performance of linear and arctangent based receivers in AWGN using a rate ½ convolutional code of constraint length 9 for N=64 with a 2X oversampling rate.

Figure 51 shows the performance of coded CE-OFDM in AWGN for the arctangent and linear receivers for the case of $2\pi h$=0.5. Both the cases of hard decision decoding (HDD) and soft decision decoding (SDD) are evaluated. The performance advantage of the linear receivers over the arctangent receiver for SDD is similar to the previously considered case of $2\pi h$=0.6 in Figure 50. The performance advantage of the linear receivers over the arctangent receiver is larger for the SDD case compared to the HDD case. This is partly due to the greater effect of phase wrapping errors at the arctangent receiver on the Viterbi decoding for the case of soft decision decoding.

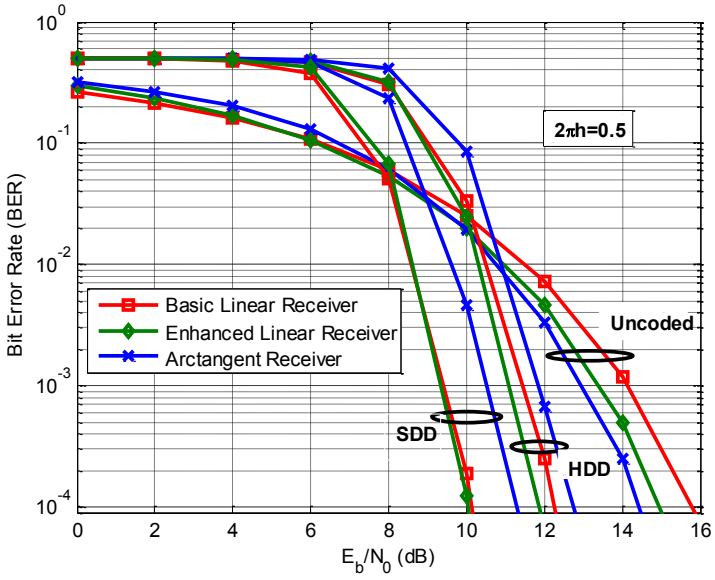

Figure 51. CE-OFDM ($2\pi h$=0.5) performance of linear and arctangent based receivers in AWGN using a rate ½ convolutional code of constraint length 9 using both hard decision decoding (HDD) and soft decision decoding (SDD) for N=64 with a 2X oversampling rate.

Finally, Figure 52 shows the performance of coded CE-OFDM in AWGN for the arctangent and linear receivers for the case of $2\pi h$=0.7. This is the highest modulation index for which the arctangent based receiver without the phase unwrapper performs well without becoming overwhelmed with degradation due to phase wrapping. This is also the highest modulation index for which the linear receivers perform well without becoming overwhelmed with distortion due to higher order terms from the Taylor series. Once again, the linear receivers display a significant performance advantage of over 1.2 dB at a BER of 10^{-3}compared to the arctangent receiver.

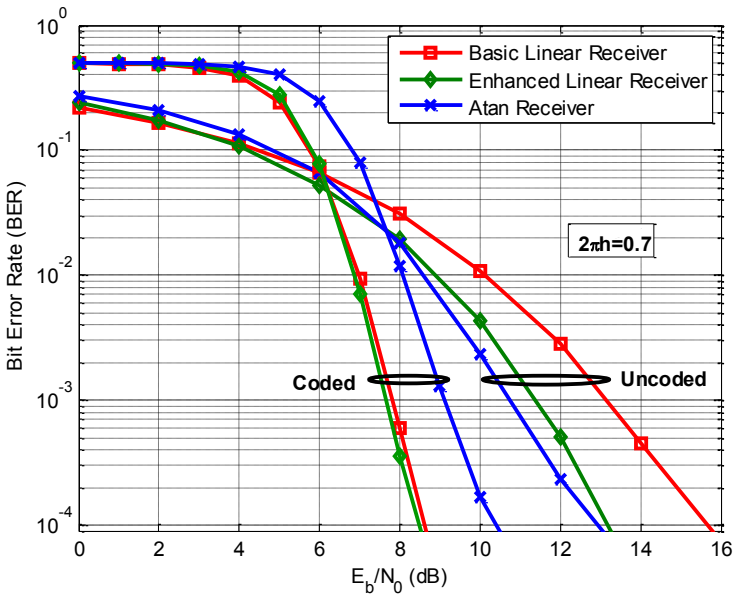

Figure 52. CE-OFDM ($2\pi h$=0.7) performance of linear and arctangent based receivers in AWGN using a rate ½ convolutional code of constraint length 9 for N=64 with a 2X oversampling rate.

6.4.2. Performance in Multipath Fading

The error correction coding performance in multipath fading channels is studied in this section. Previously defined frequency selective fading channels C and D are considered here. Channel C has an exponential power delay profile (PDP) with a delay spread of 9μs and $E\{|h[l]|^2\} \propto e^{-\tau_l/2\mu s}$. Channel D has a uniform power delay profile (PDP) with a delay spread of 9μs and all paths having equal power. These cases were evaluated with a CE-OFDM symbol period of T_s=128μs, a cyclic prefix of 10μs and FDE based equalization with perfect channel state information (CSI). The previously defined rate ½ convolutional code with a constraint length of 9 with Viterbi decoding is applied to all cases. The simulation performance evaluation of the arctangent, Basic and Enhanced linear receivers for channels C and D is presented in Figures 53-54. In Figure 53, the performance comparison is conducted for a frequency selective fading channel (Ch. C) when an FDE is employed along with error correction coding for a modulation index of $2\pi h$=0.6. Both the linear receivers outperform the arctangent receiver in this case as well, with the ELR providing better performance by over 1.6 dB at a BER of 10^{-3}.

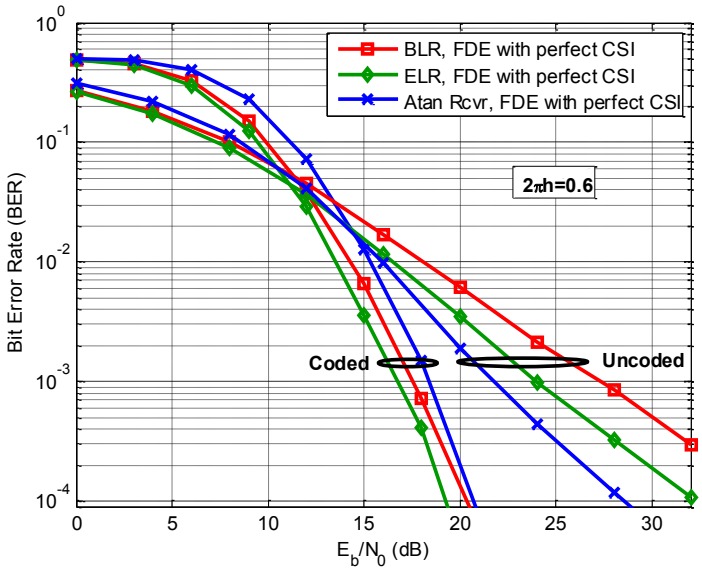

Figure 53. CE-OFDM ($2\pi h$=0.6) performance of linear and arctangent based receivers in frequency selective fading (Channel C, Exponential power delay profile) using a rate ½ convolutional code of constraint length 9 for N=64 with a 2X oversampling rate.

The performance comparison for the frequency selective fading channel (Ch. D, uniform power delay profile) is presented in Figure 54 when an FDE is employed along with error correction coding for a modulation index of $2\pi h$=0.6. Both the linear receivers outperform the arctangent receiver in this case as well, with the ELR again providing better performance by over 1.6 dB at a BER of 10^{-3}.

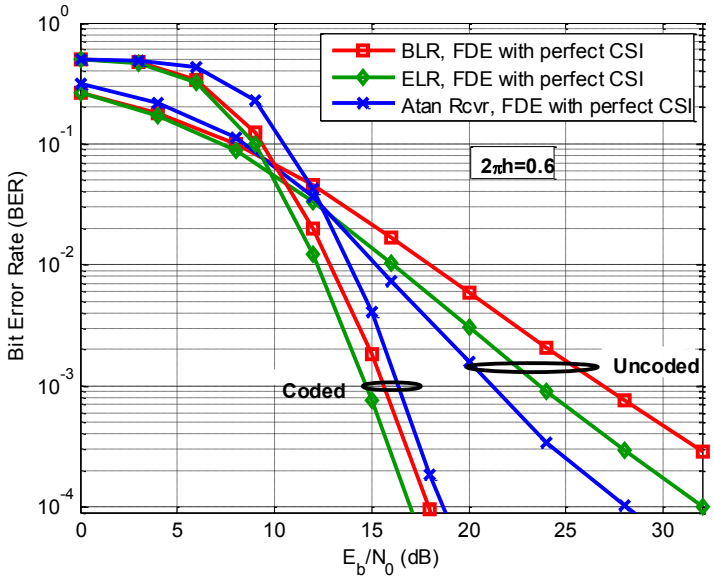

Figure 54. CE-OFDM ($2\pi h$=0.6) performance of linear and arctangent based receivers in frequency selective fading (Channel D, Uniform power delay profile) using a rate ½ convolutional code of constraint length 9 for N=64 with a 2X oversampling rate.

6.5. Soft Decision Decoding Using Quantized Levels

The soft output of the detector/matched filter may be quantized to a certain number of levels instead of having infinite precision for implementation reasons. The 16-level soft decision decoding is known to perform within a fraction of a dB of infinite precision soft decision decoding [70]. Additionally, 8 or 16-level soft decision decoding would allow an efficient implementation in a DSP. Soft decision decoding achieves an average gain of 2dB over hard decision decoding.

A Q-level quantization may be employed in soft decision decoding. The special case of Q=2 represents hard decision decoding (HDD). A Q-level quantization requires Q-1 quantization thresholds to separate between the Q levels (quantization symbols). These quantization thresholds are chosen to optimize the performance [70]. For the case of antipodal signaling with Gaussian noise, the transmit symbols are symmetric with respect to zero and the noise distribution is symmetric with respect to the symbols. Therefore, naturally one threshold is selected at T_0=0 if the Q is a power of 2. The other

thresholds can be optimally selected as described in [70]. The quantization symbols/levels are therefore symmetric around zero and can be labeled as $\pm q_1, \pm q_2, \ldots, \pm q_{Q/2}$.

The likelihood ratio of the matched filter output Y for a binary input channel is defined as

$$\lambda(\boldsymbol{Y}) = \frac{\boldsymbol{p}(\boldsymbol{Y} \mid 1)}{\boldsymbol{p}(\boldsymbol{Y} \mid 0)}. \tag{105}$$

Also, the likelihood ratio of a received quantization symbol q_i for a binary input channel is defined as

$$\lambda(\boldsymbol{q}_i) = \frac{\boldsymbol{P}(\boldsymbol{q}_i \mid 1)}{\boldsymbol{P}(\boldsymbol{q}_i \mid 0)}. \tag{106}$$

Then, the quantization threshold T_i that separates the quantization symbols q_i and q_{i+1} can be optimally computed by satisfying the condition [70]

$$\lambda(\boldsymbol{T}_i) = \sqrt{\lambda(\boldsymbol{q}_i)\lambda(\boldsymbol{q}_{i+1})}, \quad i=1, 2, \ldots, Q/2. \tag{107}$$

This condition lets us determine the optimum quantization thresholds for Q-level soft decision decoding (SDD). Since the condition is based on the probability distribution of the noise, the quantization thresholds are a function of the SNR. As an example, the figure below displays the optimum thresholds for 4-level soft decision decoding of BPSK in AWGN.

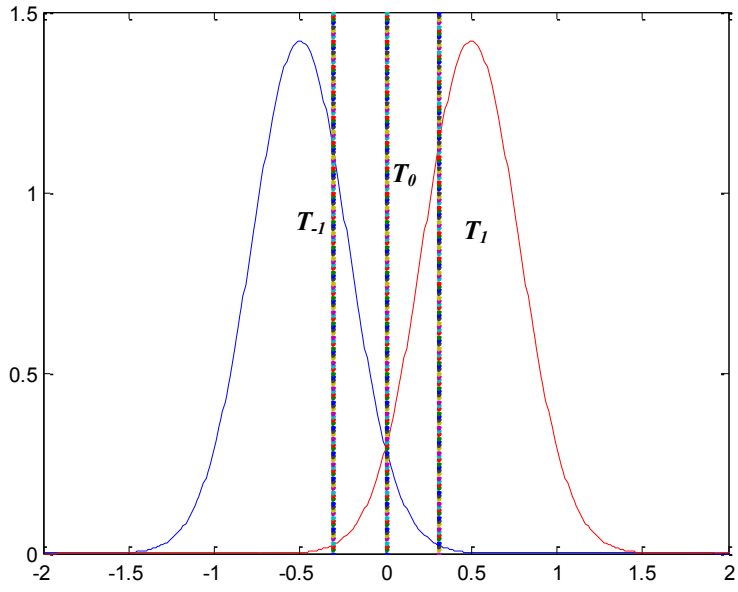

Figure 55. Example of quantization thresholds for 4-level SDD of BPSK with AWGN for E_b/N_0=5dB.

6.5.1. Performance Results

A simulation based performance evaluation of CE-OFDM employing the arctangent receiver was performed with rate ½ convolutional coding of constraint length K=9 with several quantization levels for decoding. Figure 56 shows the performance results for hard decision decoding (Q=2, blue) as well as 4 (green), 8 (orange), and 16 (purple) level soft decision decoding for modulation indices of $2\pi h$=0.1, 0.3, and 0.6.

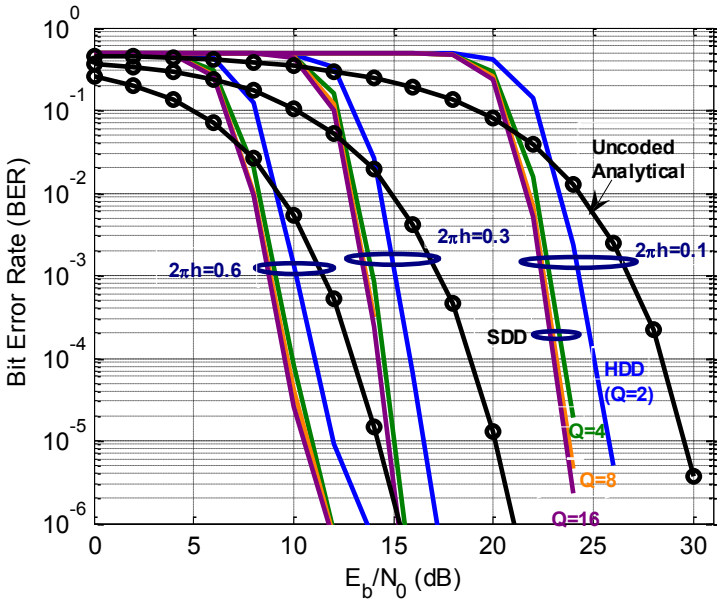

Figure 56. Performance of CE-OFDM (N=64) using the arctangent receiver while employing rate ½ convolutional coding (K=9) and Viterbi decoding with multiple quantization levels for a 4X oversampling rate.

Coding provides a performance gain for all the modulation indices; however, it is evident that the coding gain is larger for lower modulation indices compared to higher modulation indices for the arctangent receiver. Once again, this is caused by the CE-OFDM phase crossing the phase wrapping boundary at π/-π resulting in phase wrapping. Also, it should be noted that the performance gain is significant when the quantization level is increased from hard decision decoding (Q=2) to soft decision decoding with 4-level quantization (Q=4). Each subsequent increase in number of quantization levels

yields a smaller improvement in performance. Therefore, limiting the number of quantization levels to 8 or 16 results in limited loss of performance compared to the unquantized case.

6.6. Effect of Cycle Slip Noise on Coding Performance

When the arctangent based receiver is used with the phase unwrapper, it becomes prone to cycle slip noise and thus the threshold effect. Figure 57 shows the CE-OFDM performance results for the arctangent receiver with a phase unwrapper for hard decision decoding (Q=2, blue) as well as 4 (green), 8 (orange), and 16 (purple) level soft decision decoding for modulation indices of $2\pi h$=0.1, 0.3, and 0.6. These results are for the case when a phase wrapper is used after the phase demodulator.

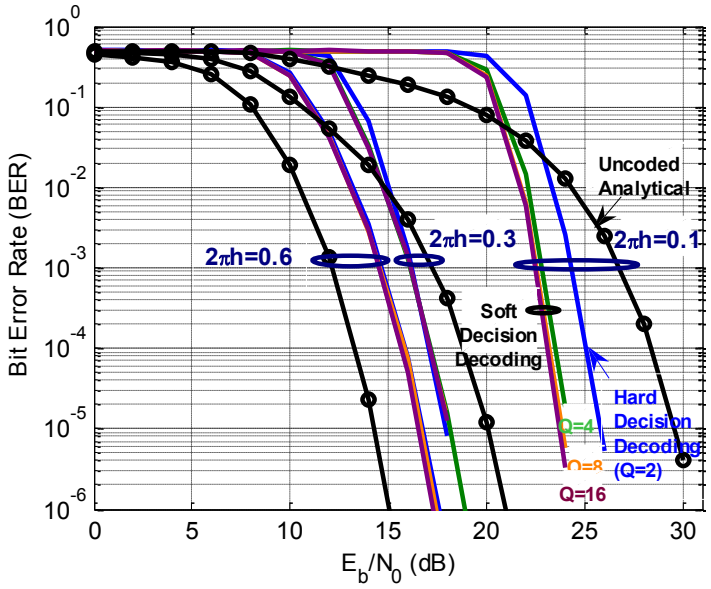

Figure 57. Performance of CE-OFDM (N=64) with a phase unwrapper employing rate ½ convolutional coding (K=9) for various modulation indices for a 4X oversampling rate.

It can be seen from Figure 55 that a gain of over 3.5dB is achieved for a modulation index of $2\pi h$=0.1 for hard decision decoding (HDD). An additional gain of about 2dB is achieved with soft decision decoding (SDD). However, the coding gains are much smaller as the modulation index is increased to $2\pi h$=0.3, with both hard decision decoding and soft decision decoding resulting in similar performance. When the modulation index is further increased to $2\pi h$=0.6, there is actually a loss in

performance compared to analytical uncoded CE-OFDM. This loss in performance at higher modulation indices is caused by the cycle slips at the phase unwrapper employed after the phase demodulator. The higher modulation index results in the demodulated CE-OFDM phase to cross the phase wrapping boundary at $\pi/-\pi$ more often. The phase unwrapper does not always perform the correct phase unwrapping due to noise (especially at lower SNRs). In fact, the phase unwrapper performs very poorly at lower SNRs causing many cycle slips. A cycle slip within an OFDM symbol results in a large number of errors within that symbol. These errors overwhelm the convolutional code and actually result in even more errors during the decoding process. Hence, the phase unwrapper not only performs poorly at low SNRs, but the resulting errors also overwhelm the coding and result in even more errors. This in turn results in performance even worse than the uncoded case. It is therefore best to only use a phase unwrapper when performance degradation due to phase wrapping is worse than the performance degradation due to the threshold induced cycle slips at low CNR. In general, a phase unwrapper should only be used at the arctangent receiver for the case of larger modulation indices, $2\pi h \geq 0.8$ when binary data symbols are employed.

6.7. Addition of an Interleaver

One reason for the worse performance at higher modulation indices as shown above in section 6.6 is burst errors generated at times when phase wrapping occurs. These burst errors overwhelm the distance properties of the convolutional code. An interleaver can be used to separate the burst of errors. Figure 58 shows the results after the application of a matrix interleaver that interleaves the data bits over 8 CE-OFDM symbols.

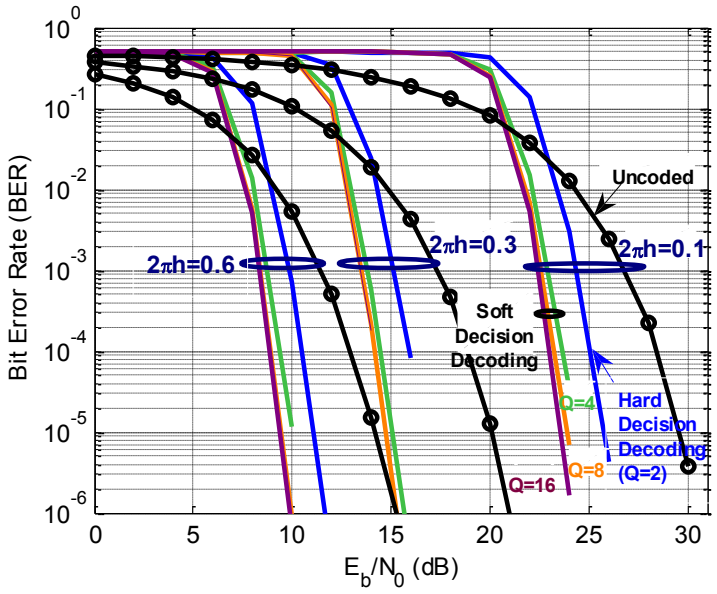

Figure 58. Performance of CE-OFDM (*N*=64) without phase unwrapper employing rate ½ convolutional coding (*K*=9) and a matrix interleaver over 8 CE-OFDM symbols.

The interleaver results in an additional gain of 1dB at higher modulation indices. This is due to the separation of burst errors.

Finally, the potential performance improvement by using an interleaver is considered for the previously considered case of the CE-OFDM performance comparison between the linear receivers and the arctangent receiver (without a phase unwrapper) in frequency selective fading (Channel C, Exponential power delay profile). A matrix interleaver that interleaves the data bits over 16 CE-OFDM symbols is employed. Only a small improvement is noted due to the addition of the interleaver unlike the previous case in which cycle slip noise was resulting in burst errors.

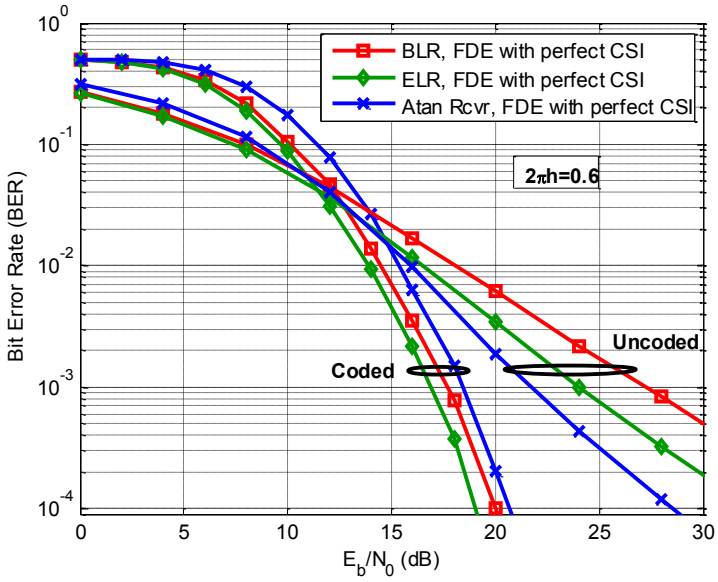

Figure 59. CE-OFDM ($2\pi h$=0.6) performance of linear and arctangent based receivers in frequency selective fading (Channel C, Exponential power delay profile) using a rate ½ convolutional code of constraint length 9 along with a matrix interleaver (16 CE-OFDM symbols) for N=64 with a 2X oversampling rate.

6.8. Performance Bound

The bit error performance of convolutionally coded communication systems is frequently studied using the union bound [43, pp. 485-490], [70, p.527], [82]. It is assumed without loss of generality that the all-zero codeword is transmitted. The bound on BER is computed by looking at all the incorrect paths that diverge from the correct path (all-zero) on the trellis. The probability of choosing a divergent path is based on the distance of that path from the correct all-zero path. An incorrect path is chosen over the correct path if the received sequence is closer (in distance) to the incorrect path compared to the correct path. The distance metric is Hamming for hard decision decoding and Euclidean for soft decision decoding. A union bound on the probability of bit error is given by [70, p. 531]

$$P_b \le \sum_{d=d_{free}}^{\infty} B[d]P_d, \tag{108}$$

where $B[d]$ is the total number of non-zero information bits on all weight d paths divided by the number of information bits k per unit time and d_{free} is the lowest Hamming weight of any error event. P_d is the pair-wise probability of choosing an incorrect path over the correct path when the distance between the two paths is d. Equation (108) is essentially the sum of the probabilities of all possible divergent (incorrect) paths times the bit errors that result from those incorrect paths.

For the case of hard decision decoding, choosing an incorrect path at a distance d from the correct path would require more than $d/2$ of the received bits to be received in error. This would cause the received sequence to be closer in distance to the incorrect path than the correct path. If P_c is the probability of a coded bit error, then the probability of choosing an incorrect path at a distance d from the correct path (for odd d) is given as [70, p. 527]

$$\boldsymbol{P_d} = \sum_{e=\frac{d+1}{2}}^{d} \binom{\boldsymbol{d}}{\boldsymbol{e}} (\boldsymbol{P_c})^{e} (1-\boldsymbol{P_c})^{d-e} < \left(2\sqrt{\boldsymbol{P_c}(1-\boldsymbol{P_c})}\right)^{d}, \tag{109}$$

where the Chernoff upper bound is used which is also an upper bound for an even distance d [43, p. 490]. Therefore, the union bound on the probability of bit error for CE-OFDM with convolutional coding and hard decision decoding can then be computed as

$$\boldsymbol{P_{b,HDD}} < \sum_{d=d_{free}}^{\infty} \boldsymbol{B}[\boldsymbol{d}]\left(2\sqrt{\boldsymbol{P_c}(1-\boldsymbol{P_c})}\right)^{d}, \tag{110}$$

where P_c is the probability of coded bit error for CE-OFDM which can be obtained for the different receiver structures from their bit error probability computed earlier for the AWGN performance in chapter 4 by replacing the bit energy (E_b) by the coded bit energy, $E_c = RE_b$. For the case of the arctangent receiver, this probability of coded bit error is given as

$$\boldsymbol{P_c} = \boldsymbol{Q}\left(2\pi\boldsymbol{h}\sqrt{\frac{2\boldsymbol{R}\boldsymbol{E_b}}{\boldsymbol{N_0}}}\right), \tag{111}$$

where R is the code rate. Similarly, expressions for the probability of coded bit error can be obtained for the linear receiver structures. The bit energy (E_b) was normalized to 1 to compute the N_0 that appears in the bound for the Enhanced linear receiver.

For the case of soft decision decoding, the Euclidean distance is computed based on the matched filter outputs for the received sequence corresponding to d independent Gaussian random variables. Therefore, the union bound for the probability of bit error is given as [70, p. 533]

$$P_{b,SDD} < \sum_{d=d_{free}}^{\infty} B[d]Q\left(2\pi h\sqrt{\frac{2dRE_b}{N_0}}\right). \tag{112}$$

B[d] can be determined for a convolutional code from its bit weight enumerating function (WEF). The bit WEF coefficients for the optimum rate ½, K=9 convolutional code are given in [83].

The performance bounds for the arctangent, Basic linear and Enhanced linear receivers are plotted for the modulation index $2\pi h$=0.3 in Figure 60-62 using the first 20 terms in (112). For this low modulation index, the AWGN performance approximation for the probability of coded bit error is very accurate for the Basic linear receiver resulting in a tight bound at low BERs. However, the bound does not hold for the arctangent receiver which suffers from cycle slip noise at low SNRs due to phase wrapping resulting in some burst errors that overwhelm the code. The Enhanced linear performance approximation is also not exact, resulting is slight deviation beyond the bound at low BERs. For higher modulation indices ($2\pi h$>0.3), the performance approximation for the probability of coded bit error is not a perfect match to the actual simulation performance and is thus the performance approximation can be considered as a low bound for higher modulation indices as shown in Figure 20, 26, and 27. Therefore, the determination of an accurate bound on the coding performance is not feasible for higher modulation indices ($2\pi h$>0.3). Overall, while the performance bound provide an estimate of the coded performance, they do not hold in most cases resulting in limited utility.

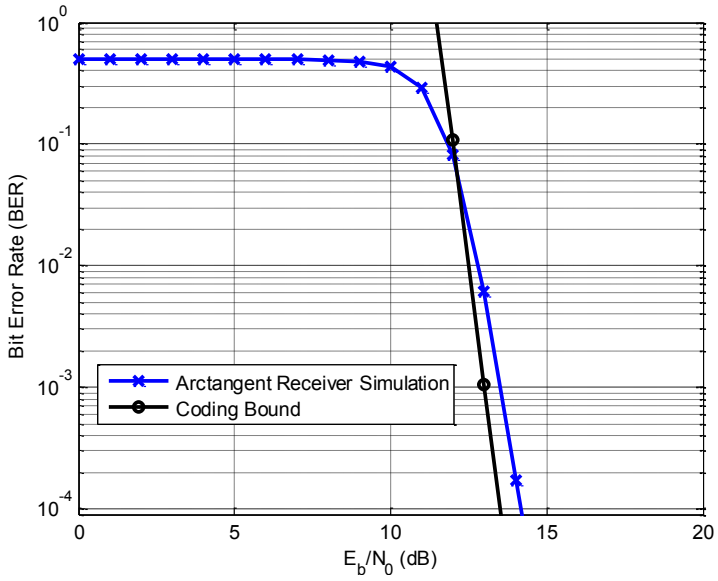

Figure 60. CE-OFDM ($2\pi h$=0.3) error correction coding (SDD) performance bound for the Arctangent Receiver in AWGN using a rate ½ convolutional code of constraint length 9 with generator polynomial [661,753].

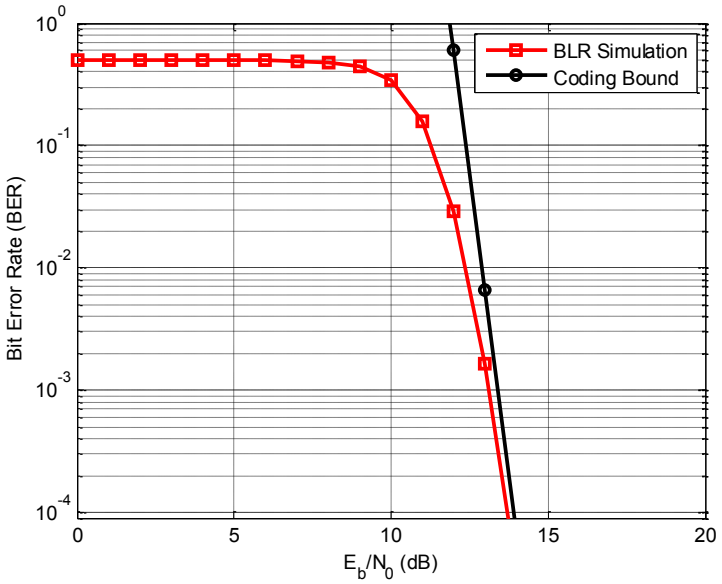

Figure 61. CE-OFDM ($2\pi h$=0.3) error correction coding (SDD) performance bound for the Basic Linear Receiver in AWGN using a rate ½ convolutional code of constraint length 9 with generator polynomial [661,753].

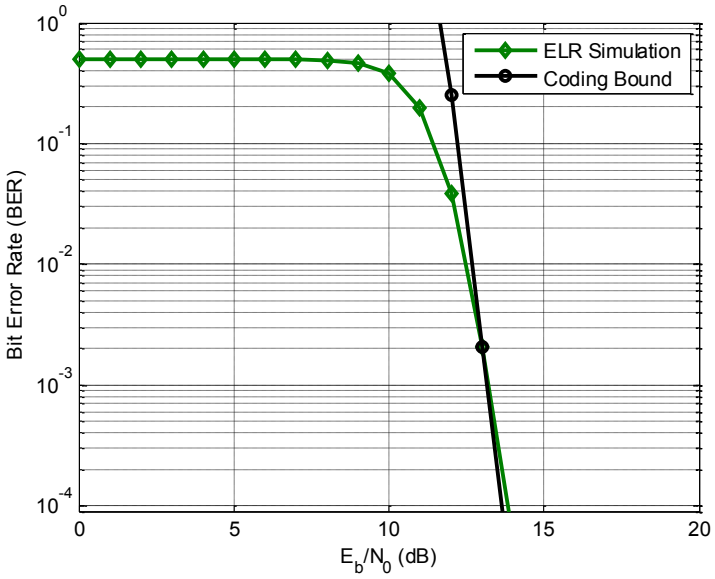

Figure 62. CE-OFDM ($2\pi h$=0.3) error correction coding (SDD) performance bound for the Enhanced Linear Receiver in AWGN using a rate ½ convolutional code of constraint length 9 with generator polynomial [661,753].

6.9. Sampling Rate at the Receiver

CE-OFDM is generally considered with a 2X or higher sampling rate at the receiver to ensure good performance. This is mainly based on the degradation in the uncoded AWGN performance of CE-OFDM when no oversampling is employed. As previously discussed in chapter 4, the Taylor series expansion of CE-OFDM includes higher order terms which are small but nonzero for small modulation indices. When no oversampling is used, the higher order terms generate distortion and resulting in an error floor at higher SNRs. However, as shown in Figure 63 for $2\pi h$=0.3, when error correction coding is employed, the errors resulting in the error floor are corrected and the coded performance is similar to the coded performance for the case of using a higher sampling rate, as shown previously in Figure 49.

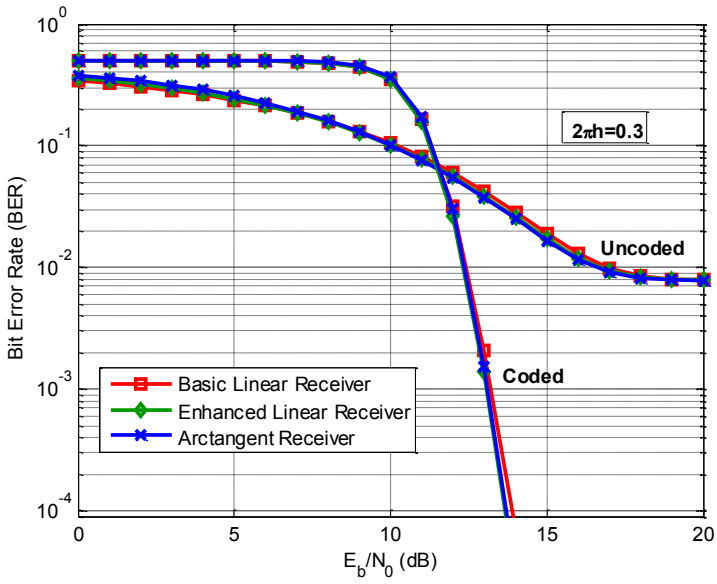

Figure 63. CE-OFDM ($2\pi h$=0.3) performance of linear and arctangent based receivers in AWGN using a rate ½ convolutional code of constraint length 9 for N=64 with no oversampling.

Similarly, for the case of $2\pi h$=0.6 shown in Figure 64, when error correction coding is employed, the errors resulting in the error floor are corrected and the coded performance is similar to the coded performance for the case of using a higher sampling rate, as shown previously in Figure 50. Basically, when error correction coding is employed, a higher sampling rate is not necessary for small and moderate modulation indices and the same sampling rate as the underlying OFDM message signal can be employed at the receiver.

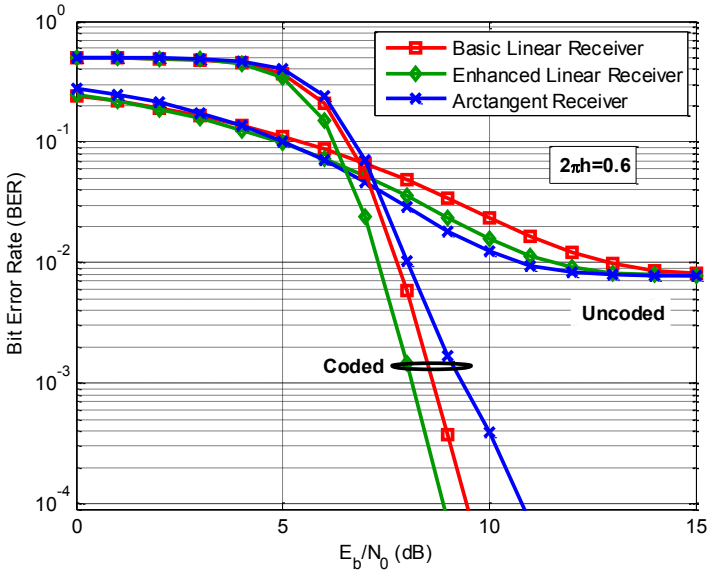

Figure 64. CE-OFDM (2πh=0.6) performance of linear and arctangent based receivers in AWGN using a rate ½ convolutional code of constraint length 9 for N=64 with no oversampling.

Finally, the case of $2\pi h$=0.6 is shown in Figure 65. The application of error correction coding corrects the errors resulting in the error floor, however, the coded performance in this case is ~1 dB worse at a BER of 10^{-3} compared to the coded performance for the case of using 2X oversampling rate, as shown in Figure 53.

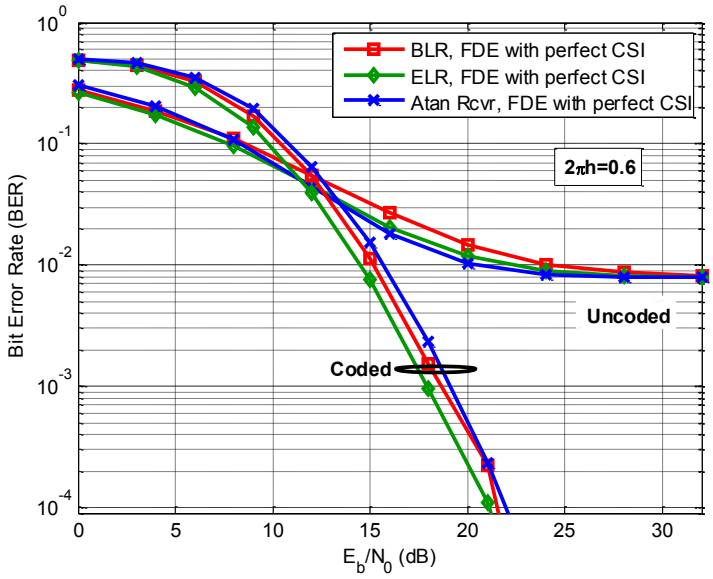

Figure 65. CE-OFDM ($2\pi h$=0.6) performance of linear and arctangent based receivers in frequency selective fading (Channel C, Exponential power delay profile) using a rate ½ convolutional code of constraint length 9 for N=64 with no oversampling.

6.10. Acknowledgements

Chapter 6 has, in part, been submitted for publication to the *IEEE Transactions on Signal Processing* as: A. U. Ahmed and J. R. Zeidler, "Novel Linear Receivers for Constant Envelope OFDM." Chapter 6 was also, in part, originally published in: A. U. Ahmed, S. C. Thompson, and J. R. Zeidler, "Constant Envelope OFDM with Channel Coding," in *Proc. of IEEE Milcom*, Washington, DC, Oct. 2006.

7. Impact of the Threshold Effect on CE-OFDM

7.1. Threshold Effect

The threshold effect is inherent in angle modulation and therefore also affects CE-OFDM. In the threshold region, at low carrier to noise ratios (CNR), the demodulated SNR falls off much more rapidly for a decrease in CNR. This results in poor performance below threshold. One property of angle modulated waveforms is the possible tradeoff between bandwidth and power with an increase in the modulation index. However, this tradeoff is limited by the threshold which appears at even higher CNRs for larger modulation indices [58, p. 32].

Threshold extension provides an increase in the range of CNR over which this tradeoff is possible. Additionally, for CE-OFDM, threshold extension would permit a larger CNR range over which channel coding would be able to provide error correction, which would be especially useful in a fading channel with interleaving. The threshold effect is accompanied by a change in the characteristics of the noise at the output of the phase demodulator.

The carrier to noise ratio (CNR) is defined as

$$CNR = \frac{A^2/2}{\sigma_n^2} = \frac{A^2/2}{N_0 B_m} \tag{113}$$

where σ_n^2 is the noise variance and $B_m = N/T_s$ is the baseband signal bandwidth.

The threshold effect is the phenomena whereby a decrease in the CNR below the threshold CNR results in a rapid nonlinear reduction in the corresponding SNR at the demodulator. This results in a large performance degradation when the CNR is below the threshold CNR. The cause of the threshold effect is the phase cycle slips that are generated at the phase demodulator as the noise entering the phase demodulator becomes large. The threshold CNR is defined as the CNR at which the output SNR has degraded 1 dB from the ideal linear SNR which is the based on the case without click or cycle slip noise.

7.2. Noise Model

In CE-OFDM, when the arctangent based receiver with a phase unwrapper is used, the phase cycle slips are generated due to the noise induced phase unwrapping errors. As the noise becomes large at lower CNRs, it can cause the phase unwrapper to both miss phase wrapping without correcting it or to incorrectly detect phase wrapping when it is not present. Each of these errors results in a 2π phase shift known as a phase cycle slip. The phase cycle slip noise in the threshold region increases with a decrease in the CNR below the threshold CNR and causes the large decrease in the SNR at the demodulator resulting in the overall performance degradation.

The demodulated CE-OFDM phase at the output of the phase demodulator can be approximated as [26],

$$\phi_r(t) = \phi(t) + Z_{CS}(t) + Z_n(t), \tag{114}$$

where $\phi(t)$ is the transmitted CE-OFDM phase (i.e. scaled OFDM) and $Z_n(t)$ can be approximated as Gaussian [20], [11] with a power spectral density that can be approximated as $S_z(f) = N_0/A^2$ W/Hz [46] where N_0 is the power spectral density of the baseband noise at the input to the receiver. $Z_{CS}(t)$ represents all the phase cycle slips generated at the phase demodulator for a given CE-OFDM symbol. In the absence of cycle slips, the ideal theoretical SNR at the demodulator output is

$$SNR_{out} = \frac{Signal\ Power}{Noise\ Power} = \frac{(2\pi h)^2}{\frac{N_0}{A^2}B_m} = 2(2\pi h)^2 CNR \tag{115}$$

where $(2\pi h)^2$ is the phase variance. This equation represents the ideal linear relationship between the input CNR and the demodulated SNR that holds true above the threshold in the absence of phase cycle slip noise. The SNR departs rapidly from this linear relationship once phase cycle slip noise appears at and below the threshold CNR.

When phase cycle slips are present, $Z_{CS}(t)$ is non-zero and can be represented as

$$Z_{CS}(t) = \sum_{l=1}^{L} 2\pi B_l u(t - t_l), \tag{116}$$

where L is total number of cycle slips over the symbol period, B_l=±1 indicates whether it is a positive or negative cycle slip and $u(t-t_l)$ is the unit step function shifted by t_l corresponding to the cycle slip start location within the CE-OFDM symbol.

The demodulated phase in (114) is further demodulated using a standard OFDM demodulator. Considering the i-th CE-OFDM symbol without loss of generality, the output of the k-th matched filter of the OFDM demodulator (corresponding to the k-th OFDM subcarrier) is

$$Y_k = \int_{(i-1)T_s}^{iT_s} \phi_r(t) q_k(t - iT_s) dt = S_k + \sum_{l=1}^{L} C_{kl} + N_k, \tag{117}$$

where

$$S_k = \int_{(i-1)T_s}^{iT_s} \phi(t) q_k(t - iT_s) dt = d_k 2\pi h C_N E_q \tag{118}$$

with the subcarrier energy $E_q = \int_0^{T_s} q_k^2(t) dt = T_s/2$ and

$$N_k = \int_{(i-1)T_s}^{iT_s} Z_n(t) q_k(t - iT_s) dt. \tag{119}$$

Since $Z_n(t)$ is well approximated as Gaussian, N_k is also Gaussian distributed with variance $\sigma_N^2 = N_0 E_q / A^2$ [20]. In the absence of phase cycle slip noise, the ideal theoretical SNR at the output of the OFDM demodulator (matched filter) is given as [12], [20]

$$SNR_{MF} = \frac{S_k^2}{\sigma_N^2} = \frac{(2\pi h C_N E_q)^2}{\frac{N_0}{A^2} E_q} = 2(2\pi h)^2 CNR. \tag{120}$$

Note that this SNR at the output of the OFDM matched filters matches the SNR at the output of the phase demodulator in (115). It represents the linear relationship between the CNR and the demodulated SNR that holds above threshold. It also signifies the tradeoff whereby the demodulated SNR increases with an increase in the modulation index at the expense of bandwidth [12, p. 52].

7.3. Cycle Slip Noise

When the CNR drops below threshold, the noise phasor in Figure 66 becomes large enough to occasionally encircle the origin resulting in a 2π phase shift (rotation) in the resultant phase [20]. This new type of additional noise is known as click noise (in FM) resulting in spikes in the demodulated FM signal or cycle slips in the demodulated PM signal. Each spike is of area 2π, while each cycle slip results in a 2π phase shift. The spikes and cycle slips contribute a significant amount of noise power for low CNR resulting in a rapid decline in demodulated SNR as the CNR falls below threshold.

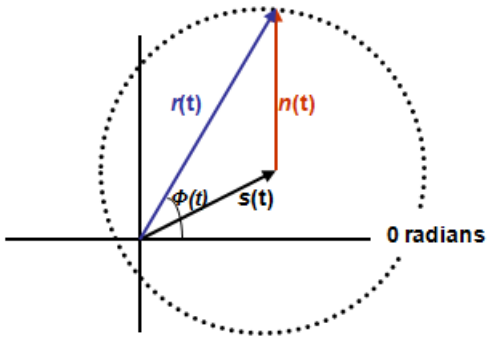

Figure 66. The noise phasor at low CNR resulting in an encirclement of the origin resulting in a phase cycle slip.

Exact analysis of noise effects below threshold is tedious if not intractable in most cases due to the inherent nonlinearities. A practical approach of an approximate noise model was presented by Rice in [72] in which he modeled the noise as having a continuous Gaussian component that is occasionally interrupted by clicks. With this model, the noise is comprised of two components: a continuous Gaussian component added to a sequence of randomly occurring clicks. For the case of phase modulation, these clicks take the form of cycle slips. The rate of clicks or cycle slips, which depends on the CNR, determines the noise power contributed by the click component. Rice's noise model has been found to be quite accurate down to CNRs as low as 2 dB [73], [74]. The realization, based on Rice's model, that click and cycle slip noise is primarily responsible for the onset of threshold supports the development of receiver structures that provide threshold extension by some form of reduction in click noise for large modulation indices. This is accomplished by either using a feedback loop mechanism

such as in PLL and FMFB based receivers [58] for click or cycle slip suppression or by employing click or cycle slip detection and elimination schemes [75] with a conventional receiver such as the limiter discriminator (LD).

7.4. Threshold Performance

7.4.1. Cross-Correlator Receiver (CCR)

In order to study the threshold effect for a CE-OFDM receiver such as the arctangent receiver with a phase unwrapper, it is important to also study the performance of a classical FM receiver such as the limiter discriminator for comparison. The conventional limiter discriminator (LD) receiver is a common practical embodiment of an ideal FM detector [73, p. 122]. It consists of a limiter followed by a discriminator [71, chap. 9]. Since the message signal in FM is embedded in the frequency, the amplitude variations of the signal are due to noise alone and therefore a limiter is used to suppress the noise induced amplitude variations. The limiter is followed by the discriminator which has a transfer characteristic which increases linearly with frequency. The discriminator is essentially a differentiator that performs differentiation in the time domain, resulting in a signal whose amplitude varies precisely as the instantaneous frequency of the signal. If the received signal is given as

$$\boldsymbol{r}(\boldsymbol{t}) = \boldsymbol{A}\cos(\omega_c \boldsymbol{t} + \phi(\boldsymbol{t})) + \boldsymbol{n}(\boldsymbol{t}) = \boldsymbol{A}_r(\boldsymbol{t})\cos(\omega_c \boldsymbol{t} + \phi_r(\boldsymbol{t})), \tag{121}$$

then the output of the limiter discriminator is

$$\boldsymbol{y}_{LD}(\boldsymbol{t}) = -\boldsymbol{A}_L\left[\omega_c + \frac{\boldsymbol{d}}{\boldsymbol{dt}}\phi_r(\boldsymbol{t})\right]\sin(\omega_c \boldsymbol{t} + \phi_r(\boldsymbol{t})), \tag{122}$$

where A_L is the limited amplitude from the limiter. For the case of FM, an envelope detector can be used at the output of the discriminator to recover the message signal embedded in the frequency. Adding an integrator at the output of the LD results in a phase demodulator [71, p. 117].

Similar to the limiter discriminator, another receiver based on the ideal FM detector [73, p. 122] is the cross-correlator receiver (CCR) which was first proposed by Park [76] who determined that the performance of the cross-correlator receiver was better than the LD at low SNR for the case with no

limiting or inverse limiting. The overall performance of the CCR has been studied in [77] and is found to be similar to that of the LD. Most importantly, the CCR is well suited for a digital implementation in a DSP.

The baseband received signal given in (3) may be written as

$$\boldsymbol{r(t)} = \boldsymbol{A}\cos\boldsymbol{\phi(t)} + \boldsymbol{n_c(t)} + \boldsymbol{j}(\boldsymbol{A}\sin\boldsymbol{\phi(t)} + \boldsymbol{n_s(t)}) = \boldsymbol{I(t)} + \boldsymbol{jQ(t)}, \tag{123}$$

where $I(t)$ and $Q(t)$ are the quadrature components. The phase of the received signal is

$$\hat{\boldsymbol{\phi}}\boldsymbol{(t)} = \tan^{-1}\frac{\boldsymbol{Q(t)}}{\boldsymbol{I(t)}} \tag{124}$$

and the output of the ideal FM detector [76] is then given as

$$\begin{aligned}\hat{\boldsymbol{\phi}}'\boldsymbol{(t)} &= \frac{\boldsymbol{d}}{\boldsymbol{dt}}\hat{\boldsymbol{\phi}}\boldsymbol{(t)} = \frac{\boldsymbol{d}}{\boldsymbol{dt}}\tan^{-1}\frac{\boldsymbol{Q(t)}}{\boldsymbol{I(t)}} \\ &= \frac{\boldsymbol{I(t)Q'(t) - Q(t)I'(t)}}{\boldsymbol{I^2(t) + Q^2(t)}}.\end{aligned} \tag{125}$$

This is known as the cross-correlator receiver. It is shown in Fig. 67 and lends itself well to a digital implementation. Since the output is the instantaneous frequency, adding an integrator results in a phase demodulator as needed for CE-OFDM.

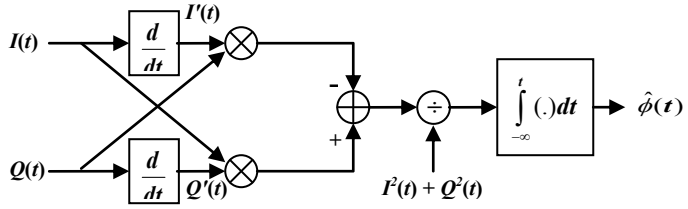

Figure 67. Cross-correlator receiver (CCR) as phase demodulator.

The cross-correlator receiver in Figure 67 can be implemented in discrete time using the sampled baseband quadrature components, $I(n)$ and $Q(n)$. The differentiators can be implemented in a DSP or FPGA environment for varying degrees of fidelity and complexity [78]. The central difference differentiator ($I'(n) = (I(n+1) - I(n-1))/2$) provides a very simple differentiator which is linear for small frequencies ($f < 0.08F_s$) and provides good attenuation at higher frequencies. A higher order differentiator can be designed to attain greater accuracy at the cost of complexity. An FIR filter of length 19 is used in this thesis. It is designed using the Parks-McClellan optimal filter design algorithm

(*firpm* in MATLAB) with a frequency response that increases linearly up to a normalized frequency of 0.5 and a stop band from 0.7 to 1 as shown in Figure 68 (where the frequencies are normalized by $F_s/2$).

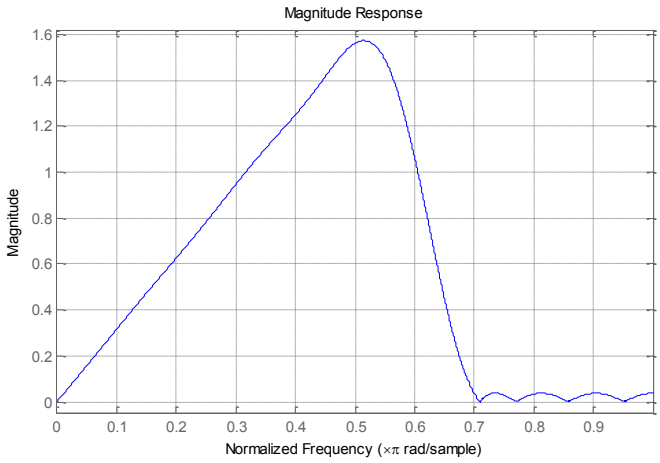

Figure 68. FIR differentiator of length 19 used in the cross-correlator receiver.

7.4.2. Arctangent Based Receiver

The arctangent based receiver for CE-OFDM was previously discussed. The arctangent provides the instantaneous phase which is restricted to the –π to +π range. This results in phase wrapping when the phase crosses the –π/+π phase boundary such as for high OFDM signal peaks. In such cases, it is necessary to use a phase unwrapper to reconstruct the original unrestricted phase.

The phase unwrapper (*unwrap* in MATLAB) operates on a sample by sample basis by searching for phase jumps larger than π and replacing them by their 2π complement. The phase unwrapper is prone to making errors due to the presence of noise and performs especially poorly at low CNR when significant noise is present. The phase unwrapper errors result in 2π phase jumps in the demodulated phase, analogous to cycle slips described earlier. For small modulation indices where an equalizer corrects any phase shifts due to the channel resulting in a 0 radian phase reference, the phase wrapping is very infrequent and hence, better performance is attained by operating without the phase unwrapper. Conversely, the phase unwrapper is essential for higher modulation indices.

7.4.3. Performance Comparison

The performance of the cross-correlator receiver (CCR) along with the arctangent based receiver both with and without a phase unwrapper is shown in Figure 69 for an oversampling factor of R_{OS}=4. The arctangent receiver without the phase unwrapper requires an equalizer to undo the random channel phase shift. The linear demodulated SNR computed for high CNR in (115) is also plotted. Both the CCR and the arctangent receiver with the unwrapper show the onset of threshold as indicated by the deviation of the demodulated SNR from the linear model. However, the arctangent receiver without the unwrapper does not show any signs of the threshold effect. This can be explained from the fact that this receiver only provides a sample by sample estimate of the phase and therefore isn't prone to cycle slips which result in 2π phase jumps in the demodulated phase. However, the demodulated SNR for it does deviate slightly from the linear model for low CNR which is due to the reduced accuracy at low CNR of the approximations used to obtain the linear model in (115). For modulation indices higher than $2\pi h$=0.6, there is significant amount of phase wrapping and hence the arctangent based receiver without a phase unwrapper has a significant loss over the linear model. The arctangent based receiver with the phase unwrapper shows a lower threshold (of around 11.25 dB) compared to the CCR (around 12 dB). This is mainly because of the amplification of high frequency noise by the differentiators in the CCR.

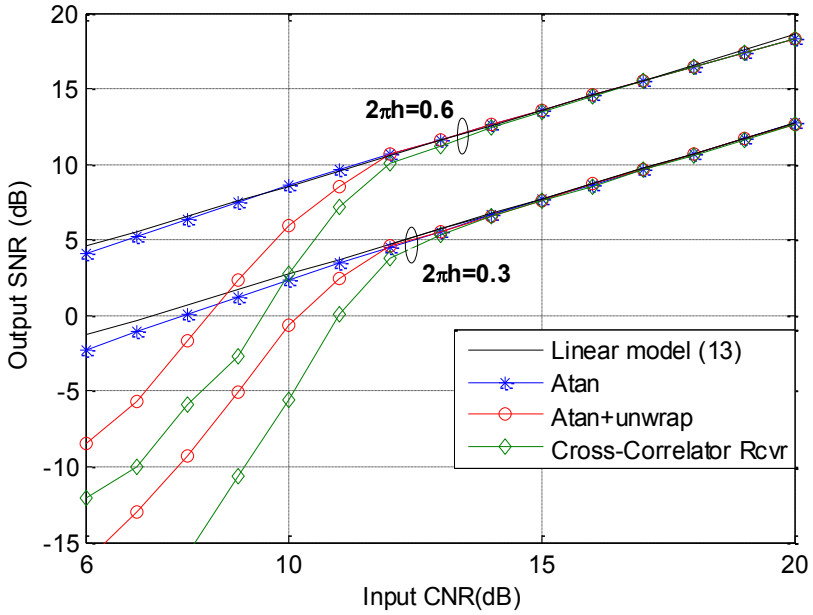

Figure 69. Demodulated SNR as a function of CNR with R_{OS}=4 with a predetection filter (fT_b=0.6 for $2\pi h$= 0.3 and fT_b=0.8 for $2\pi h$= 0.6).

7.5. Threshold Performance on a Subcarrier Basis

Consider the impact of the phase cycle slip noise at the output of the matched filters of the OFDM demodulator for both cosine and sine subcarriers. For a single positive cycle slip appearing at t_l in the CE-OFDM symbol, the matched filter outputs for the k-th cosine and the k-th sine subcarriers are

$$C_{kl}^{cos} = \int_0^{T_s} 2\pi u(t-t_l)\cos\left(\frac{2\pi kt}{T_s}\right)dt = 2\pi\int_{t_l}^{T_s}\cos\left(\frac{2\pi kt}{T_s}\right)dt = -\frac{T_s}{k}\sin\left(\frac{2\pi kt_l}{T_s}\right) \quad (126)$$

and

$$C_{kl}^{sin} = \int_0^{T_s} 2\pi u(t-t_l)\sin\left(\frac{2\pi kt}{T_s}\right)dt = 2\pi\int_{t_l}^{T_s}\sin\left(\frac{2\pi kt}{T_s}\right)dt = \frac{T_s}{k}\left(\cos\left(\frac{2\pi kt_l}{T_s}\right)-1\right). \quad (127)$$

Using these results and (118) in (117) along with normalizing shows the impact of a single positive cycle slip on the matched filter outputs for both cosine and sine subcarriers

$$Y_k^{cos} = d_k - \frac{1}{k\pi hC_N}\sin\left(\frac{2\pi kt_l}{T_s}\right) + \frac{1}{2\pi hC_N E_q}N_k \quad (128)$$

and

$$Y_k^{sin} = d_k + \frac{1}{k\pi hC_N}\left(\cos\left(\frac{2\pi kt_l}{T_s}\right) - 1\right) + \frac{1}{2\pi hC_N E_q} N_k. \quad (129)$$

The noise component at the output of the k-th cosine and k-th sine matched filters given in (128) and (129) due to a single positive cycle slip is plotted in Figures 70 and 71 respectively as a function of the cycle slip location for subcarriers k from 1 to 10 for CE-OFDM with $2\pi h$=0.8.

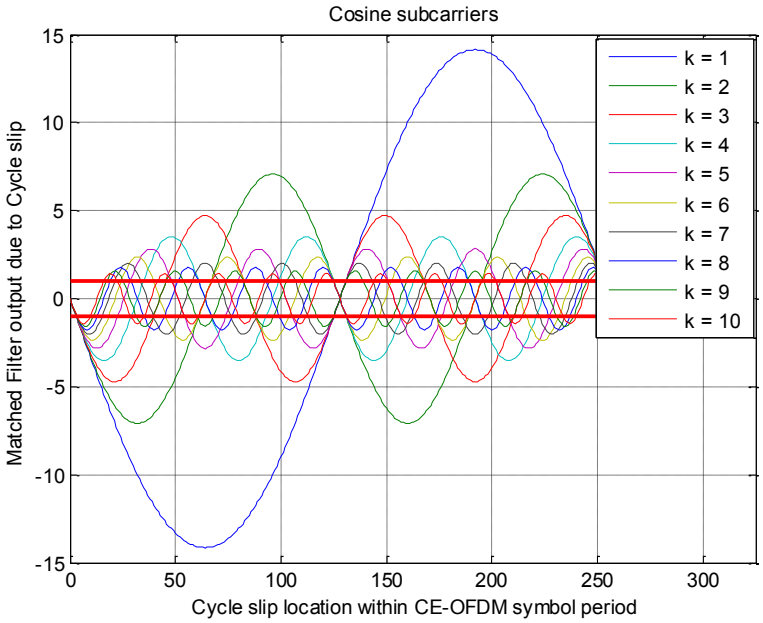

Figure 70. Cosine subcarrier matched filter output during CE-OFDM demodulation due to a single cycle slip as a function of the cycle slip location for $2\pi h$=0.8.

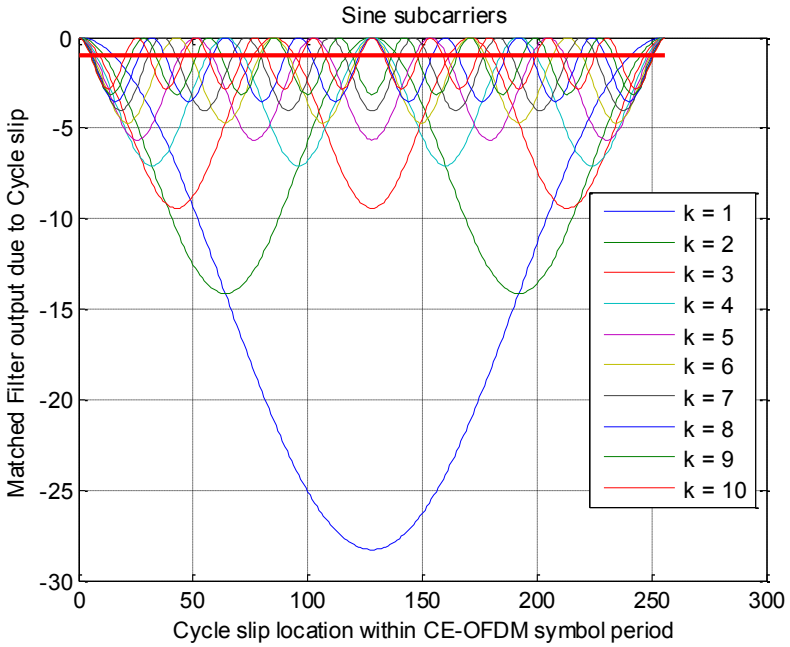

Figure 71. Sine subcarrier matched filter output during CE-OFDM demodulation due to a single cycle slip as a function of the cycle slip location for $2\pi h$=0.8.

In these figures, the x-axis represents the location of the phase cycle slip in the CE-OFDM symbol period (with an oversampling rate of 4). The solid red line shows the level of the demodulated data bits at the matched filters. It is clear that even a single cycle slip has a major impact on the matched filter output and in most cases drowns out the data bit. Secondly, it is also evident that the impact of matched filter outputs due to cycle slips at lower frequency subcarriers is much greater than higher frequency ones. Additionally, the phase cycle slip noise levels at the output of the sine subcarrier matched filters is greater than the corresponding cosine subcarriers. Finally, these figures show why there is such a large degradation in the SNR and thus overall performance below threshold as the phase cycle slips start to appear. Figure 72 shows the maximum possible matched filter output on a subcarrier basis for cosine and sine subcarriers due to a cycle slip within the CE-OFDM symbol period. As expected, the largest impact of a cycle slip occurs at the lowest frequency subcarriers.

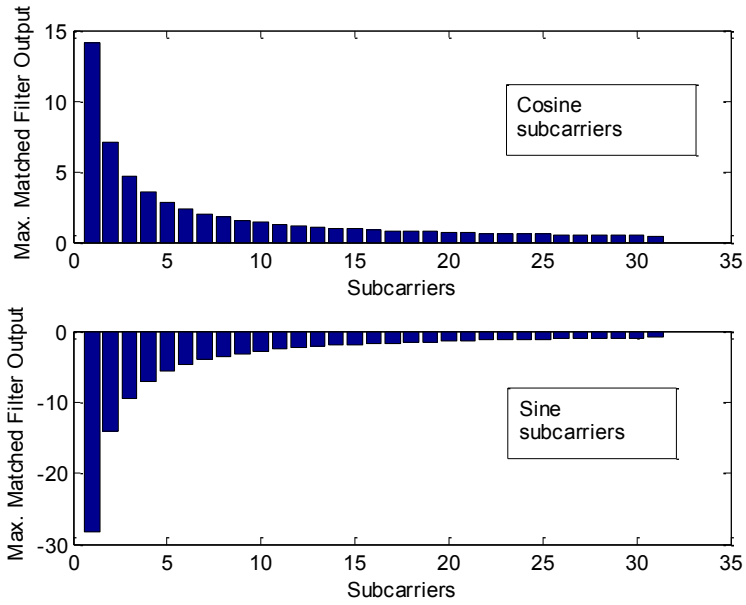

Figure 72. Maximum possible matched filter output for cosine and sine subcarriers due to a cycle slip during CE-OFDM demodulation for $2\pi h$=0.8.

7.5.1. Performance Results

The previous figures showed the impact of a single cycle slip occurring at a specific location on the underlying cosine and sine subcarriers. The simulation results on the overall threshold performance of CE-OFDM as a function of the CNR are given here including threshold and performance results on a subcarrier basis. CE-OFDM with a modulation index of $2\pi h$=0.8 is employed and the arctangent based receiver with a phase unwrapper is used. The overall SNR as a function of the CNR is shown in Figure 73. The ideal linear model which does not take phase cycle slip noise into account is plotted against the actual CE-OFDM threshold performance. Threshold is defined as the CNR at which the output SNR falls 1 dB below the linear model, in this case the threshold occurs at 12.2 dB. Below this CNR, the output SNR decreases rapidly with a decrease in the CNR.

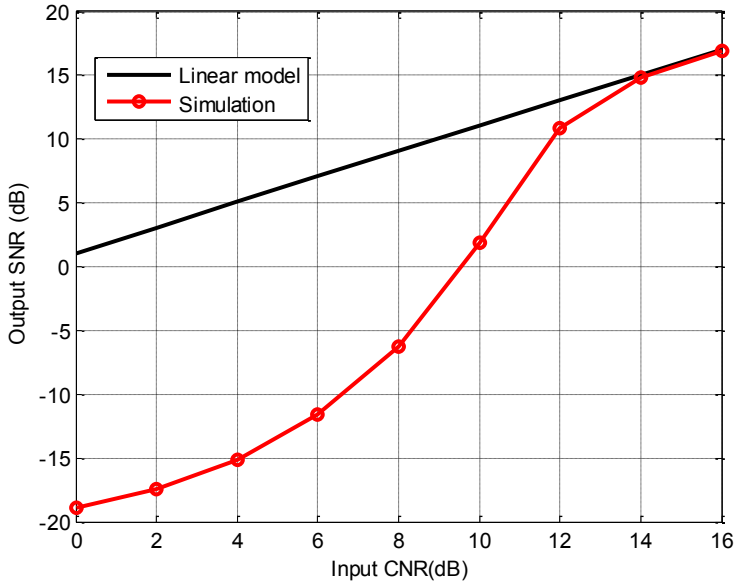

Figure 73. Demodulated SNR as a function of the CNR for CE-OFDM with $2\pi h$=0.8 (4X oversampling, predetection filter with fT_b=0.625).

The threshold performance on a subcarrier basis for the various CNRs is shown for both cosine and sine subcarriers in Figures 74 and 75 respectively.

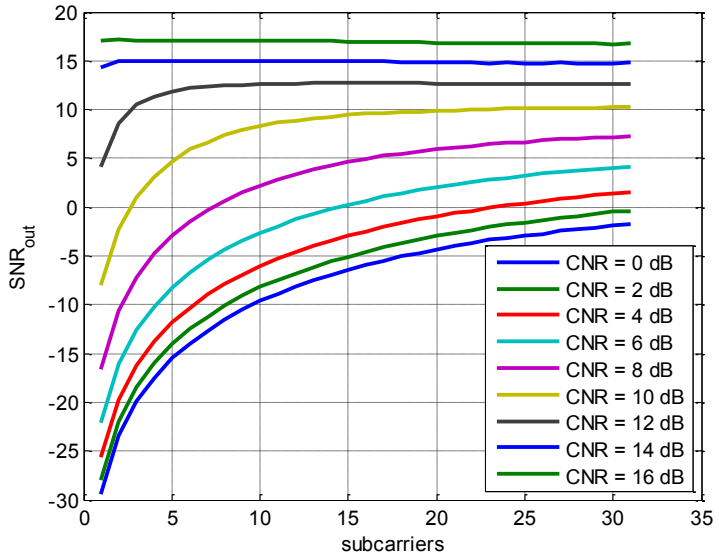

Figure 74. Demodulated SNR for cosine subcarriers for various CNRs for CE-OFDM with $2\pi h$=0.8 (4X oversampling, predetection filter with fT_b=0.625).

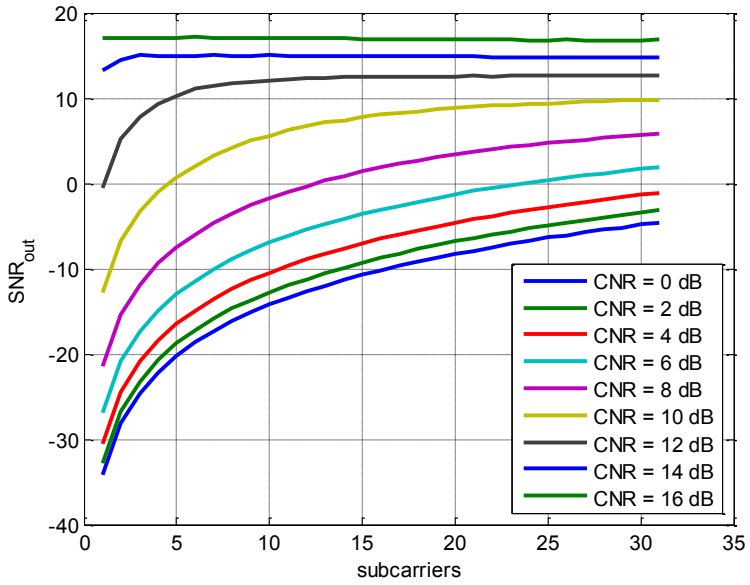

Figure 75. Demodulated SNR for sine subcarriers for various CNRs for CE-OFDM with $2\pi h$=0.8 (4X oversampling, predetection filter with fT_b=0.625).

As expected, these results follow the analytical results presented in the previous section on the impact of a cycle slip on a subcarrier basis. For high CNRs above the threshold, the SNR at the demodulator output is relatively constant across all subcarriers. However, as the CNR is reduced, the appearance of the threshold effect is evident in the SNR degradation especially at lower frequency subcarriers. In fact, for CNRs below 10 dB, the SNR at the demodulator drops more than 20 dB when going from high frequency subcarriers to low frequency subcarriers for the same CNR. This shows just how much more phase cycle slip noise is present at low frequency subcarriers, especially at the first few subcarriers. The figures also show that the threshold SNR is lower for sine subcarriers compared to cosine subcarriers for low frequency subcarriers.

Finally, it is important to understand the impact of the threshold effect not only on the demodulated SNR but also on the CE-OFDM bit error rate (BER) performance on a subcarrier basis. The BER on a subcarrier basis is shown for both cosine and sine subcarriers in Figures 76 and 77.

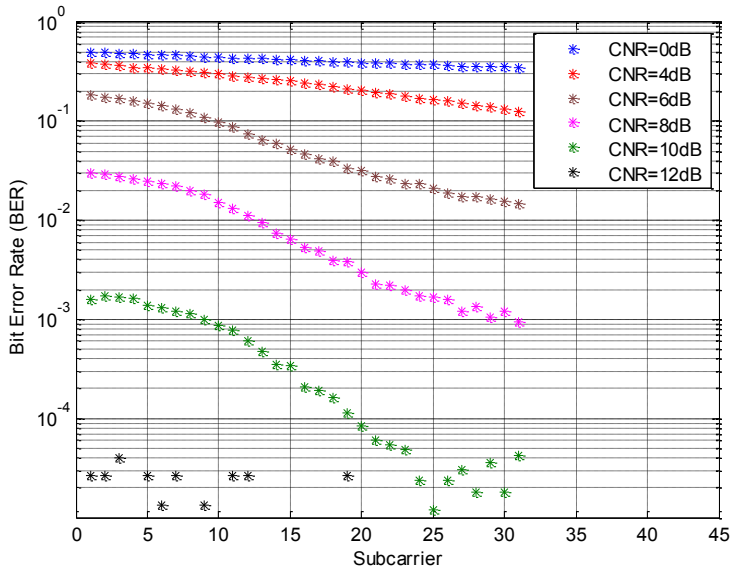

Figure 76. BER for cosine subcarriers for various CNRs for CE-OFDM with $2\pi h$=0.8 (4X oversampling, predetection filter with fT_b=0.625).

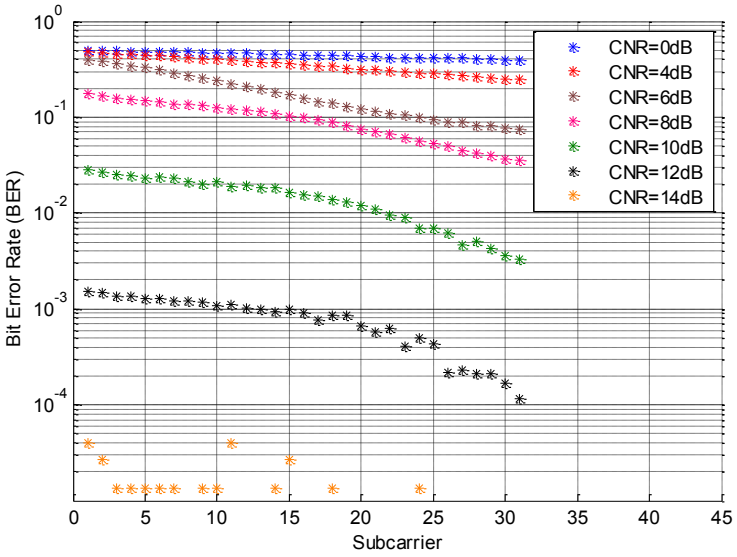

Figure 77. BER for sine subcarriers for various CNRs for CE-OFDM with $2\pi h$=0.8 (4X oversampling, predetection filter with fT_b=0.625).

The BER follows the same trend on a subcarrier basis as the SNR at the demodulator. For CNRs of 10dB and below, in most cases there is a tenfold or more increase in the bit errors going from the highest to lowest frequency subcarriers. It is interesting to note that the BER performance improves

more quickly for the cosine subcarriers than the sine subcarriers when going from low to high frequency subcarriers. Overall, while the BER performance degradation is not catastrophic at the low frequency subcarriers compared to the high frequency subcarriers as one may have thought based on the earlier SNR curves, it is important to note that even the highest frequency subcarriers suffer degradation due to the threshold effect and the errors are not limited to only low frequency subcarriers.

7.6. A Phase Cycle Slip Mitigation Technique

From the results in the previous sections, it is clear that phase cycle slip noise results in a major degradation in CE-OFDM performance at low CNRs in the threshold region. While modern communication systems employ error correction coding, too many errors can overwhelm any error correction technique. Therefore, it is important to minimize the phase cycle slip noise at the demodulator before any error correction. A low complexity cycle slip detection and mitigation technique is presented in Figure 78.

The detection of cycle slips in the CE-OFDM demodulated phase is a detection problem in the presence of the OFDM message signal and the AWGN induced phase noise which was shown in chapter 4 to be well modeled as Gaussian distributed. The OFDM message signal samples are also well modeled as jointly Gaussian distributed due to the central limit theorem as shown in [52]. Also, oversampling results in correlation between the OFDM phase samples. As shown in appendix D, with sampling rate (F_s=1/T_0, T_0=T_s/(NR_{OS})), the phase correlation between two OFDM message samples separated by *i-j* is given as

$$R_{i,j} = (2\pi h)^2 \frac{2}{N} \sum_{k=0}^{N/2} cos\left(\frac{2\pi k(i-j)}{NR_{os}}\right). \tag{130}$$

where R_{os} is the oversampling factor. Therefore, due to this correlation, the problem of detecting of cycle slips is essentially their detection in correlated, Gaussian distributed signal plus noise. The terms of the correlation matrix for the signal plus noise are

$$C_{i,j} = \sigma_n^2 \delta(i-j) + R(i,j). \tag{131}$$

To accomplish the detection of the phase cycle slips in the presence of the OFDM message phase and the phase noise, the optimum detector for the case of correlated 'noise' whitens the spectrum by employing the correlation matrix at the receiver [79]. With the received phase vector given as $\underline{\phi}_r$ and the signal of interest (reference cycle slip) given by the vector $\underline{x}$, the optimum detector computes the metric

$$T(\phi_r) = \underline{\phi}_r^T C^{-1} \underline{x} \tag{132}$$

where C^{-1} is the inverse correlation matrix. This results in prewhitening of the spectrum for optimum detection. This optimum detector is known as the generalized matched filter and provides the basis for the cycle slip mitigation technique discussed here. When the correlation between samples is ignored, prewhitening is not performed and the detector defaults to the standard matched filter which is well known in wireless communication for detection in white Gaussian noise.

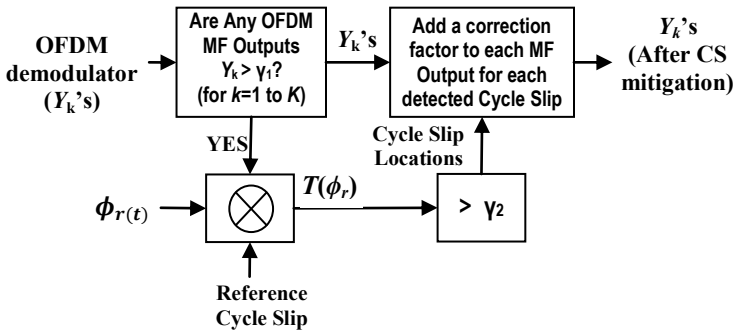

Figure 78. Phase Cycle slip mitigation at OFDM demodulator matched filter (MF) output.

To implement the overall cycle slip detection technique, the OFDM demodulator matched filter outputs for the first K subcarriers are first compared to a predetermined threshold (γ_1). Since each cycle slip results in a large cycle slip noise component especially at the low subcarriers as shown in Figures 74 and 75, this provides a very accurate general detector to estimate whether or not a phase cycle slip is present within the CE-OFDM symbol. Once it is established that one or more cycle slips (CS) are present, a correlator employing a reference cycle slip is employed to detect the exact cycle slip locations within the demodulated phase. Essentially the demodulated phase is correlated with a reference cycle slip and compared to a threshold (γ_2) to accurately detect all cycle slips within the demodulated phase. Finally the location and polarity of the detected cycle slips is used to compute

correction factors based on (126) and (127) to completely mitigate the cycle slip noise due to the detected cycle slips at the output of the OFDM demodulator. Figure 79 shows the threshold performance improvement when this cycle slip mitigation technique is employed for CE-OFDM with $2\pi h=0.8$.

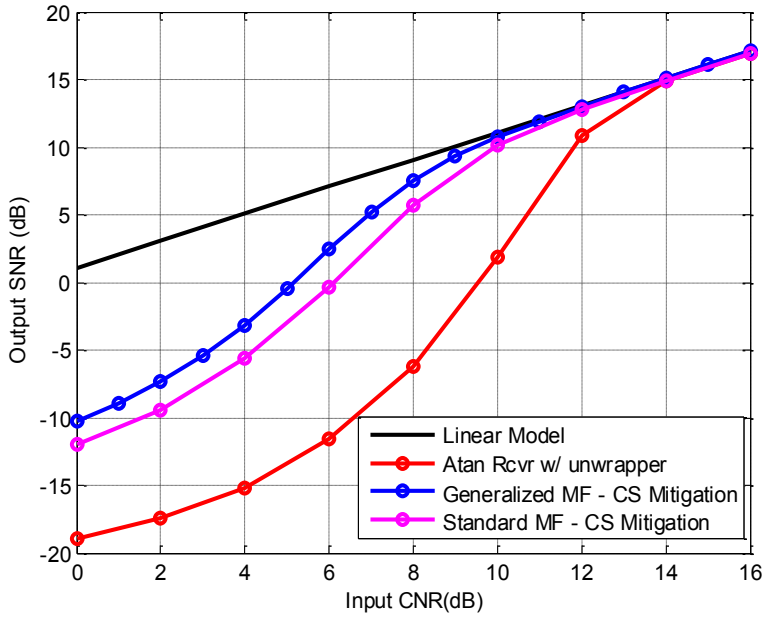

Figure 79. Demodulated SNR as a function of the CNR for CE-OFDM with $2\pi h=0.8$ (4X oversampling, predetection filter with $fT_b=0.625$, $K=5$, $\gamma_1=2.5$, $\gamma_2=\pi/2$, length of ref. cycle slip =16 samples).

The threshold mitigation technique provides a significant threshold extension of over 3 dB. Both the performance of the generalized matched filter that uses the channel correlation and the standard matched filter that ignores it is plotted. The generalized matched filter provides around 1 dB greater threshold extension. Finally the BER performance comparison is shown in Figure 80. The cycle slip mitigation technique provides significant BER performance improvement. At a BER of 10^{-3}, a performance improvement of around 2dB is present. It should be noted that the extra threshold extension due to the generalized matched filter over the standard matched filter does not translate into any extra bit error rate performance improvement.

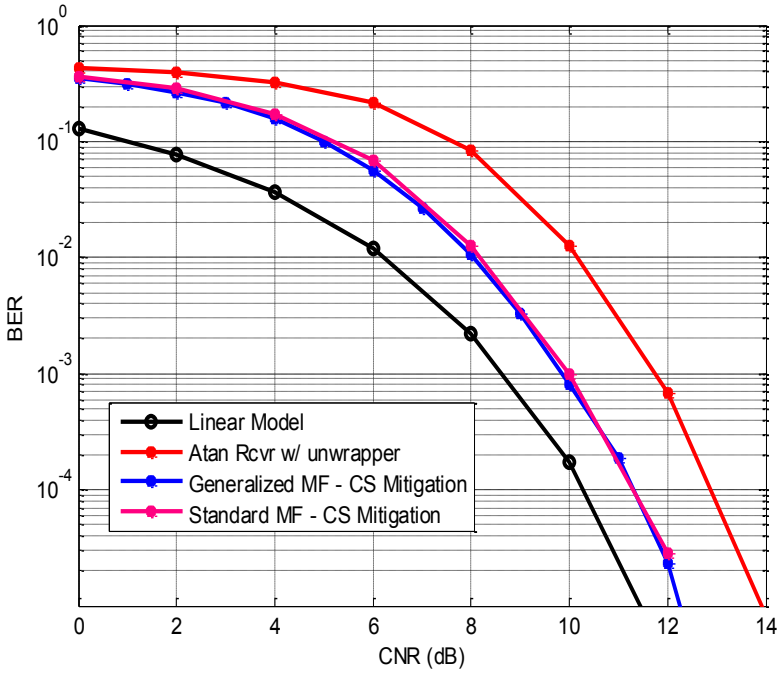

Figure 80. Bit error rate (BER) as a function of the CNR for CE-OFDM with $2\pi h$=0.8 (4X oversampling, predetection filter with fT_b=0.625, K=5, γ_1=2.5, γ_2=π/2, length of ref. CS=16 samples).

The various parameters (K, γ_1, γ_2, and length of the reference cycle slip) for the cycle slip mitigation technique presented here can be further optimized for performance improvement based on system requirements.

7.7. Acknowledgements

Chapter 7 was, in part, originally published in: A. U. Ahmed, S. C. Thompson, and J. R. Zeidler, "Threshold extending receiver structures for CE-OFDM," in *Proc. of IEEE Milcom*, Orlando, FL, Nov. 2007 and A. U. Ahmed, S. C. Thompson, D. W. Chi, and J. R. Zeidler, "Subcarrier based threshold performance enhancement in Constant Envelope OFDM," in *Proc. of IEEE Milcom*, Orlando, FL, Nov. 2012.

8. Impact and Mitigation of Narrowband Interference in CE-OFDM

8.1. Narrowband Interference

Narrowband interference (NBI) is a major issue in OFDM where an interferer anywhere within the band can result in severe degradation in performance for signal to interference ratios (SIRs) as high as 0 dB [80]. This is because the interferer power is spread out over multiple subcarriers during demodulation. The performance of CE-OFDM, with its underlying OFDM structure, is similarly degraded in the presence of narrowband interference.

The narrowband interferer is defined as

$$i_n = \sqrt{E_i} e^{j\left(\frac{2\pi}{N_s} f_i n T_s + \theta\right)} = \sqrt{E_i} e^{j\left(\frac{2\pi}{N_s}(m+\alpha)n + \theta\right)} \tag{133}$$

where $f_i = (m+\propto)\, {}^{f_s}/_{N_s}$ with N_s as the samples per symbol and $f_s = 1/T_0$ is the sampling frequency. m is the discrete frequency closest to the interferer and α is the fractional offset from it. θ is the random phase distributed between [-π, π] and n is the sample index. It can be shown that the effect of the interference in the frequency domain at discrete frequencies is given as [81]

$$I_k = \sqrt{\frac{E_i}{N}} \frac{(1-e^{2\pi\alpha})e^{j\theta}}{1-e^{\frac{2\pi}{N}(m-k-\alpha)}}. \tag{134}$$

with the interference power at the discrete frequencies given as [84]

$$\sigma_{I_k}^2 = E[|I_k|^2] = \frac{E_i}{N} \frac{(1-\cos(2\pi\alpha))}{1-cos\frac{2\pi}{N}(m-k+\alpha)}. \tag{135}$$

This interference power in the frequency domain is plotted in Figure 81 for the case of an interferer near the center of the frequency band with m=0, α=0.5.

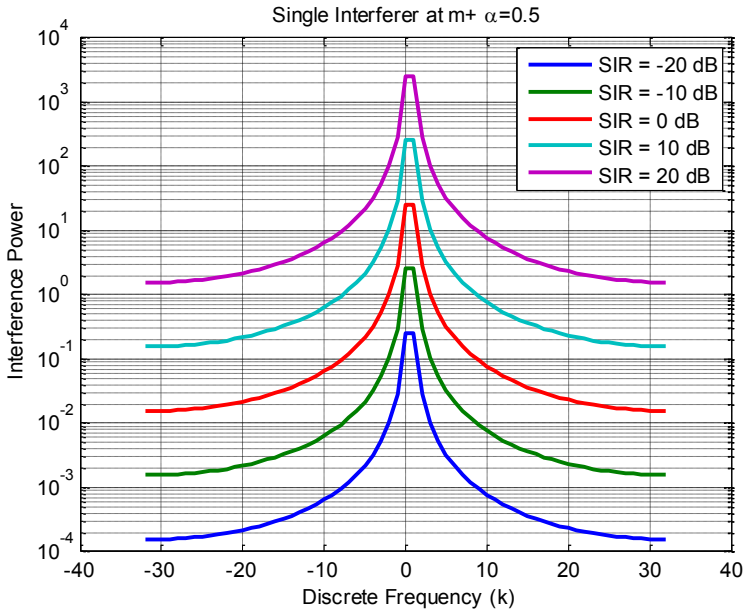

Figure 81. Interference in the frequency domain for various signal to interference ratios (SIRs) for a single interferer (m=0, α=0.5).

It is evident that while the interferer power is greatest near its vicinity, its power is spread out over the whole signaling band. Due to this reason, even a narrowband interferer results in significant overall performance degradation in OFDM as well as CE-OFDM.

8.2. Impact of Interference on CE-OFDM Performance

It has been previously shown that narrowband interference results in severe degradation in OFDM performance for signal to interference (SIR) ratios as high as 0 dB [80]. The performance of CE-OFDM is studied here in the presence of narrowband interference for the alternate receiver structures. The performance of CE-OFDM in AWGN for the case of the Arctangent receiver in the

presence of a single narrowband interferer for various SIRs is shown in Figure 82. The performance degradation is severe for SIRs up to 0 dB with an error floor above BER=0.1. Even for the case of low interference power with an SIR of 10dB, an error floor appears around a BER of 10^{-2}.

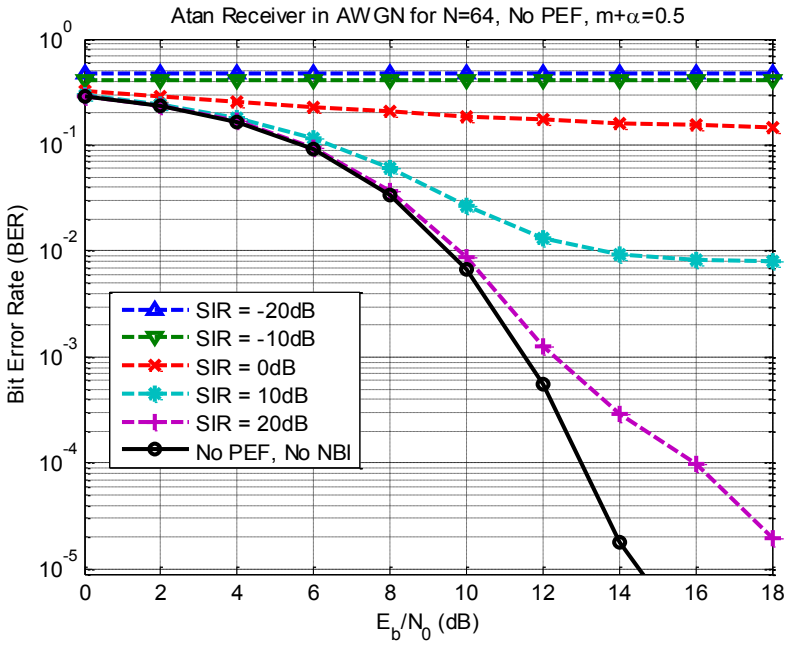

Figure 82. Performance of CE-OFDM (N=64, R_{os}=2, $2\pi h$=0.6) in AWGN while employing the Arctangent receiver in the presence of a single narrowband interferer (m=0, α=0.5).

The performance of CE-OFDM in AWGN for the case of the Enhanced linear receiver in the presence of a single narrowband interferer for various SIRs is shown in Figure 83. Once again, the performance degradation is severe for SIRs up to 0 dB with an error floor slightly lower compared to the case of the arctangent receiver. And again, even for the case of low interference power with an SIR of 10dB, an error floor appears around a BER of 10^{-2}.

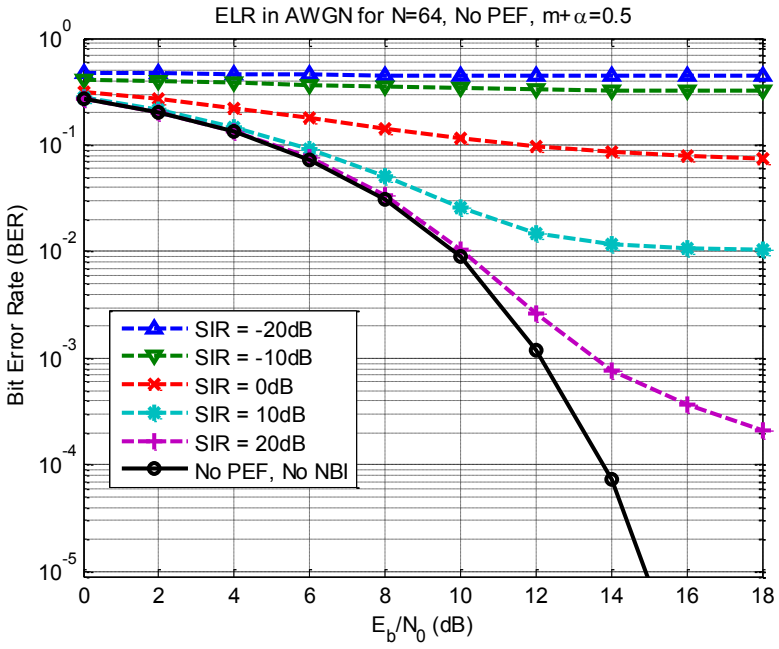

Figure 83. Performance of CE-OFDM (N=64, R_{os}=2, $2\pi h$=0.6) in AWGN while employing the Enhanced linear receiver in the presence of a single narrowband interferer (m=0, α=0.5).

Finally, the performance of CE-OFDM in AWGN for the case of the Basic linear receiver in the presence of a single narrowband interferer for various SIRs is shown in Figure 84. While the performance degradation is severe as well for the Basic linear receiver for SIRs up to 0 dB, interestingly error floors are lower for SIRs of 0 dB and -10 dB indicating that the Basic linear receiver is least affected by interference in these cases.

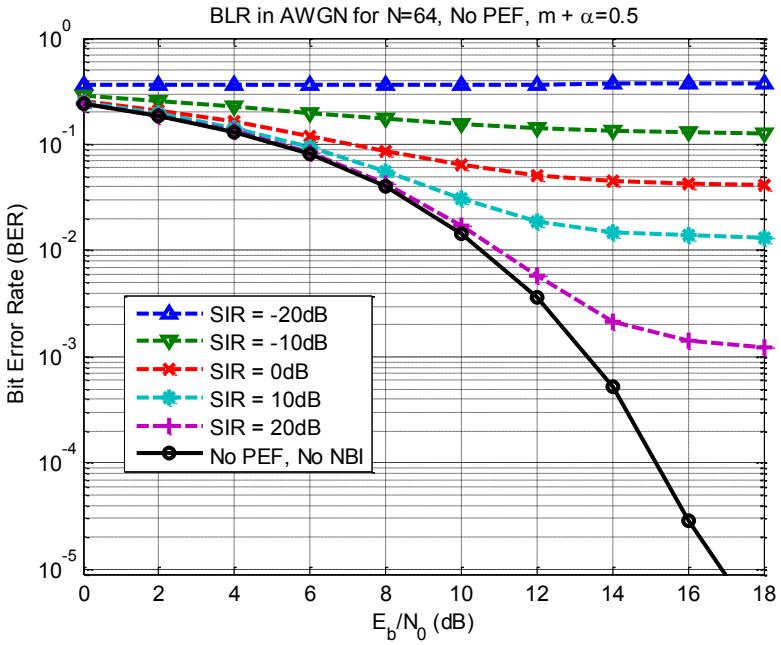

Figure 84. Performance of CE-OFDM (N=64, R_{os}=2, $2\pi h$=0.6) in AWGN while employing the Basic linear receiver in the presence of a single narrowband interferer (m=0, α=0.5).

Overall, based on the results for the Arctangent, Basic and Enhanced linear receivers, it is clear that the performance degradation is severe for SIRs of 0 dB and below. In these cases, error correction coding will not be sufficient to address this degradation, therefore an interference mitigation technique using a prediction error filter (PEF) is studied in the next section.

8.3. Interference Mitigation using a Prediction Error Filter (PEF)

A prediction error filter (PEF) is a well known structure based on the method of linear prediction. It has been previously used to remove narrowband interference from wideband signals [43], [85], [80]. The prediction error filter uses the correlation between samples past samples of the received signal to form an estimate of the interference which is then removed from the received signal. By removing the correlation between received signal samples, the prediction error filter essentially whitens the spectrum. In essence, it creates a notch at the interferer location to remove the interferer while resulting in limited distortion to signal components over the full band [80].

The structure of the prediction error filter is shown in Figure 85. It is a transversal filter of length *L*. *d* is the decorrelation delay to ensure that the current received sample is uncorrelated from the previous received samples that are used to form an estimate of the interference.

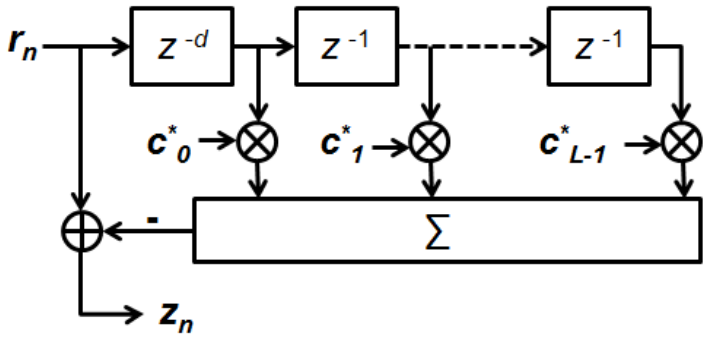

Figure 85. The prediction error filter of length *L*.

The output of the prediction error filter is given as

$$z_n = r_n - \sum_{l=0}^{L-1} c_l^* r_{n-d-l} \tag{136}$$

where c_k's are the prediction error filter coefficients for which the optimum weights under the minimum mean square error (MMSE) have been previously shown to be [85], [84] , [80]

$$c_l = Ke^{-j\frac{2\pi}{N_s}(m+\alpha)(l+d)} \tag{137}$$

where

$$K = \frac{E_i}{E_b+\sigma_n^2+LE_i}. \tag{138}$$

For the case of low signal to interference ratios and low noise to interference ratios, the approximation, K=1/L, becomes feasible.

The prediction error filter can be implemented using the low complexity least mean squares (LMS) algorithm. For the LMS algorithm, the filter weights are adaptively obtained based on the error signal as

$$\underline{c}_{l+1} = \underline{c}_l + \mu e_l^* \underline{r}_l$$

where μ is the filter step size, $\underline{c}_l$ and $\underline{c}_{l+1}$ represent the vectors with the prediction error filter coefficients at time instants l and l+1 and $\underline{r}_l$ is the vector of previous received signal samples inside the prediction error filter at time instant l. These samples are delayed by decorrelation delay d. The error signal, e_l, can be shown to simply be the output of the prediction error filter, z_n. The convergence properties of the LMS have been well described before [80].

8.4. CE-OFDM Performance with a Prediction Error Filter (PEF)

The performance of CE-OFDM for N=64 and modulation index $2\pi h$=0.6 is studied when a prediction error filter (PEF) is used for interference mitigation is studied here. A prediction error filter of length L=32 was implemented with a step size (μ) of 10^{-9}. The step size was set to 10^{-5} for the first 16 CE-OFDM symbols for faster convergence. The performance of the Arctangent, Basic linear and Enhance linear receivers is given in Figures 86-88. The performance with the prediction error filter (solid lines) is plotted in comparison to the performance without interference mitigation (dashed lines).

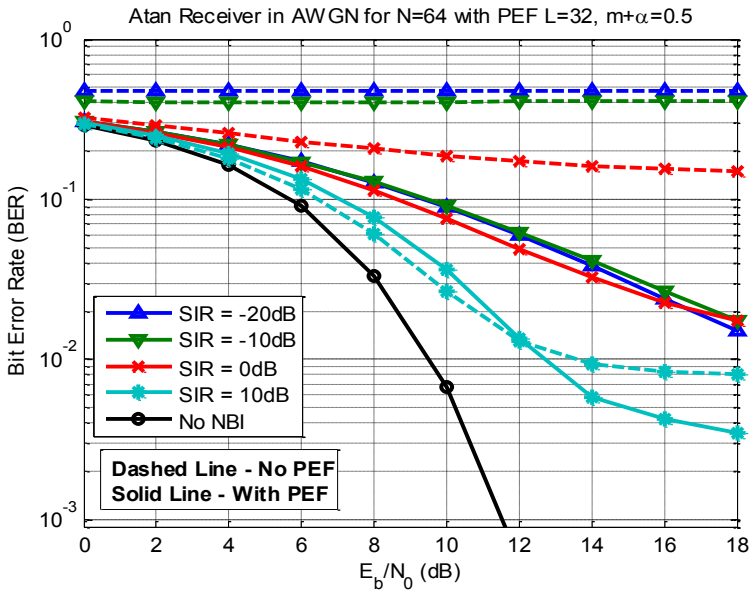

Figure 86. Performance of CE-OFDM (N=64, R_{os}=2, $2\pi h$=0.6) in AWGN while employing the Arctangent receiver in the presence of a single narrowband interferer (m=0, α=0.5) with interference mitigation using a PEF (L=32, μ=10^{-9}).

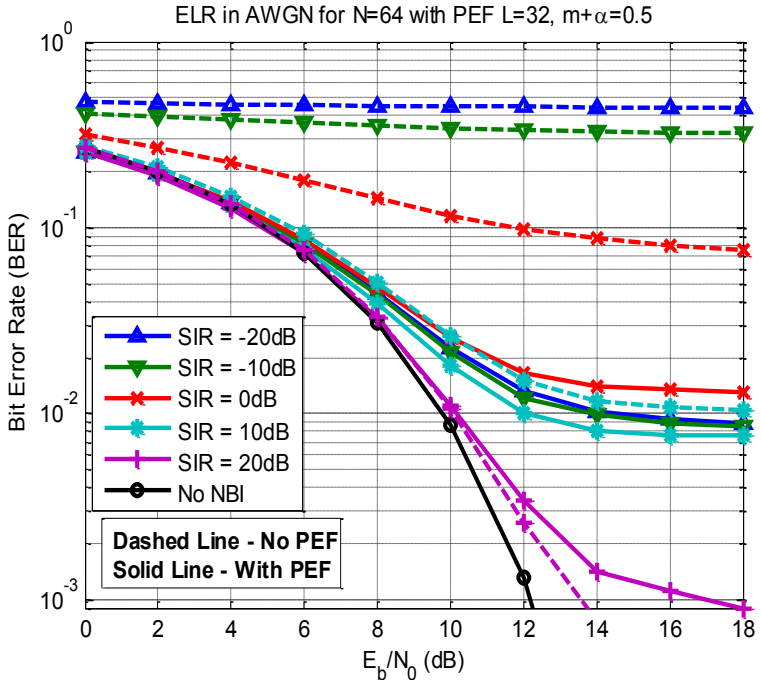

Figure 87. Performance of CE-OFDM (N=64, R_{os}=2, $2\pi h$=0.6) in AWGN while employing the Enhanced linear receiver in the presence of a single narrowband interferer (m=0, α=0.5) with interference mitigation using a PEF (L=32, μ=10^{-9}).

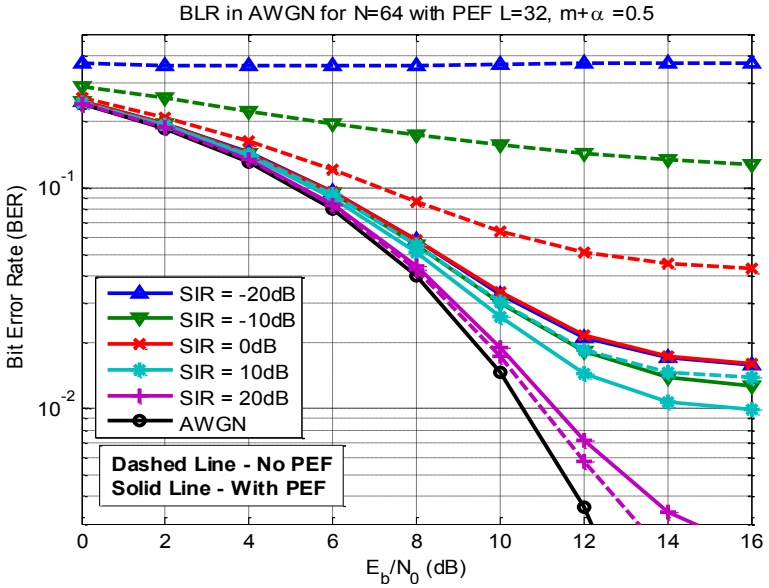

Figure 88. Performance of CE-OFDM (N=64, R_{os}=2, $2\pi h$=0.6) in AWGN while employing the Basic linear receiver in the presence of a single narrowband interferer (m=0, α=0.5) with interference mitigation using a PEF (L=32, μ=10^{-9}).

For the Arctangent receiver, performance improvement is evident for low SIR cases of 0 dB and below with significant performance improvement. For the high SIR case of 10 dB, the arctangent receiver performs worse below an SNR of 12 dB. This is consistent with the sensitivity of the phase demodulator to noise and distortion at low SNRs. The performance gains for the Enhanced linear receiver are even more significant, especially at low SNRs. The Basic linear receiver also provides significantly improved performance at low SIRs while using the prediction error filter for interference mitigation. The significant improvements for all the receiver structures at low SIRs makes the use of error correction coding feasible for robust performance in the presence of narrowband interference.

It should be noted that the prediction error filter provides the most performance improvement for the low SIR cases of -10 dB and -20 dB. In these cases, with the signal and noise power much lower than the interferer power, the PEF is able to mitigate the interference much better. For higher SIR cases, while the PEF does not provide significant gain, it also does not cause any added performance degradation.

8.5. Receiver Performance Comparison with a Prediction Error Filter (PEF)

While all the receiver structures obtained significant gains while using a prediction error filter, it is important to compare their performance to determine which receiver performs best under which circumstances. For all the cases, a prediction error filter of length L=32 was implemented with a step size (μ) of 10^{-9}. The step size was set to 10^{-5} for the first 16 CE-OFDM symbols for faster convergence.

8.5.1. Single Interferer

Figure 89 shows the comparison of the performance of the Arctangent and Enhanced Linear Receivers in AWGN with a single narrowband interferer located near the center of the signal band (m=0, α=0.5). The Enhanced linear receiver significantly outperforms the arctangent receiver for all the low SIR cases. Only for the high SIR case of 10 dB, the Arctangent provides better performance at high

SNRs. It is believed that the sensitivity of the phase demodulator to the distortion caused by the notch created by the PEF is mainly responsible for the smaller gain. However, in spite of this sensitivity, the Arctangent receiver performs significantly better at low SIRs when the PEF is used. In terms of overall performance, the Enhanced linear receiver provides significantly better performance when the PEF is used for interference mitigation.

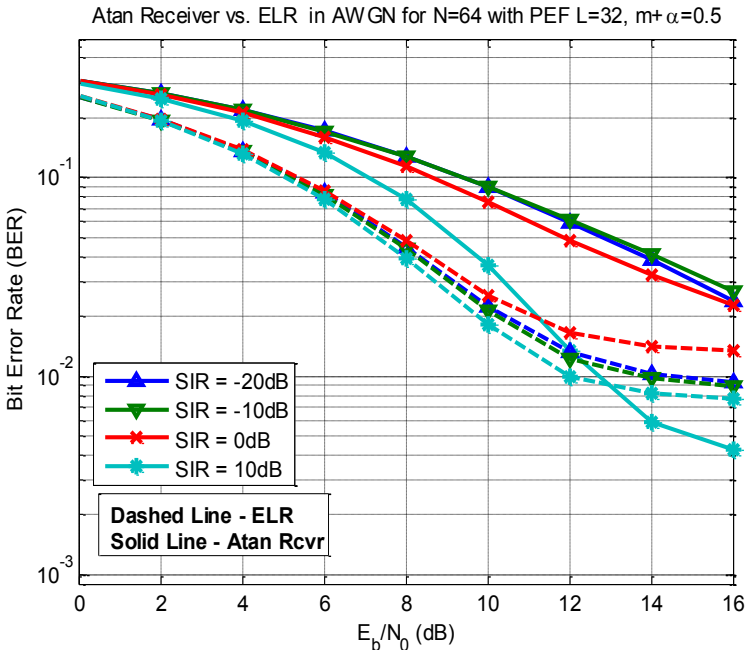

Figure 89. Performance comparison of the Arctangent receiver (solid lines) and Enhanced linear receiver (dashed lines) for CE-OFDM (N=64, R_{os}=2, $2\pi h$=0.6) in AWGN in the presence of a single narrowband interferer (m=0, α=0.5) with interference mitigation using a PEF (L=32, μ=10^{-9}).

Figure 90 shows the comparison of the performance of the Basic and Enhanced Linear Receivers in AWGN with a single narrowband interferer located near the center of the signal band (m=0, α=0.5). The Enhanced linear receiver outperforms the Basic linear receiver for all the cases, however not as significantly as the previous case of the Arctangent receiver.

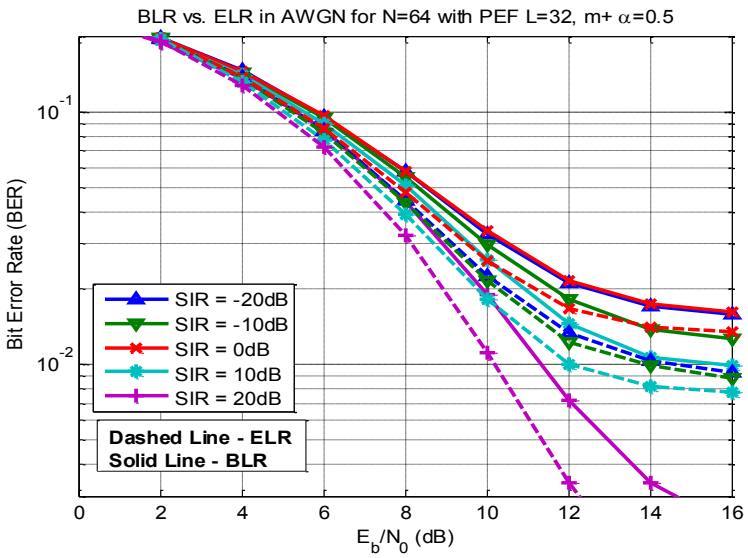

Figure 90. Performance comparison of the Basic linear receiver (solid lines) and Enhanced linear receiver (dashed lines) for CE-OFDM (N=64, R_{os}=2, $2\pi h$=0.6) in AWGN in the presence of a single narrowband interferer (m=0, α=0.5) with interference mitigation using a PEF (L=32, μ=10^{-9}).

Figure 91 shows the comparison of the performance of the Arctangent and Enhanced Linear Receivers in AWGN with a single narrowband interferer located away from the center of the signal band (m=6, α=0.5). The previously observed trends still hold for these cases as the Enhanced linear receiver still outperforms the Arctangent linear receiver for all the cases, however the Arctangent receiver performance is much improved at high SNR over 14 dB where it is comparable or better than the Enhanced linear receiver. The effect of the notch created by the PEF on the phase demodulator is less severe in this case for high SNRs. It should be noted that low SNR performance is much more critical in a communication system as it has a significant impact on the error correction coding performance, as previously shown in chapter 6. For the same conditions, Figure 92 shows the performance comparison between the Basic and Enhanced linear receivers and as before, the Enhanced linear receiver provides better performance than the Basic linear receiver for all cases.

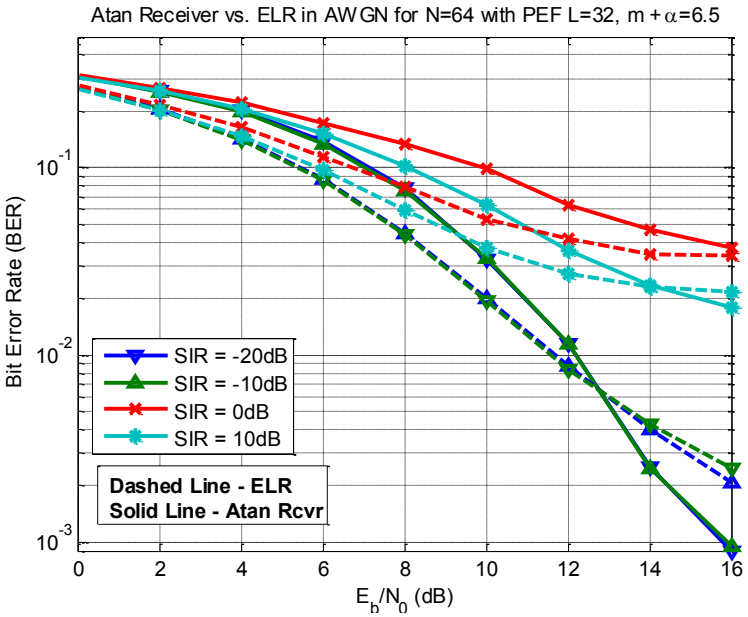

Figure 91. Performance comparison of the Arctangent receiver (solid lines) and Enhanced linear receiver (dashed lines) for CE-OFDM (N=64, R_{os}=2, $2\pi h$=0.6) in AWGN in the presence of a single narrowband interferer (m=6, α=0.5) with interference mitigation using a PEF (L=32, μ=10^{-9}).

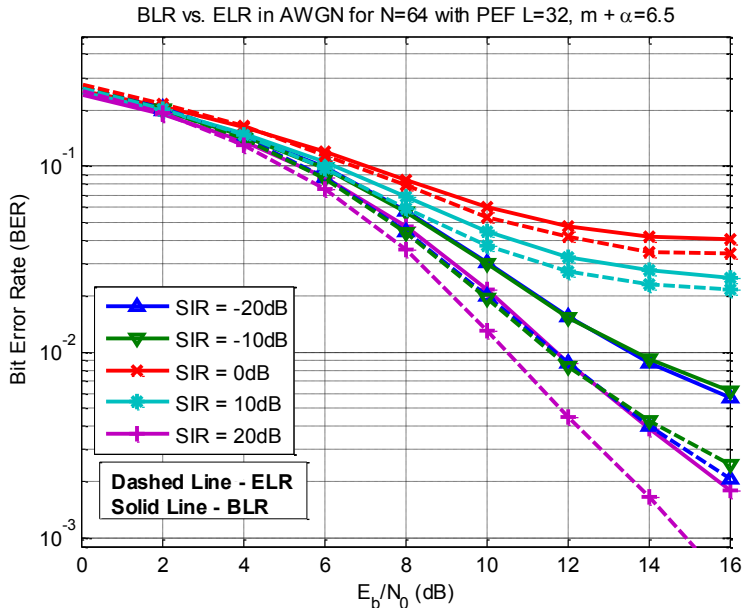

Figure 92. Performance comparison of the Basic linear receiver (solid lines) and Enhanced linear receiver (dashed lines) for CE-OFDM (N=64, R_{os}=2, $2\pi h$=0.6) in AWGN in the presence of a single narrowband interferer (m=6, α=0.5) with interference mitigation using a PEF (L=32, μ=10^{-9}).

Finally, Figure 93 shows the comparison of the performance of the Arctangent and Enhanced Linear Receivers in AWGN with a single narrowband interferer located even further away from the center of the signal band (m=16, α=0.5). The previously observed trends still hold for this cases as the Enhanced linear receiver still outperforms the Arctangent linear receiver for all the cases, however the Arctangent receiver performance is again much improved at high SNR over 14 dB where it is comparable or better than the Enhanced linear receiver.

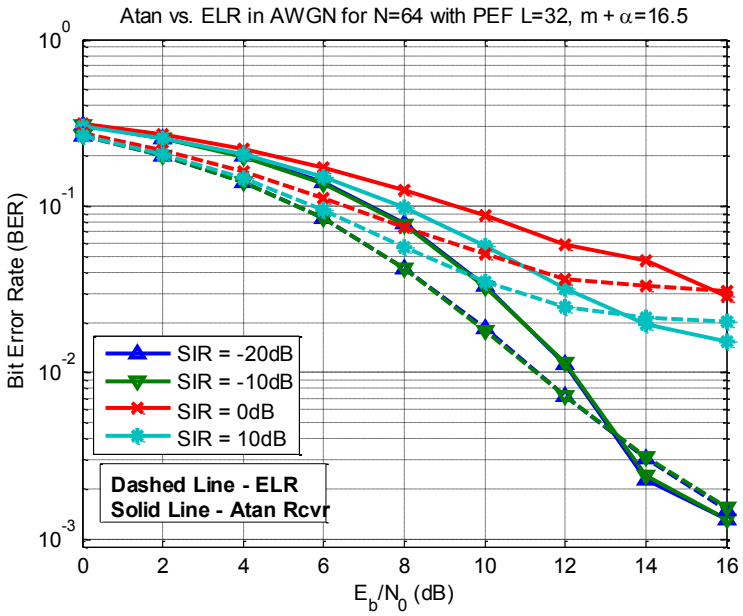

Figure 93. Performance comparison of the Arctangent receiver (solid lines) and Enhanced linear receiver (dashed lines) for CE-OFDM (N=64, R_{os}=2, $2\pi h$=0.6) in AWGN in the presence of a single narrowband interferer (m=16, α=0.5) with interference mitigation using a PEF (L=32, $\mu=10^{-9}$).

8.5.2. Multiple Interferers

A case of two simultaneous interferers in the signal band, each with half of the overall interference power, is considered here. In this case, the PEF attempts to simultaneously mitigate both the interferers. Figures 94 and 95 show the performance of the Arctangent and the Enhanced Linear

Receivers respectively in AWGN with two narrowband interferers within the band, one located near the center of the signal band (m=0, α=0.5) and one away from the center (m=16, α=0.5). For both the receivers, significant performance improvement is attained for low SIRs below 0 dB. The Enhanced linear receiver attains an especially large performance improvement for SIRs of -10 dB and -20 dB.

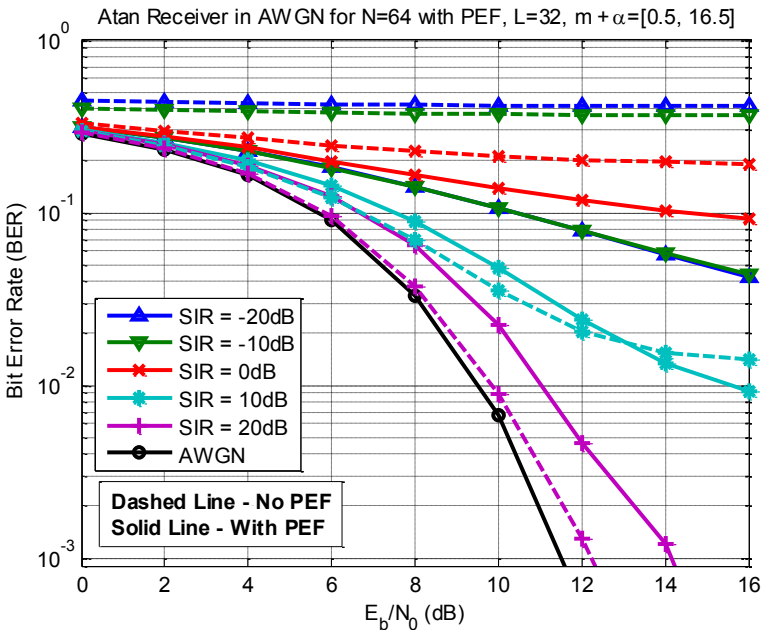

Figure 94. Performance of CE-OFDM (N=64, R_{os}=2, 2πh=0.6) in AWGN while employing the Arctangent receiver in the presence of two narrowband interferers (m=0, α=0.5 and m=16, α=0.5) with interference mitigation using a PEF (L=32, μ=10^{-9}).

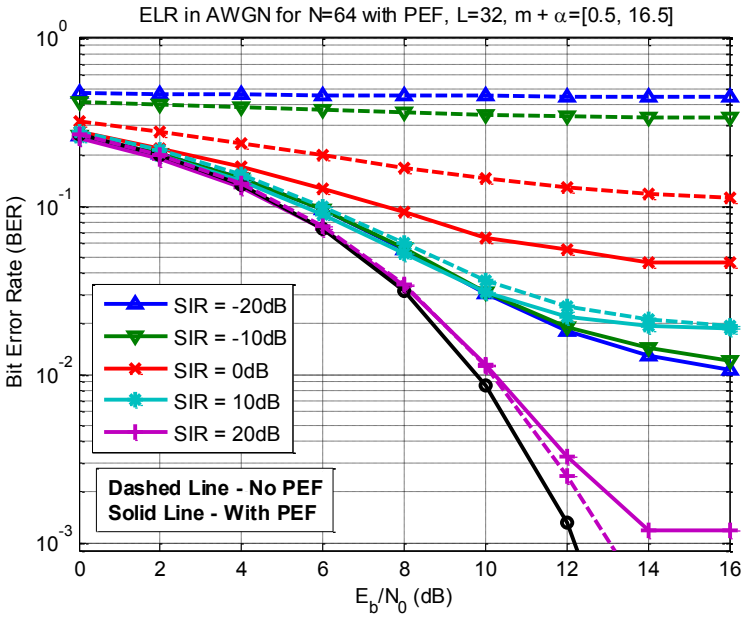

Figure 95. Performance of CE-OFDM (N=64, R_{os}=2, $2\pi h$=0.6) in AWGN while employing the Enhanced linear receiver in the presence of two narrowband interferers (m=0, α=0.5 and m=16, α=0.5) with interference mitigation using a PEF (L=32, μ=10^{-9}).

Finally, the performance comparison of the Arctangent and Enhanced Linear Receivers in AWGN is shown in Figure 96 with two narrowband interferers within the band, one located near the center of the signal band (m=0, α=0.5) and one away from the center (m=16, α=0.5). The Enhanced linear receiver significantly outperforms the arctangent receiver for all the cases with an especially significant performance advantage at low SIRs of -10dB and -20dB. For high SIRs (e.g. 10dB), the Arctangent receiver performs better at high SNRs above 12 dB, although such gains are unlikely to translate into an advantage in a coded system.

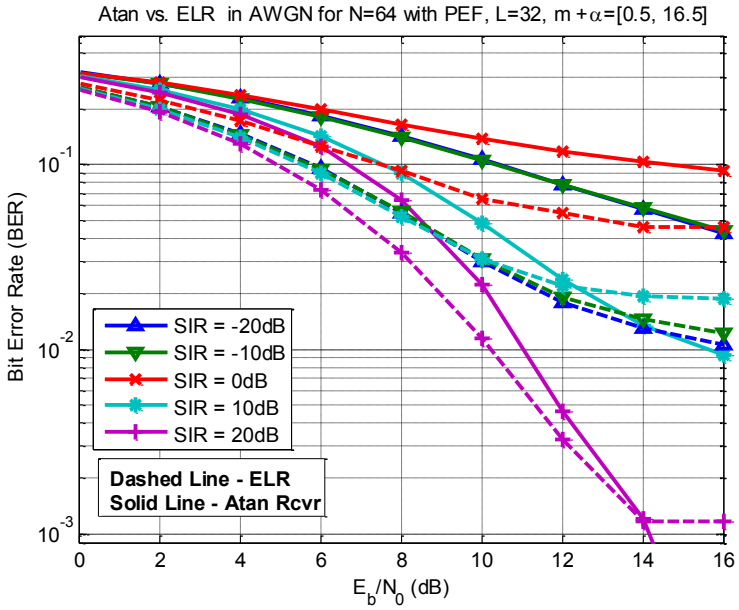

Figure 96. Performance comparison of the Arctangent receiver (solid lines) and Enhanced linear receiver (dashed lines) for CE-OFDM (N=64, R_{os}=2, $2\pi h$=0.6) in AWGN in the presence of two narrowband interferers (m=0, α=0.5 and m=16, α=0.5) with interference mitigation using a PEF (L=32, $\mu=10^{-9}$).

For all the cases considered in this section, including a single as well as two interferers, the prediction error filter (PEF) provides significant performance improvement at low SIRs of 0 dB and below for all receiver structures. Also, comparison of the receiver structures for the various cases shows that, with a very few exceptions, the Enhanced linear receiver provides the best performance in the presence of a strong narrowband interferer when a PEF is used for interference mitigation.

9. Conclusion

Constant Envelope OFDM is a novel communication waveform that addresses one of the major issues with OFDM, namely the high peak-to-average power ratio (PAPR). With its constant envelope, CE-OFDM, permits highly efficient operation near the saturation point in a power amplifier where the amplifier operation is most efficient. Not only does this result in maximum transmit power due to the lack of any backoff at the amplifier but it also results in the most efficient use of power, which is especially critical for mobile communications applications using batteries. Furthermore, CE-OFDM alleviates any linearity constraints on the amplifier or other hardware, permitting the selection of the most efficient, economical and best performing components to be employed. This is an important consideration at extremely high frequencies above 60 GHz where a large amount of unused bandwidth is available but limitations on hardware design or operation has rendered its use beyond reach. With its constant envelope, CE-OFDM provides an ideal candidate for communication at extremely high frequencies free of constraints and limitations that have hindered rapid expansion to unused higher frequency bands. Due to its constant envelope, CE-OFDM has attracted a lot of interest in recent years for applications as varied as wireless, optical, wireline and satellite communications as well as radar. As interest in CE-OFDM continues to build, further applications for CE-OFDM will continue to be explored.

CE-OFDM is based on angle modulation, and unlike linear modulations techniques such as OFDM and CDMA, CE-OFDM presents its own unique challenges in reception, equalization, coding and interference mitigation. These challenges were explored and addressed in this thesis. The threshold effect, which is caused by noise induced cycle slips is well known in angle modulation, and was studied in this thesis. It should be noted that the threshold effect is generally only encountered when a phase demodulator with some form of memory or tracking is employed such as such an arctangent receiver with a phase unwrapper or a phase locked loop (PLL). When a small or moderate modulation index

($2\pi h \leq 0.7$) is employed, the threshold effect can be avoided by using a sample by sample phase estimate provide by the arctangent receiver (without a phase unwrapper). For proper operation, the phase of the channel in this case does need to be estimated and removed from the receiver signal so the receiver phase is centered around 0 radian with reduced likelihood of phase wrapping due to crossing the $-\pi/\pi$ boundary. By operating in this manner, the arctangent receiver provides good performance. However, phase wrapping does still occur infrequently resulting in some degradation in performance at low SNRs. However, this degradation is much less significant compared to a phase demodulator prone to the threshold effect. For higher modulation indices ($2\pi h \geq 0.8$), phase wrapping is much more frequent and thus a phase demodulator with memory or tracking is needed. The effect of cycle slip noise was studied in this thesis and it was shown to affect low frequency subcarrier in the embedded OFDM message signal much more severely than high frequency subcarriers. The threshold performance of alternate receivers was studied and a novel cycle slip mitigation technique was developed for CE-OFDM, resulting in 3-4 dB of threshold extension.

The novel basic and enhanced linear receiver structures were developed for CE-OFDM. These receiver structures do not rely on a phase demodulator and provide complete immunity from cycle slip noise. This results in excellent performance at low SNRs and relatively good performance at high SNRs, for both AWGN as well as flat and frequency selective multipath fading channels. Additionally, due to their superior low SNR performance, these receivers were shown to outperform the arctangent receiver when error correction coding was used, as would be the case in a real world communication system. These receiver structures are very low complexity compared to phase demodulators such as the Arctangent receiver making them a competitive choice.

Finally, the performance of CE-OFDM in narrowband interference was studied and it was shown that just like OFDM, CE-OFDM performance is severely degraded in strong narrowband interference for signal-to-interference ratios of 0 dB and below. A prediction error filter (PEF) was applied to CE-OFDM for interference mitigation resulting in significant performance improvement. The

Enhanced linear receiver was shown to provide the best overall performance in strong narrowband interference when a prediction error filter was used for interference mitigation.

In conclusion, the techniques studied in this thesis for reception, equalization, error correction coding and narrowband interference mitigation enable robust CE-OFDM in challenging multipath fading and interference environments. This research work indicates that with its many advantages and good performance, CE-OFDM provides a competitive choice as a communication waveform to overcome challenges encountered in real world environments.

Appendix A: Simplification of the cubic term

For the case of sine and cosine subcarriers, the CE-OFDM phase signal is given as

$$x(t) = 2\pi h C_N \left(\sum_{k=1}^{N/2} dc_k \cos\left(\frac{2\pi kt}{T_s}\right) + ds_k \sin\left(\frac{2\pi kt}{T_s}\right) \right) \tag{A1}$$

where N is the total number of sine/cosine OFDM subcarriers, T_s is the CE-OFDM/OFDM block period, C_N is the normalizing constant equaling $\sqrt{\frac{2}{N}}$ for the case of binary data and ds_k and dc_k are the k-th data symbols present on the sine and cosine subcarriers respectively. Based on this, the cubic term is then given as

$$x^3(t) = \left(2\pi h C_N \left(\sum_{k=1}^{\frac{N}{2}} dc_k cos\left(\frac{2\pi kt}{T_s}\right) + ds_k sin\left(\frac{2\pi kt}{T_s}\right) \right) \right)^3. \tag{A2}$$

It can be simplified to the following form by expanding out the terms,

$$\begin{aligned} x^3(t) = (2\pi h C_N)^3 \sum_{l=1}^{N/2} \sum_{m=1}^{N/2} \sum_{n=1}^{N/2} \Bigg(& dc_l dc_m dc_n cos\left(\frac{2\pi lt}{T_s}\right) cos\left(\frac{2\pi mt}{T_s}\right) cos\left(\frac{2\pi nt}{T_s}\right) \\ & + dc_l ds_m dc_n cos\left(\frac{2\pi lt}{T_s}\right) sin\left(\frac{2\pi mt}{T_s}\right) cos\left(\frac{2\pi nt}{T_s}\right) + ds_l dc_m dc_n sin\left(\frac{2\pi lt}{T_s}\right) cos\left(\frac{2\pi mt}{T_s}\right) cos\left(\frac{2\pi nt}{T_s}\right) \\ & + ds_l ds_m dc_n sin\left(\frac{2\pi lt}{T_s}\right) sin\left(\frac{2\pi mt}{T_s}\right) cos\left(\frac{2\pi nt}{T_s}\right) + dc_l dc_m ds_n cos\left(\frac{2\pi lt}{T_s}\right) cos\left(\frac{2\pi mt}{T_s}\right) sin\left(\frac{2\pi nt}{T_s}\right) \\ & + dc_l ds_m ds_n cos\left(\frac{2\pi lt}{T_s}\right) sin\left(\frac{2\pi mt}{T_s}\right) sin\left(\frac{2\pi nt}{T_s}\right) + ds_l dc_m ds_n sin\left(\frac{2\pi lt}{T_s}\right) cos\left(\frac{2\pi mt}{T_s}\right) sin\left(\frac{2\pi nt}{T_s}\right) \\ & + ds_l ds_m ds_n sin\left(\frac{2\pi lt}{T_s}\right) sin\left(\frac{2\pi mt}{T_s}\right) sin\left(\frac{2\pi nt}{T_s}\right) \Bigg). \end{aligned} \tag{A3}$$

This expression consists of a product of cosines and sines. Such trigonometric products can be represented in the form given below through the application of trigonometric identities,

$$dc_l dc_m dc_n \cos\left(\frac{2\pi lt}{T_s}\right)\cos\left(\frac{2\pi mt}{T_s}\right)\cos\left(\frac{2\pi nt}{T_s}\right) = dc_l dc_m dc_n \frac{1}{2}\left(\cos\left(\frac{2\pi(l-m)t}{T_s}\right)+\cos\left(\frac{2\pi(l+m)t}{T_s}\right)\right)\cos\left(\frac{2\pi nt}{T_s}\right)$$
$$= dc_l dc_m dc_n \frac{1}{4}\left(\cos\left(\frac{2\pi(l-m-n)t}{T_s}\right)+\cos\left(\frac{2\pi(l-m+n)t}{T_s}\right)+\cos\left(\frac{2\pi(l+m-n)t}{T_s}\right)+\cos\left(\frac{2\pi(l+m+n)t}{T_s}\right)\right)$$

$$dc_l ds_m dc_n \cos\left(\frac{2\pi lt}{T_s}\right)\sin\left(\frac{2\pi mt}{T_s}\right)\cos\left(\frac{2\pi nt}{T_s}\right) = dc_l ds_m dc_n \frac{1}{2}\cos\left(\frac{2\pi lt}{T_s}\right)\left(\sin\left(\frac{2\pi(m-n)t}{T_s}\right)+\sin\left(\frac{2\pi(m+n)t}{T_s}\right)\right)$$
$$= dc_l ds_m dc_n \frac{1}{4}\left(\sin\left(\frac{2\pi(-l+m-n)t}{T_s}\right)+\sin\left(\frac{2\pi(l+m-n)t}{T_s}\right)+\sin\left(\frac{2\pi(-l+m+n)t}{T_s}\right)+\sin\left(\frac{2\pi(l+m+n)t}{T_s}\right)\right)$$

$$ds_l dc_m dc_n \sin\left(\frac{2\pi lt}{T_s}\right)\cos\left(\frac{2\pi mt}{T_s}\right)\cos\left(\frac{2\pi nt}{T_s}\right) = ds_l dc_m dc_n \frac{1}{2}\sin\left(\frac{2\pi lt}{T_s}\right)\left(\cos\left(\frac{2\pi(m-n)t}{T_s}\right)+\cos\left(\frac{2\pi(m+n)t}{T_s}\right)\right)$$
$$= ds_l dc_m dc_n \frac{1}{4}\left(\sin\left(\frac{2\pi(l-m+n)t}{T_s}\right)+\sin\left(\frac{2\pi(l+m-n)t}{T_s}\right)+\sin\left(\frac{2\pi(l-m-n)t}{T_s}\right)+\sin\left(\frac{2\pi(l+m+n)t}{T_s}\right)\right)$$

$$ds_l ds_m dc_n \sin\left(\frac{2\pi lt}{T_s}\right)\sin\left(\frac{2\pi mt}{T_s}\right)\cos\left(\frac{2\pi nt}{T_s}\right) = ds_l ds_m dc_n \frac{1}{2}\left(\cos\left(\frac{2\pi(l-m)t}{T_s}\right)-\cos\left(\frac{2\pi(l+m)t}{T_s}\right)\right)\cos\left(\frac{2\pi nt}{T_s}\right)$$
$$= ds_l ds_m dc_n \frac{1}{4}\left(\cos\left(\frac{2\pi(l-m-n)t}{T_s}\right)+\cos\left(\frac{2\pi(l-m+n)t}{T_s}\right)-\cos\left(\frac{2\pi(l+m-n)t}{T_s}\right)-\cos\left(\frac{2\pi(l+m+n)t}{T_s}\right)\right)$$

$$dc_l dc_m ds_n \cos\left(\frac{2\pi lt}{T_s}\right)\cos\left(\frac{2\pi mt}{T_s}\right)\sin\left(\frac{2\pi nt}{T_s}\right) = dc_l dc_m ds_n \frac{1}{2}\left(\cos\left(\frac{2\pi(l-m)t}{T_s}\right)+\cos\left(\frac{2\pi(l+m)t}{T_s}\right)\right)\sin\left(\frac{2\pi nt}{T_s}\right)$$
$$= dc_l dc_m ds_n \frac{1}{4}\left(\sin\left(\frac{2\pi(-l+m+n)t}{T_s}\right)+\sin\left(\frac{2\pi(l-m+n)t}{T_s}\right)+\sin\left(\frac{2\pi(-l-m+n)t}{T_s}\right)+\sin\left(\frac{2\pi(l+m+n)t}{T_s}\right)\right)$$

$$dc_l ds_m ds_n \cos\left(\frac{2\pi lt}{T_s}\right)\sin\left(\frac{2\pi mt}{T_s}\right)\sin\left(\frac{2\pi nt}{T_s}\right) = dc_l ds_m ds_n \frac{1}{2}\cos\left(\frac{2\pi lt}{T_s}\right)\left(\cos\left(\frac{2\pi(m-n)t}{T_s}\right)-\cos\left(\frac{2\pi(m+n)t}{T_s}\right)\right)$$
$$= dc_l ds_m ds_n \frac{1}{4}\left(\cos\left(\frac{2\pi(l-m+n)t}{T_s}\right)+\cos\left(\frac{2\pi(l+m-n)t}{T_s}\right)-\cos\left(\frac{2\pi(l-m-n)t}{T_s}\right)-\cos\left(\frac{2\pi(l+m+n)t}{T_s}\right)\right)$$

$$ds_l dc_m ds_n \sin\left(\frac{2\pi lt}{T_s}\right)\cos\left(\frac{2\pi mt}{T_s}\right)\sin\left(\frac{2\pi nt}{T_s}\right) = ds_l dc_m ds_n \frac{1}{2}\left(\cos\left(\frac{2\pi(l-n)t}{T_s}\right)-\cos\left(\frac{2\pi(l+n)t}{T_s}\right)\right)\cos\left(\frac{2\pi mt}{T_s}\right)$$
$$= ds_l dc_m ds_n \frac{1}{4}\left(\cos\left(\frac{2\pi(l-m-n)t}{T_s}\right)+\cos\left(\frac{2\pi(l+m-n)t}{T_s}\right)-\cos\left(\frac{2\pi(l-m+n)t}{T_s}\right)-\cos\left(\frac{2\pi(l+m+n)t}{T_s}\right)\right)$$

$$ds_l ds_m ds_n \sin\left(\frac{2\pi lt}{T_s}\right)\sin\left(\frac{2\pi mt}{T_s}\right)\sin\left(\frac{2\pi nt}{T_s}\right) = ds_l ds_m ds_n \frac{1}{2}\sin\left(\frac{2\pi lt}{T_s}\right)\left(\cos\left(\frac{2\pi(m-n)t}{T_s}\right)-\cos\left(\frac{2\pi(m+n)t}{T_s}\right)\right)$$
$$= ds_l ds_m ds_n \frac{1}{4}\left(\sin\left(\frac{2\pi(l-m+n)t}{T_s}\right)+\sin\left(\frac{2\pi(l+m-n)t}{T_s}\right)-\sin\left(\frac{2\pi(l-m-n)t}{T_s}\right)-\sin\left(\frac{2\pi(l+m+n)t}{T_s}\right)\right)$$

Using these identities, the cubic term in (A3) can be simplified to obtain,

$$x^3(t) = (2\pi h C_N)^3 \sum_{l=1}^{\frac{N}{2}} \sum_{m=1}^{\frac{N}{2}} \sum_{n=1}^{\frac{N}{2}} \Bigg(\frac{1}{4}(dc_l dc_m dc_n + ds_l ds_m dc_n - dc_l ds_m ds_n + ds_l dc_m ds_n) cos\left(\frac{2\pi(-l+m+n)t}{T_s}\right)$$
$$+ \frac{1}{4}(dc_l dc_m dc_n + ds_l ds_m dc_n + dc_l ds_m ds_n - ds_l dc_m ds_n) cos\left(\frac{2\pi(l-m+n)t}{T_s}\right)$$
$$+ \frac{1}{4}(dc_l dc_m dc_n - ds_l ds_m dc_n + dc_l ds_m ds_n + ds_l dc_m ds_n) cos\left(\frac{2\pi(l+m-n)t}{T_s}\right)$$
$$+ \frac{1}{4}(dc_l dc_m dc_n - ds_l ds_m dc_n - dc_l ds_m ds_n - ds_l dc_m ds_n) cos\left(\frac{2\pi(l+m+n)t}{T_s}\right)$$
$$+ \frac{1}{4}(dc_l ds_m dc_n - ds_l dc_m dc_n + dc_l dc_m ds_n + ds_l ds_m ds_n) sin\left(\frac{2\pi(-l+m+n)t}{T_s}\right)$$
$$+ \frac{1}{4}(-dc_l ds_m dc_n + ds_l dc_m dc_n + dc_l dc_m ds_n + ds_l ds_m ds_n) sin\left(\frac{2\pi(l-m+n)t}{T_s}\right)$$
$$+ \frac{1}{4}(dc_l ds_m dc_n + ds_l dc_m dc_n - dc_l dc_m ds_n + ds_l ds_m ds_n) sin\left(\frac{2\pi(l+m-n)t}{T_s}\right)$$
$$+ \frac{1}{4}(dc_l ds_m dc_n + ds_l dc_m dc_n + dc_l dc_m ds_n - ds_l ds_m ds_n) sin\left(\frac{2\pi(l+m+n)t}{T_s}\right)\Bigg).$$

(A4)

Appendix B: Analysis of the cubic term

Consider only the first cosine term from (11), more specifically the cases of interest are

$$cos\left(\frac{2\pi(-l+m+n)t}{T_s}\right) = cos\left(\frac{2\pi kt}{T_s}\right) \text{ for all } l,m,n \in \left[1,\frac{N}{2}\right]. \quad \text{(B1)}$$

This represents all the cases for different combinations of l, m, n that result in a cosine term that impacts the k-th cosine matched filter. These cases are given by all possible combinations that result in $m+n-l=k$. For example, for the case of k=1, we have combinations of the following forms:

For $m+n$=2, there is 1 combination, (l,m,n)= (1,1,1).

For $m+n$=3, there are 2 combinations, (l,m,n)= (2,1,2), (2,2,1).

For $m+n$=4, there are 3 combinations, (l,m,n)= (3,2,2), (3,3,1), (3,1,3).

…

For $m+n = N/2+1$, there are $N/2$ combinations.

Therefore, for the case of k=1, the triple sum (over l, m, n) of the first cosine term in (33) results in $\sum_{p=1}^{N/2} p$ cosine terms from all l, m, n combinations that impact the k=1 cosine matched filter.

Generalizing over any k-th matched filter, the number of cosine terms generated due to the triple sum (over l, m, n) of the first cosine term in (33) is given as

$$\sum_{p=k}^{\frac{N}{2}-1+k} p - 2\sum_{p=1}^{k}(p-1). \quad \text{(B2)}$$

The second and third cosine terms in (33) also generate the same number of cosine terms that impact the k-th matched filter. By going through a similar exercise, it can be shown that the fourth cosine term in (33) results in $\sum_{p=3}^{k}(p-2)$ cosine terms that impact the k-th cosine matched filter, with $k \in \left[3, N/2\right]$.

Therefore, the total number of terms from (33) that impact the k-th cosine matched filter is

$$3\left(\sum_{p=k}^{\frac{N}{2}-1+k} p - 2\sum_{p=1}^{k}(p-1)\right) + \sum_{p=3}^{k}(p-2)\,u[k-3] \quad \text{(B3)}$$

where $u[k\text{-}3]$ is the unit step function that equals 1 for $k \geq 3$ and is 0 otherwise. The identity $\sum_{p=1}^{P} p = P(P+1)2$ can be used to further simplify this expression as

$$N_{Total}^{k} = 3\left(\frac{N^2}{8} - \frac{N}{4} + \frac{kN}{2} - k^2 + k\right) + \left(\frac{k^2}{2} - \frac{3k}{2} + 1\right)u(k-3). \quad \text{(B4)}$$

This expression represents the number of terms from the triple sum representing the cubic term in (33) that impact the k-th cosine matched filter at the OFDM receiver. This expression is also valid for the case of the sine terms from (33) that impact the k-th sine matched filter.

The number of these interfering terms that contribute constructively at the matched filter need to be determined i.e., all such terms that not only impact the k-th matched filter but also have the correct data symbols as well (dc_k and ds_k for the k-th cosine and sine matched filters respectively). Considering the first cosine term from (33), the $N/2$ -1 cases corresponding to $m=k$ and $l=n$ (with $m \neq l$) results in $\frac{1}{4}(dc_n dc_k dc_n + ds_n ds_k dc_n - dc_n ds_k ds_n + ds_n dc_k ds_n)cos\left(\frac{2\pi kt}{T_s}\right) = \frac{1}{4}2dc_k cos\left(\frac{2\pi kt}{T_s}\right)$, where $dc_k^2 = ds_k^2 = 1$ was employed. In these $N/2$ -1 cases, the correct data symbols (dc_k) are present on the terms and these contribute constructively at the receiver. Similarly, it can be shown that the $N/2$ -1 cases corresponding to $n=k$ and $l=m$ (with $n \neq l$) also have the correct data symbols. Finally, the case of $l=m=n=k$ also results in one term with the correct data symbol (since $dc_k^3 = dc_k$). Therefore, the total number of terms that are generated from the first term of (33) for different combinations of l, m, n with the correct data symbol is $2\left(\frac{N}{2} - 1\right) + 1$. It can similarly be shown that the second and third terms of (33) also contribute this number of terms with the correct data symbol at the k-th cosine matched filter while the fourth term does not contribute any terms. Therefore, the total number of terms that contribute constructively at the k-th cosine or the k-th sine matched filter of the OFDM receiver is

$$N_{correct} = 6\left(\frac{N}{2} - 1\right) + 3 = 3(N-1). \quad \text{(B5)}$$

Appendix C: Noise Modeling for the Enhanced Linear Receiver

The total noise at the output of the *k*-th matched filter of the OFDM demodulator of the Enhanced linear receiver is

$$N_{k,Total} = \sum_{n=1}^{N_s} X_n \cos\left(\frac{2\pi k(n-1)}{N_S}\right) \tag{C1}$$

where $X_n \equiv n_1((n-1)T_o) + n_2((n-1)T_o) + n_3((n-1)T_o)$ and $\sigma_{n,Total}^2 = \sigma_{n1}^2 + \sigma_{n2}^2 + \sigma_{n3}^2 = E_b N\left(AN_0 + BN_0 + {N_0}^2\right)$ with $A = 1 + (2\pi h)^2 + \frac{1}{2}(2\pi h)^4 - \frac{7}{12}(2\pi h)^6$ and $B = (2\pi h)^2 - (2\pi h)^4 - \frac{2}{3}(2\pi h)^6$.

For a given message signal, the random variables, X_n's, are independent since they are based on independent in phase and quadrature noise samples. The Lindberg condition [49] is given for $N_{k,Total}$ as follows. For every $\epsilon > 0$,

$$\frac{1}{\sigma_{n,Total}^2} \sum_{n=1}^{N_s} E\left((C_n X_n)^2 I\{|C_n X_n| \geq \epsilon \sigma_{n,Total}\}\right) \to 0 \text{ as } N_s \to \infty$$

where $\boldsymbol{C_n} = \cos\left(\frac{2\pi k(n-1)}{N_S}\right)$ and $I\{\}$ is the indicator function. Since $2 - \cos(x(t)) \leq 3$ and $|sin(x(t))| \leq 1$, we define $n_{1,b}(t) \equiv 3n_s(t)$ and $n_{2,b}(t) \equiv n_c(t)$ with $W_n \equiv n_{1,b}((n-1)T_o) + n_{2,b}((n-1)T_o) + n_3((n-1)T_o)$**.** Based on this and since W_n's are identically distributed,

$$\frac{1}{\sigma_{n,Total}^2} \sum_{n=1}^{N_s} C_n^2 E\left({X_n}^2 I\{|C_n X_n| \geq \epsilon \sigma_{n,Total}\}\right) \tag{C2}$$

$$\leq \frac{1}{\sigma_{n,Total}^2} \sum_{n=1}^{N_s} C_n^2 E\left({W_n}^2 I\{|C_n W_n| \geq \epsilon \sigma_{n,Total}\}\right) \tag{C3}$$

$$= \frac{1}{2\sigma_{n,Total}^2} \sum_{n=1}^{N_s} \left(E\left({W_1}^2 I\{|C_n W_1| \geq \epsilon \sigma_{n,Total}\}\right) + \cos\left(\frac{4\pi k(n-1)}{N_S}\right) E\left({W_1}^2 I\{|C_n W_1| \geq \epsilon \sigma_{n,Total}\}\right)\right) \tag{C4}$$

$$= \frac{1}{2E_b\left(AN_0+BN_0+{N_0}^2\right)/R_{os}} E\left({W_1}^2 I\left\{|C_n W_1| \geq \epsilon\sqrt{E_b N_S\left(AN_0 + BN_0 + {N_0}^2\right)/R_{os}}\right\}\right). \quad \text{(C5)}$$

Let Z_n denote the random variable ${W_1}^2 I\left\{|C_n W_1| \geq \epsilon\sqrt{E_b N_S\left(AN_0 + BN_0 + {N_0}^2\right)/R_{os}}\right\}$. In order to show that $E(Z_n) \rightarrow 0$, it should be noted that Z_n is nonzero if and only if $|C_n W_1| \geq \epsilon\sqrt{E_b N_S\left(AN_0 + BN_0 + {N_0}^2\right)/R_{os}}$. Since this event has probability that tends to zero as $N_s \rightarrow \infty$, it can be concluded that $Z_n \xrightarrow{P} 0$ by the definition of convergence in probability [51]. Since $|Z_n| \leq {W_1}^2$ and $E({W_1}^2) < \infty$, based on the dominated convergence theorem [51], $E(Z_n) \rightarrow 0$ and the Lindberg condition is satisfied.

Appendix D: CE-OFDM phase signal correlation

The CE-OFDM signal is given as

$$s(t) = Ae^{j\phi(t)} \tag{D1}$$

where the CE-OFDM phase was previously defined as

$$\phi(t) = 2\pi h C_N \sum_{k=0}^{N/2-1} d_{kc} \cos\left(\frac{2\pi kt}{T_s}\right) + d_{ks} \sin\left(\frac{2\pi kt}{T_s}\right). \tag{D2}$$

The phase correlation is then given as

$$R(t_1, t_2) = E\left[\phi(t_1)\phi(t_2)\right] \tag{D3}$$

$$R(t_1, t_2) = E\left[\left(2\pi h C_N \sum_{k=0}^{N/2-1} d_{kc} \cos\left(\frac{2\pi kt_1}{T_s}\right) + d_{ks} \sin\left(\frac{2\pi kt_1}{T_s}\right)\right)\left(2\pi h C_N \sum_{k=0}^{N/2-1} d_{kc} \cos\left(\frac{2\pi kt_2}{T_s}\right) + d_{ks} \sin\left(\frac{2\pi kt_2}{T_s}\right)\right)\right]. \tag{D4}$$

We know that,

$$\begin{cases} E\left[d_{k_{c1}} d_{k_{c2}}\right] = E\left[d_{k_{s1}} d_{k_{s1}}\right] = \sigma_{d_k}^2 \delta(k_{c1} - k_{c2}) \\ E\left[d_{k_c} d_{k_s}\right] = 0 \end{cases}. \tag{D5}$$

Therefore,

$$R(t_1, t_2) = (2\pi h)^2 C_N^2 \sum_{k=0}^{N/2-1} \sigma_{d_k}^2 \left[\cos\left(\frac{2\pi kt_1}{T_s}\right)\cos\left(\frac{2\pi kt_2}{T_s}\right) + \sin\left(\frac{2\pi kt_1}{T_s}\right)\sin\left(\frac{2\pi kt_2}{T_s}\right)\right] \tag{D6}$$

$$R(t_1, t_2) = (2\pi h)^2 \frac{2}{N\sigma_{d_k}^2} \sum_{k=0}^{N/2-1} \sigma_{d_k}^2 \cos\left(\frac{2\pi k(t_2 - t_1)}{T_s}\right) = R(t_2 - t_1) \tag{D7}$$

$$R(\tau) = (2\pi h)^2 \frac{2}{N\sigma_{d_k}^2} \sigma_{d_k}^2 \sum_{k=0}^{N/2-1} \cos\left(\frac{2\pi k\tau}{T_s}\right) \tag{D8}$$

$$R(\tau) = (2\pi h)^2 \frac{2}{N} \sum_{k=0}^{N/2-1} \cos\left(\frac{2\pi k\tau}{T_s}\right) \text{ where } \tau = t_2 - t_1 \tag{D9}$$

Note that the correlation is only a function of the time difference. As expected, the phase variance is given as

$$\sigma_\phi^2 = R(0) = (2\pi h)^2 \tag{D10}$$

With sampling rate (F_s=1/T_0, T_0=T_s/(NR_{OS})),and the phase correlation between two samples separated by l=i-j as a result of oversampling is given as

$$R(\tau) = (2\pi h)^2 \frac{2}{N} \sum_{k=0}^{N/2} cos\left(\frac{2\pi kl}{NR_{os}}\right) = (2\pi h)^2 \frac{2}{N} \sum_{k=0}^{N/2} cos\left(\frac{2\pi k(i-j)}{NR_{os}}\right) \tag{D11}$$

where R_{os} is the oversampling factor.

Bibliography

[1] R. W. Chang, "Synthesis of band-limited orthogonal signals for multichannel data transmission," *Bell Syst. Tech. J.*, vol. 45, pp. 1775-1796, Dec. 1966.

[2] S. B. Weinstein and P. M. Ebert, "Data transmission by frequency division multiplexing using the discrete Fourier transform," *IEEE Trans. Commun. Technol.*, vol. 19, no. 5, pp. 628–634, Oct. 1971.

[3] L. J. Cimini, Jr., "Analysis and simulation of a digital mobile channel using orthogonal frequency division multiplexing," *IEEE Trans. Commun.*, vol. 33, no. 7, pp. 665–675, July 1985.

[4] J. A. C. Bingham, "Multicarrier modulation for data transmission: An idea whose time has come," *IEEE Commun. Mag.*, vol. 28, pp. 5-14, May 1990.

[5] W. Y. Zou and Y. Wu, "COFDM: an overview," *IEEE Trans. Broadcast.*, vol. 41, no. 1, pp. 1–8, Mar. 1995.

[6] H. Ochiai and H. Imai, "On the distribution of the peak-to-average power ratio in OFDM signals," *IEEE Trans. Commun.*, vol. 49, no. 2, pp. 282-289, Feb. 2001.

[7] S. H. Hang and J. H. Lee, "An overview of peak-to-average power ratio reduction techniques for multicarrier transmission," *IEEE Wireless Communications*, vol. 12, issue 2, pp. 56- 65, Apr. 2005.

[8] F. H. Raab, P. Asbeck, S. Cripps, P. B. Kenington, Z. B. Popovic, N. Pothecary, J. F. Sevic, and N. O. Sokal, "Power amplifiers and transmitters for RF and microwave," *IEEE Trans. Microwave Theory Tech.*, vol. 50, no. 3, pp. 814–826, Mar. 2002.

[9] T. Svensson and T. Eriksson, "On Power Amplifier Efficiency with Modulated Signals," in *Proc. of IEEE Vehicular Tech. Conf.*, May 2010.

[10] G. Breed, "The Quest for Power Amplifier Linearity and Efficiency," in *High Frequency Electronics*, Vol. 10, No. 6, June 2011.

[11] S. C. Thompson, A. U. Ahmed, J. G. Proakis, J. R. Zeidler and M. J. Geile, "Constant Envelope OFDM," *IEEE Trans. on Comm.*, Aug. 2008.

[12] S.C. Thompson, "Constant Envelope OFDM Phase Modulation," Ph.D. dissertation, University of California, San Diego, 2005. [Online]. Available: http://zeidler.ucsd.edu/students/thesis_sthompson.pdf

[13] S.C. Thompson, J.G. Proakis, and J.R. Zeidler, "Binary OFDM Phase Modulation," in *Proc. of IEEE Milcom 2003*, Boston, MA, Oct. 2003.

[14] S.C. Thompson, A.U. Ahmed, J.G. Proakis, and J.R. Zeidler, "Constant Envelope OFDM Phase Modulation: Spectral Containment, Signal Space Properties and Performance," in *Proc. of IEEE Milcom 2004*, Monterey, CA, Nov. 2004.

[15] S. C. Thompson, J. G. Proakis, and J. R. Zeidler, "Noncoherent reception of constant envelope OFDM in flat fading channels," in *Proc. IEEE PIMRC*, vol. 1, Berlin, Sept. 2005, pp. 517–521.

[16] Y. Tsai and G. Zhang, "Orthogonal Frequency Division Multiplexing with Phase Modulation and Constant Envelope Design," in *Proc. of IEEE Milcom 2005*, Atlantic City, NJ, Oct. 2005.

[17] M. Kiviranta, A. Mammela, D. Cabric, D. A. Sobel, and R. W. Brodersen, "Constant Envelope Multicarrier Modulation: Performance Evaluation in AWGN and Fading Channels," in *Proc. of IEEE Milcom 2005*, Atlantic City, NJ, Oct. 2005.

[18] R. A. Pacheco and D. Hatzinakos, “Error Rate Analysis of Phase-Modulated OFDM (OFDM-PM) in AWGN Channels,” in *Proc. of IEEE ICASSP*, Toulouse, France, May 2006.

[19] A. U. Ahmed, S. C. Thompson, and J. R. Zeidler, “Constant Envelope OFDM with Channel Coding,” in *Proc. of IEEE Milcom 2006*, Washington, DC, Oct. 2006.

[20] A. U. Ahmed, S. C. Thompson, and J. R. Zeidler, “Threshold extending receiver structures for CE-OFDM,” in *Proc. of IEEE Milcom 2007*, Orlando, FL, Nov. 2007.

[21] A. U. Ahmed, S. C. Thompson, and J. R. Zeidler, “Channel estimation and equalization for CE-OFDM in multipath fading channels,” in *Proc. of IEEE Milcom 2008*, San Diego, CA, Nov. 2008.

[22] J. Nieto, “Constant envelope waveforms for use on HF multipath fading channels,” in *Proc. of IEEE Milcom 2008*, San Diego, CA, Nov. 2008.

[23] E. S. Hassan, S. E. El-Khamy, M. I. Dessouky, S. A. El-Dolil, and F. E. A. El-Samie, “New interleaving scheme for CE-OFDM systems using chaotic maps,” in *Proc. of the Sixth international conference on Wireless and Optical Communications Networks*, Apr. 2009.

[24] Char-Dir Chung, “Spectral precoding for constant-envelope OFDM,” in *IEEE Trans. on Communications*, Feb. 2010.

[25] Zujun Liu, “Reducing specific inter-symbol interference of constant envelope OFDM system through optimizing zero-padding pattern” in *Proc. of ICSPCC*, Sept. 2011.

[26] A. U. Ahmed, S. C. Thompson, D. W. Chi, and J. R. Zeidler, “Subcarrier based threshold performance enhancement in Constant Envelope OFDM,” in *Proc. of IEEE Milcom 2012*, Orlando, FL, Nov. 2012.

[27] J. A. L. Silva, A. V. T. Cartaxo, and M. E. V. Seggato, “A PAPR Reduction Technique Based on a Constant Envelope OFDM Approach for Fiber Nonlinearity Mitigation in Optical Direct-Detection Systems,” in *Journal of Optical Communications and Networking*, Apr 2012.

[28] J. A. Silva, T. M. Alves, A. Cartaxo, and M. Seggato, “Experimental Demonstration of a Direct-Detection Constant Envelope OFDM System,” in *Signal Processing in Photonic Communications*, Germany, June 2010.

[29] J. von Hoyningen-Huene, “Constant Envelope Optical OFDM for Improved Nonlinear and Phase Noise Tolerance,” in *Proc. of Optical Fiber Comm. Conf.*, March 2011.

[30] J.M. Fabrega, “Constant envelope coherent optical OFDM based on fast Hartley transform,” in *Proc. of Conf. on Transparent Optical Networks*, June 2011.

[31] J . von Hoyningen-Huene, J. Leibrich, A. Ali, W. Rosenkranz, "Constant envelope optical OFDM for improved nonlinear and phase noise tolerance", in *Proc. of Optical Fiber Comm. Conf. and Expo. and the National Fiber Optic Engineers Conf.*, pp. 1-3, 6-10 March 2011.

[32] El Ghzaoui Mohammed, B. Jamal, and B. Ali, “Performance Evaluation of CE-OFDM in PLC Channel,” in *Signal Processing: An international journal (SPIJ)*, 2011.

[33] E. Cianca, T. Rossi, A. Yahalom, Y. Pinhasi, J. Farserotu, and C. Sacchi, “EHF for Satellite Communications: The New Broadband Frontier,” in the *Proceedings of the IEEE*, Nov. 2011.

[34] S.C. Thompson and J.P. Stralka, "Constant envelope OFDM for power-efficient radar and data communications," in *Proc. of Int. Waveform Diversity and Design Conference*, pp. 291-295, 8-13 Feb. 2009.

[35] S. Sen and A. Nehorai, “Adaptive OFDM Radar for Target Detection in Multipath Scenarios,” in *IEEE Trans. on Signal Processing*, Jan. 2011.

[36] J. P. Stralka and G. G. L. Meyer, "Constant Envelope Orthogonal Frequency-Division Multiplexing Phase Modulation for Radar Pulse Compression," in *Proc. of the conf. on Information Sciences and Systems*, Mar. 2007.

[37] van Genderen, P., "Recent advances in waveforms for radar, including those with communication capability," in *Proc. of European Radar Conference (EuRAD)*, pp. 318 - 325, Sept. 2009.

[38] K. Davaslioglu and E. Ayanoglu, "Quantifying Potential Energy Efficiency Gain in Green Cellular Wireless Networks," accepted for publication in *IEEE Communications Surveys and Tutorials*.

[39] T. Rappaport, J. Murdock, and F. Gutierrez, "State of the Art in 60-GHz Integrated Circuits and Systems for Wireless Communications," in *Proceedings of the IEEE*, Vol. 99, Issue 88, Aug. 2011.

[40] C. Doan, S. Emami, D. Sobel, A. Niknejad, and R. Brodersen, "Design Considerations for 60 GHz CMOS Radios," in *IEEE Communications Magazine*, Dec. 2004.

[41] Ahmed El Oualkadi (2011). Trends and Challenges in CMOS Design for Emerging 60 GHz WPAN Applications, Advanced Trends in Wireless Communications, Dr. Mutamed Khatib (Ed.), ISBN: 978-953-307-183-1, InTech, 2011.

[42] R. Daniels and R. Heath, "60 GHz wireless communications: emerging requirements and design recommendations," in *IEEE Vehicular Tech. Magazine*, Vol. 2, Issue 3, Sept. 2007.

[43] J. G. Proakis, *Digital Communications*. NY: McGraw Hill, 2001.

[44] Ray Andraka, "A survey of CORDIC algorithm for FPGA based computers", in the *Proceedings of the ACM/SIGDA sixth international symposium on Field programmable gate arrays*, pp 191-200, Feb. 1998.

[45] J. Vijn, "Off on a tangent: A look at arctangent implementations," 2009. [Online]. Available: http://www.coranac.com/documents/arctangent/

[46] J. G. Proakis and M. Salehi, *Communication Systems Engineering*. Upper Saddle River, NJ: Prentice Hall, 2002.

[47] M. Scutari, "Structure Variability in Bayesian Networks," *Statistics Methodology*, arXiv:0909.1685v4 [stat.ME], 2010.

[48] C. M. Grinstead and J. L. Snell, *Introduction to Probability.* Providence, RI: American Mathematical Society, 1997, pp. 325-337.

[49] D. H. Hong, "A remark on the C.L.T for sums of pairwise I.I.D. random variables," in *Math. Japonica*. 42(1). pp. 87-89, 1995.

[50] Andrzej Krajka, "On an example of sums of pairwise independent random variables for which the central limit theorem holds," *Yokohama Mathematical*, Vol. 45, 1998.

[51] R. Durrett, *Probability: Theory and Examples*. NY: Cambridge University Press, 2010.

[52] Cui, T., & Tellambura, C., "Semiblind channel estimation and data detection for OFDM systems with optimal pilot design," in *IEEE Transactions on Communications*, 55(5), 1053-1062, 2007.

[53] A. Winkelbauer, "Moments and Absolute Moments of the Normal Distribution," *Statistics Theory*, arXiv:1209.4340 [math.ST], 2012.

[54] J.G. Proakis and D. G. Manolakis, *Digital Signal Processing: Principles, Algorithms, and Applications.* New Jersey: Prentice-Hall Inc., 1996.

[55] S.O. Rice, "Statistical Properties of a Sine Wave plus Random Noise," *Bell System Tech. J.,* vol. 27, no. 3, pp. 109-157, Jan. 1948.

[56] D. Middleton, *An Introduction to Statistical Communication Theory*, Los Altos, CA: Peninsula Publishing, 1987.

[57] C. R. Cahn, "Performance of Digital Phase-Modulation Communication Systems," *IRE Trans. on Comm. Sys.*, vol. 7, no. 1, pp. 3-6, May 1959.

[58] J. Klapper and J. T. Frankle, *Phase-Locked and Frequency-Feedback Systems*. New York: Academic Press, 1972.

[59] Ove Edfors, Magnus Sandell, Jan-Jaap van de Beek and Sarah Kate Wilson, "OFDM Channel Estimation by Singular Value Decomposition," *IEEE Transactions on Communications*, July 1998.

[60] G. S. Prabhu and P. M. Shankar, "Simulation of Flat Fading Using MATLAB for Classroom Instruction," *IEEE Trans. Educ.*, vol 45, no. 1, pp. 19-25, Feb 2002.

[61] M. K. Simon and M. S. Alouini, Digital Communication over Fading Channels: A Unified Approach to Performance Analysis. New York: John Wiley & Sons, 2000.

[62] H. Sari, G. Karam, and I. Jeanclaud, "Frequency-domain equalization of mobile radio and terrestrial broadcast channels," in *Proc. of IEEE GLOBECOM*, 28 Nov.-2 Dec. 1994.

[63] C. E. Tan and I. J. Wassell, "Near-Optimum Training Sequences for OFDM Systems," in *Proc. of the 9th Asia-Pacific Conference on Communications,* 2003.

[64] X. Gao, B. Jiang, X. You, Z. Pan, Y. Xue, and E. Schulz, "Efficient Channel Estimation for MIMO Single-Carrier Block Transmission With Dual Cyclic Timeslot Structure," in *IEEE Trans. on Commun.,* vol. 55, no. 11, Nov. 2007.

[65] S. Barbarossa and A. Swami, "Estimation of time-varying multipath channel parameters using chirp signals," in *Proc. of IEEE International Symposium on Information Theory*, Washington, DC, June 2001.

[66] M. K. Ozdemir and H. Arslan, "Channel Estimation for Wireless OFDM Systems," in IEEE Communications Surveys, vol. 9, no. 2, 2nd Quarter, 2007.

[67] E. Costa, M. Midrio, and S. Pupolin, "Impact of Amplifier Nonlinearities on OFDM Transmission System Performance," *IEEE Commun. Lett*., vol. 3, no. 2, pp. 37–39, Feb. 1999.

[68] A. A. M. Saleh, "Frequency-Independent and Frequency-Dependent Nonlinear Models of TWT Amplifiers," *IEEE Trans. Commun.*, vol. 29, no. 11, pp. 1715–1720, Nov. 1981.

[69] R. van Nee and R. Prasad, OFDM for Wireless Multimedia Communications. Boston, MA: Artech House, 2000, pp. 119-129.

[70] Shu Lin and Daniel J. Costello, *Error Control Coding*, Prentice Hall, Upper Saddle River, NJ, 2004.

[71] H. Taub and D. L. Schilling, *Principles of Communication Systems*. McGraw Hill, 1971.

[72] S. O. Rice, "Noise in FM Receivers," *Time Series Analysis,* ed. M. Rosenblatt (Wiley 1963), pp. 395-422, 1963.

[73] M. Schwartz, W. Bennett, and S. Stein, *Communication Systems and Techniques*, Piscataway, NJ: IEEE Press, 1995.

[74] I. Bar-David and S. Shamai, "On the Rice Model of Noise in FM Receivers," *IEEE Trans. on Info. Theory*, vol. 34, no. 6, Nov. 1988.

[75] M. Polacek, S. Shamai, and I. Bar-David, "On FM Threshold Extension by Click Noise Elimination," *IEEE Trans. on Comm.*, vol. 36, no. 3, March 1988.

[76] J. H. Park, "An FM Detector for Low S/N," *IEEE Trans. on Comm. Tech.*, vol. 18, no. 2, pp. 110-118, April 1970.

[77] K. A. Farrell and P. J. McLane, "Performance of the Cross-Correlator Receiver for Binary Digital Frequency Modulation," *IEEE Trans. on Comm.*, vol. 45, no. 5, pp. 573-582, May 1997.

[78] R. Lyons, "Novel Differentiator Handles Discrete Time-Domain Signals," *Electonic Design* [Online], Sept. 2006. Available: http://www.elecdesign.com/Articles/Index.cfm?ArticleID=13358

[79] L. L. Scharf, *Statistical Signal Processing: Detection, Estimation, and Time Series Analysis*. New Jersey: Prentice-Hall Inc., 1991.

[80] A. Batra, "Mitigation techniques for severe narrowband interference," Ph.D. dissertation, University of California, San Diego, 2009.

[81] A. Batra and J. R. Zeidler, "Narrowband Interference Mitigation in BICM OFDM Systems," in *Proc. of IEEE International Conference on Acoustics, Speech, and Signal Processing (ICASSP) 2009*, Taipei, Taiwan, Apr. 2009.

[82] J. Lassing, T. Ottosson, and E. Strom, "On the union bound applied to convolutional codes," in *Proc. of IEEE VTC 2001*, Atlantic City, NJ, Oct. 2001.

[83] P. Frenger, P. Orten, and T. Ottosson, "Convolutional Codes with Optimum Distance Spectrum," *IEEE Communications Letter,* vol. 3, no. 11, pp. 317-319, Nov. 1999.

[84] A. Batra and J. R. Zeidler, "Narrowband Interference Mitigation in OFDM Systems," in *Proc. of IEEE Milcom 2008*, San Diego, CA, Nov. 2008.

[85] L.-M. Li and L. B. Milstein, "Rejection of CW interference in QPSK systems using decision-feedback filters," in *IEEE Transactions on Communications*, vol. COM-31, pp. 473-483, Apr. 1983.

[86] J. R. Zeidler, E. H. Satorius, D. M. Chabries, and H. T. Wexler, "Adaptive Enhancement of Multiple Sinusoids in Uncorrelated Noise,' in *IEEE Transactions on Acoustic, Speech and Signal Processing,* vol. ASSP-26, pp. 240-254, June 1978.

[87] Ahmad R.S. Bahai and Burton R. Saltzberg, *Multi-Carrier Digital Communications: Theory and Applications of OFDM*, New York, NY, 1999.

[88] David V. Roderick, A Coded Orthogonal Frequency Division Multiplexing Simulation of a High Data Rate, Line-of-Sight, Digital Radio for Mobile Maritime Communications, Thesis, Naval Postgraduate School, June 1997.

[89] P. H. Moose, D. Roderick, R. North, and M. Geile, "A COFDM based Radio for HDR LOS Networked Communications," in *Proc. of IEEE Int. Conf. on Comm.*, Vancouver, BC, June 1999.

[90] J. C. Allen, M. Reuter, and R.C. North, "Scattering Functions from the Naval Communication Channels Dataset," in *Proc. of IEEE MILCOM*, 31 Oct.-3 Nov. 1999.

[91] L. Schilling and J. Billig, "On the Threshold Extension Capability of PLL and FDMFB," *IEEE Trans. Comm. Tech.*, vol. 52, no. 5, pp. 621-622, May 1964.

[92] W. C. Lindsey and C. M. Chie, "A Survey of Digital Phase-Locked Loops," *Proc. of the IEEE*, vol. 69, no. 4, pp. 410-431, Apr. 1981.

[93] J. Garodnick, J. Greco, and D. L. Schilling, "Response of an All Digital Phase-Locked Loop," *IEEE Trans. on Comm.*, vol. 22, no. 6, pp. 751-764, June 1974.

[94] S. Ono, T. Aoyama, M. Hagiwara and M. Nakagawa, "Implementation of a new DSP DPLL using high performance DSP DSSP-1," in *Proc. of ICASSP 1986*, Tokyo, Japan, Apr. 1986.

[95] Y. Iwanami and T. Ikeda, "An adaptive control method of a digital signal processing DPLL FM demodulator under a fading environment," in *Proc. of Globecom 1987*, Tokyo, Japan, Nov. 1987.

[96] Y. Iwanami, "Demodulation of CPFSK and GMSK Signals using Digital Signal Processing DPLL with Sequence Estimator," *IEICE* Trans. on Comm., vol. 84-B, no. 1, pp. 26-35, Jan. 2001.

[97] G. D. Arndt and F. J. Loch, "A study of FM threshold extension techniques," *NASA Tech. Rpt. R-384*, Washington, DC, Apr. 1972.